Energetics of Small Molecules and Molecular Fragments on Model Catalyst Surfaces: Calorimetric Adsorption and Adhesion Energies on Pt, Ni and Cu(111)

S. Elizabeth Harman

A dissertation

submitted in partial fulfillment of the

requirements for the degree of

Doctor of Philosophy

University of Washington

2022

Reading Committee:

Charles T. Campbell, Chair

Anne McCoy

Cody Schlenker

Bo Zhang

Program Authorized to Offer Degree:

Chemistry

University of Washington

Abstract

Energetics of Small Molecules and Molecular Fragments on Model Catalyst Surfaces: Calorimetric Adsorption and Adhesion Energies on Pt, Ni and Cu(111)

S. Elizabeth Harman

Chair of the Supervisory Committee:
Professor Charles T. Campbell
Chemistry

Heterogenous catalysts are essential for our society. From the production of food and energy to the manufacture of chemicals and the mitigation of pollution, catalysts touch every facet of our lives. In order to maintain our way of life and improve our energy systems it is critical to seek out new and better catalysts. We need continual improvement in our catalysts and processes to continue supporting our society's growth. Modeling methods such as Density Functional Theory (DFT) do great work in exploring new catalyst materials. By using quantum mechanical first principles and experimentally determined adsorbate bond enthalpies of catalytic intermediates, DFT can predict the energetics of individual steps of complex reactions on catalyst surfaces. However, DFT suffers from errors in absolute energy accuracy, which in turn leads to large errors in predicted reaction rates. It's imperative that we improve these models. By experimentally measuring the energetics of catalytically relevant species on catalysts surfaces,

critical benchmarks for DFT and other modeling methods can be provided. Of the available experimental methods, Single-Crystal Adsorption Calorimetry (SCAC) is the only technique capable of directly measuring the binding energies of adsorbates on surfaces that do not adsorb and then desorb reversibly.

This dissertation details the use of SCAC to measure the heats of adsorption of a variety of catalytically relevant molecular fragments on the Pt(111), Ni(111) and Cu(111) surfaces, including the first direct measurement of the heat of adsorption of any molecular fragment on a Cu surface. These measurements continue a decades-long effort by the Campbell group to supply critical benchmarks of experimentally determined energetics of small molecules and molecular fragments on model catalyst surfaces. This work also details the calculated adhesion energies of several small molecules on these transition metal surfaces using a method recently developed by the Campbell group.

In the following chapters, SCAC is used to measure the heats of adsorption of methanol and methoxy on Ni(111). Ni is a common catalyst for steam reforming and methanol synthesis, while methoxy is a common intermediate in those processes. SCAC is also used to make the first measurement of the energetics of adsorption of any molecular fragment on a Cu surface, here the dissociative adsorption of formic acid on oxygen-precovered Cu(111) to form bidentate formate and gaseous water. Cu is a promising monometallic catalysts for the reduction of CO_2, where formate is an intermediate. The adhesion energy of molecular formic acid on Cu(111) is also presented. The energetics of several species to Pt(111) are measured via SCAC. We use azulene as an analogue for defects in graphene, and its isomer naphthalene for well ordered graphene, to examine their energetic differences on Pt(111). The heat of adsorption of *n*-decane on Pt(111) is measured and compared to previous work via Temperature Programmed

Desorption (TPD). The adhesion energy of *n*-decane is calculated and compared to the adhesion energy of shorter linear alkanes on Pt(111) to show that adhesion energy remains nearly constant as chain length increases due to the per unit area definition of adhesion energy. Finally, the heat of adsorption and adhesion energy of acetonitrile on Pt(111) are reported. Acetonitrile is a common solvent in electrocatalysis, where Pt is a common electrode material, in addition to being the simplest organic nitrile. These fundamental energetics provide important benchmarks for DFT modeling, especially on Cu(111) where there is a lack of experimental measurements.

Table of Contents

List of Figures

List of Tables

Acknowledgments

To begin, I would like to thank my advisor and mentor Dr. Charles T. Campbell. His guidance, wealth of knowledge and support have made my time at the University of Washington a rewarding experience. I would also like to thank the members of my committee, Dr. Anne McCoy, Dr. Cody Schlenker, Dr. Bo Zhang and Dr. Oscar Vilches for their time and aid. I would like to thank Dr. Spencer Carey for his training both on the calorimeter and how to succeed in graduate school. I cannot begin to thank Dr. Griffin Ruehl enough for both his collaboration in our work and his friendship and support throughout this process. I would also like to thank the other members of the Cambell group, past and present – Dr. Jack Rumptz, Dr. Wei Zhang, Dr. Zhongtian Mao, Nida Janulaitus, Dr. Kun Zhao, Dr. Wei Zhao and the excellent undergraduate research assistants Oliva Gluth and David LaVoy. It has been a pleasure to work with and learn from all of you. I would like to thank the expert stuff of the UW Chemistry Electronic Shop – Lon Buck, Bill Beaty and Rachel Huffman – and the UW Chemistry Machine Shop – Eric Strakbein, Brian Wadey and Kevin Sonderlund – for their repairs to our equipment and creative problem solving. I would also like to thank Loch Hickok of the chemistry stockroom for his support and guidance. I would like to thank all of my friends and family, especially my mom Janet, my sister Rachelq and my partner Vishal. Your support, love and patience have made all this possible. Last and certainly not least I would be remiss not the thank the cats Aoife, Mozzarella and Orange Boi for the levity and joy they've brought me during this journey.

Chapter 1 Introduction

Heterogeneous catalysis is critical to the development and maintenance of our society. From the production of fertilizer that facilitates feeding the world's growing population, to the refining of fuels in the energy sector, to the production of chemicals needed for a wide range of applications, catalysts touch every aspect of our lives.[1–3] It would be impossible to produce these products on the necessary scale without catalysts lowering energy barriers and increasing reaction rates. Catalysts even mitigate pollution from myriad sources, including these industrial processes and even transportation.[4]

As our population continues to grow, energy demands increase alongside greenhouse gas emissions that are driving climate change. It is crucial to investigate solutions on a variety of fronts, from stepping away from fossil fuels and replacing that energy with sustainable sources, as well as improving the activity and selectivity of our current catalysts to minimize the production of harmful waste species and reduce energy demands. This can be achieved by developing new and better catalysts. However, there are many unknowns when it comes to what makes a catalyst effective for a specific reaction. Testing potential catalyst materials via a trial-and-error method is far too slow and expensive. While some educated guesses can be made using the known bond strengths between common catalytic materials like transition metals and some key intermediates,[5] this quickly falls apart when considering the complexity of not only the chemical processes being studied but also the wide variety of potential catalysts surfaces. Beyond individual transition metals, various oxides,[6] metal-organic frameworks (MOFs),[7] supported nanoparticles[8] and single-atom catalysts[9] are all options that need to be investigated. In principle, if one knew the energies (and standard-state entropies) of all the adsorbed

intermediates and transition states in the reaction mechanism on all the materials of interest, one could solve the rate equations to estimate the net catalytic rates on potential new catalyst materials.

To develop new and better catalysts, some of this investigative research has moved to computational modeling for estimating these needed energies and entropies. A popular and powerful method for estimating the bond energies of catalytically relevant intermediates and elementary-step transition states on catalyst surfaces is Density Functional Theory (DFT). This method, especially when done with functionals that consider additional complications such as van der Waals forces, can predict bond energy trends of reactants and intermediates on a wide variety of transition metal surfaces.[10–16] However, even the best DFT functionals for adsorbate energies are limited by rather large errors (20 kJ/mol or more) in absolute energy accuracy.[17] Even small errors in estimated adsorbate energies can lead to large errors in reaction rates. An error of 20 kJ/mol in the rate determining step of reaction at 200 C results in a 160-fold error in the rate of reaction. To develop better DFT functionals or other fast methods for solving the ground state electronic energies with improved energy accuracy, more adsorbate-energy benchmarks are needed to validate accuracy for a wider range of systems. Since no existing computational methods provide the needed energy accuracy for adsorbate energies on extended solids or large particles, experimental benchmarks of adsorbate energies on clean single crustal surfaces are the only energies of sufficient accuracy for well-defined adsorbate structures. The current number of such benchmarks is rather limited, and most molecular fragments are only reported on the Pt(111) surface.[17,18] A primary goal of the work presented in this dissertation is to provide more experimental benchmark energies for adsorbates of interest in catalysis for an expanded range of adsorbate classes and metals.

There are three ways to experimentally measure these benchmark energies of well-defined adsorbates structures on clean single crystal surfaces. One method is Temperature Programmed Desorption (TPD), which takes the desorption energy of a molecule from a surface to be equivalent to the adsorption energy.[19,20] Another is to measure equilibrium adsorption isotherms.[20,21] However, these methods require that a molecule desorbs reversibly; that is to say the molecule does not undergo any dissociation on the catalyst surface or fragment during heating, or, if it does dissociate, that the fragments reversibly recombine to make the same gas upon heating. In practice, the only such fragments that could so far be measured by those methods are H, O and N, produced from the dissociative adsorption of their diatomic gases.[22] The most important species other than molecularly adsorbed species that require experimental energy benchmarks for DFT are other more complex dissociatively adsorbed molecular fragments and transition state species. The focus of this dissertation is to provide some benchmark energies for such fragments on well-defined late transition metal model catalyst surfaces.

The only method currently available to directly measure the irreversible adsorption of molecules on a well-defined (i.e., single crystal) surfaces was developed by Sir David King in the 1990's, Single-Crystal Adsorption Calorimetry (SCAC).[20,23] This original calorimeter used a remote infrared temperature sensing via a broadband infrared photon detector to measure heats of adsorption. The Campbell group updated this method over time, changing the heat detector to a pyroelectric β-polyvinylidene fluoride (PVDF) ribbon that makes physical contact with the back of the sample surface, directly measuring the temperature change that occurs when a bond is formed between an incoming molecule and a model catalyst surface. This direct measurement of heat improved the heat detector sensitivity by an order of magnitude,[24] enabling the

measurement of these irreversible adsorptions under a greater range of experimental conditions. This technique and its instrumentation will be employed in this dissertation to provide new benchmark adsorbate energies and will be discussed in greater detail in **Chapter 2**.

While SCAC is a powerful technique it is also slow, time consuming and expensive. Because of this, it is important to carefully select which experimental systems will provide the greatest value as DFT benchmarks. For the projects discussed in this work, three different model catalyst surfaces were selected – Ni(111), Pt(111) and Cu(111). These metals are all catalytically relevant and are also predicted by DFT to have significantly different bond energies to adsorbates of interest.[25–27] By measuring benchmarks on a wide range of surfaces, DFT can improve the energy accuracy of its models. The (111) surface is chosen here since it is the most thermodynamically stable surface structure of these FCC, consisting of a smooth hexagonally-close packed layer of atoms. The (111) surface is also easily modeled by DFT with periodic boundary conditions.

In addition to the careful selection of the model catalyst surface, the molecular fragments studied were also specifically selected. The simplest examples of the common surface fragments, including hydroxyls, alkoxys, carboxylates, alkyls and carbynes, were selected to produce a broad range of benchmarks. These fragments are formed from the dissociative adsorption of water, methanol, formic acid and methyl iodide. In this work, I will present the results for the adsorption of various species on all three of these model catalyst surfaces, including the first measurement of the heat of adsorption of any molecular fragment to any Cu surface. This provides the first experimental benchmark of a direct measurement of heat of adsorption of a fragment on Cu for comparison to various DFT functionals.

It is also of interest to understand the energetics of liquid solvents used in electrocatalysis and liquid phase catalysis. The Campbell group has developed a method to calculate the adhesion energies of solvent molecules as a liquid to these surfaces using our calorimetrically measured gas-phase heat of adsorption values. The adhesion energy of solvents can be calculated by using low-temperature SCAC measurements out to multilayers of adsorbate coverage, integrating the heats of adsorption above the bulk-like multilayer enthalpy of sublimation, and using several known values from the literature such as surface energy of a liquid. The derivation for this technique is described in detail in **Chapter 5** as well as in several other papers from this group.[28–30] Note that this method was not available when older papers, such as those discussed in **Chapters 3** and **7**, were published. Work by Rumptz et.al.[30] extracts the adhesion energies of 5 solvents on Pt(111) and Ni(111) from work previously published concerning SCAC of small molecules on model catalyst surfaces.

In this work, each chapter will report calorimetrically-measured energetics of a different adsorbate / surface combination. We next explain the motivations for studying each of these systems.

Many important catalytic reactions involving adsorbed methoxy occur on Ni and other transition metal surfaces such as steam reforming reactions, methanol synthesis, and direct alcohol fuel cell reactions.[31–33] **Chapter 3** will detail the energetics of methanol molecularly adsorbed on clean Ni(111) and methanol dissociatively adsorbed on oxygen-precovered Ni(111) to produce adsorbed methoxy and hydroxy.[34]

Formic acid and formate are common intermediates in industrial scale reactions such as methanol synthesis, water-gas shift and steam reforming of methane.[35–38] **Chapter 4** presents the adsorption and adhesion energies of molecular formic acid on clean Cu(111) at 120 K, along

with the adsorption energy of bidentate formate on oxygen-precovered Cu(111) at 240 K.[39] This is also the first measurement of any molecular fragment on any Cu surface.

Acetonitrile is a common electrochemical solvent that possesses a high dielectric constant and an aprotic nature, which make it of great use in electrocatalysis[40–45] as well as in batteries and capacitors.[46–50] **Chapter 5** presents the adsorption and adhesion energies of acetonitrile to Pt(111) at 100 and 180 K.[51] Platinum is a commonly used electrode material, making measuring the energetics of this solvent/metal pair of even greater interest.

The desorption, and subsequently adsorption, energies of smaller linear alkanes ($C_1 - C_6$) have previously been measured via TPD,[52] but larger alkanes do not adsorb reversibly. **Chapter 6** details adsorption and adhesion energies of *n*-decane on Pt(111) at 150 K.[53] The resulting adhesion energy of *n*-decane on Pt(111) is also compared to the adhesion energies of linear alkanes on Pt(111), MgO(100) and C(0001)/Pt(111)[54] to demonstrate trends in adhesion energy versus alkane size.

Azulene and naphthalene are aromatic and antiaromatic molecules that are the simplest models for large, multi-ring conjugated hydrocarbon adsorbates expected to be present on Pt catalysts during hydrocarbon conversion reactions used in petroleum refining. They also serve as simple models for defects in graphene sheets, where naphthalene is used to model defect-free graphene. Additionally, azulene is used as an analog to the common pentagon-heptagon (5-7) defect. The presence of these defects can greatly alter the characteristics of the graphene/metal interface, which in turn influences the chemical and physical properties of the graphene sheet.[55–64] **Chapter 7** reports the adsorption energy of azulene to the Pt(111) surface and compares it to naphthalene,[65] previously measured by the Campbell group in 2006.[66]

Chapter 2 Experimental

Single-Crystal Adsorption Calorimetry (SCAC) is performed in an ultrahigh vacuum (UHV) surface science instrument with a base pressure of $<2 \times 10^{10}$ mbar. The instrument consists of a main chamber comprised of upper and lower sections and a molecular beam. Figure 2.1 shows an exterior view of the entire apparatus. The specific details of this instrument and its operation have previously been described in depth[24,67,68] but this chapter will outline the instrumentation and methods, along with the preparation of the single-crystal samples used.

The upper portion of the main chamber contains instrumentation used to determine the cleanliness of the single-crystal metal's surface and its elemental composition and to ensure the single-crystal maintains a well ordered 111 crystalline surface. It is equipped with X-Ray Photoelectron Spectroscopy (XPS), Auger Electron Spectroscopy (AES), and Low Energy Electron Diffraction (LEED). This upper section also contains the ion gun used for sample cleaning by sputtering with Ar^+ ions.

The lower portion of the main chamber is where SCAC experiment are carried out. Figure 2.2 depicts the inside of the lower chamber. In the center is the single-crystal metal sample, ~1 cm in diameter and 1 μm thick Pt(111), 1 μm thick Ni(111) or 2 μm thick Cu(111) samples, positioned in front of a pulsed molecular beam of 4.36 mm diameter. Behind the sample is the pyroelectric β-polyvinylidene fluoride (PVDF) ribbon heat detector which translates into contact with the back of the sample. This heat detector measures small changes in the sample's temperature (or heat content) from the heat released when a molecular bond is formed on the sample surface to a voltage.[69] To the sides are a quadrupole mass spectrometer (QMS), a gold flag, a quartz-crystal microbalance (QCM), and a resistive heater that anneals the sample via thermal radiation.

The molecular beam contains a heated glass capillary array (GCA) to ensure a Boltzmann distribution of temperature for the incoming molecules and a series of liquid nitrogen cooled orifices that collimate the molecules and produce a consistent spot size with an effective beam diameter of 4.36 mm. At the beginning of the molecular beam is either a glass bulb that holds the molecule of interest that can be cooled to ~ -2 deg C with a salt-ice-water bath, or a metal tube that can be heated to increase the vapor pressure of a solid molecule using heat tape, depending on the molecule being studied. A chopper at the end of the molecular beam creates pulses 102 ms in length with a 3 or 5 second repeat period. Around the apparatus are three rough (mechanical) pumps, three turbo pumps and a titanium sublimation pump that maintain the UHV state of the chamber.

The thin single crystal samples are purchased from Jacques Chevallier and Bine Hansen at the Thin Film Laboratory at Aarhus University in Denmark. They arrive as grown, on NaCl blocks, with the metal's (111) side facing (epitaxial to) the block surface. The salt on the crystals is gently washed away by dripping deionized water over the salt surface. During this cleaning the crystal is placed atop a tantalum disc with a circular hole in its center, and once clean a second tantalum disc is set on the exposed (111) surface. Once the sample is dry, these two rings are spot welded together, leaving a thin sheet of (111) metal suspended in the center with ~ 1 cm diameter of exposed surface area. The heat detector ribbon will press into the back of this sheet while the (111) front will be exposed to the flux of the molecular beam. This completed sample is placed in a copper sample holder, and set in the middle of the lower chamber (see Figure 2.2). Repeated cycles of Ar^+ ion sputtering and annealing clean the sample surface of any contaminants and create the desired (111) surface crystallinity.

SCAC experiments can be carried out with the sample held at any constant temperature desired between 100 and 350 K.[24] The sample holder is positioned on top of a large copper block which serves as a temperature reservoir. To perform experiments at low temperatures, nitrogen gas is cooled with liquid nitrogen outside of the chamber and circulated through the reservoir. the flow rate of the gas controls the temperature. A hot water bath can instead be used for experiments above room temperature. The internal reservoir is also connected to the pyroelectric detector with thick copper braids to simultaneously cool the heat detector. Thermocouples are attached to the heat detector and to the copper reservoir to monitor the temperature. The temperature of the sample is recorded as the average of these two temperatures. Experiments are only performed when the difference between the two temperatures is less than 10 K.

The heat detector is calibrated by using a diffuse, intensity-stabilized HeNe laser (632.8 nm) shined through the molecular beam's beam-defining orifice column while the chopper is open. This guarantees that the molecular beam and the laser will have the same spot size and location. A mirror is used to reflect the laser out of a port window where the intensity can be measured with an optical power meter to determine the absolute power of the laser. The intensity of the laser can be adjusted with a set of filters. The heat from a series of laser pulses on the single-crystal surface is measured and this heat signal is compared to that of the signal produced from the pulsed molecular beam. The response signal of the PVDF ribbon at any time scales linearly with energy absorbed by the metal, even at cryogenic temperatures, so the energy released from the surface reaction is simple to calculate.

Short-term and long-term sticking probabilities are concurrently measured with the heat of adsorption using a quadrupole mass spectrometer (QMS). "Long-term sticking" is defined as the probability that a gas molecule adsorbs to the surface and stays adsorbed until the next pulse

3 (or 5) seconds later. “Short-term sticking probability” is the probability that the gas molecule stays adsorbed only for the 102 ms window in which heat measurement occurs. The QMS detects any molecules that either do not adsorb to the sample or desorb from the sample surface after transient adsorption. The QMS signal for the entire 3 (or 5) second pulse repeat period is used to calculate the long-term sticking probability, which determines the coverage on the surface after each pulse. The signal obtained during the pulse is used to calculate the short-term sticking and determines what percentage of molecules in each pulse contribute to the heat measurement. A zero-sticking measurement is needed to convert the QMS signal to a sticking probability. This is done by translating a room-temperature gold flag in front of the sample. The molecules selected for our SCAC have very minimal adsorption onto gold at room temperature. Therefore after several pulses to saturate the gold surface, all incoming molecules leave the gold surface quickly, allowing QMS to measure all molecules in the pulse. This signal represents a sticking probability of zero. A sticking probability of one indicates all the molecules adsorbed and stayed adsorbed to the sample, meaning there is no mass spec signal. The QMS signal scales linearly between a probability of one and zero, allowing the sticking to be calculated.[70]

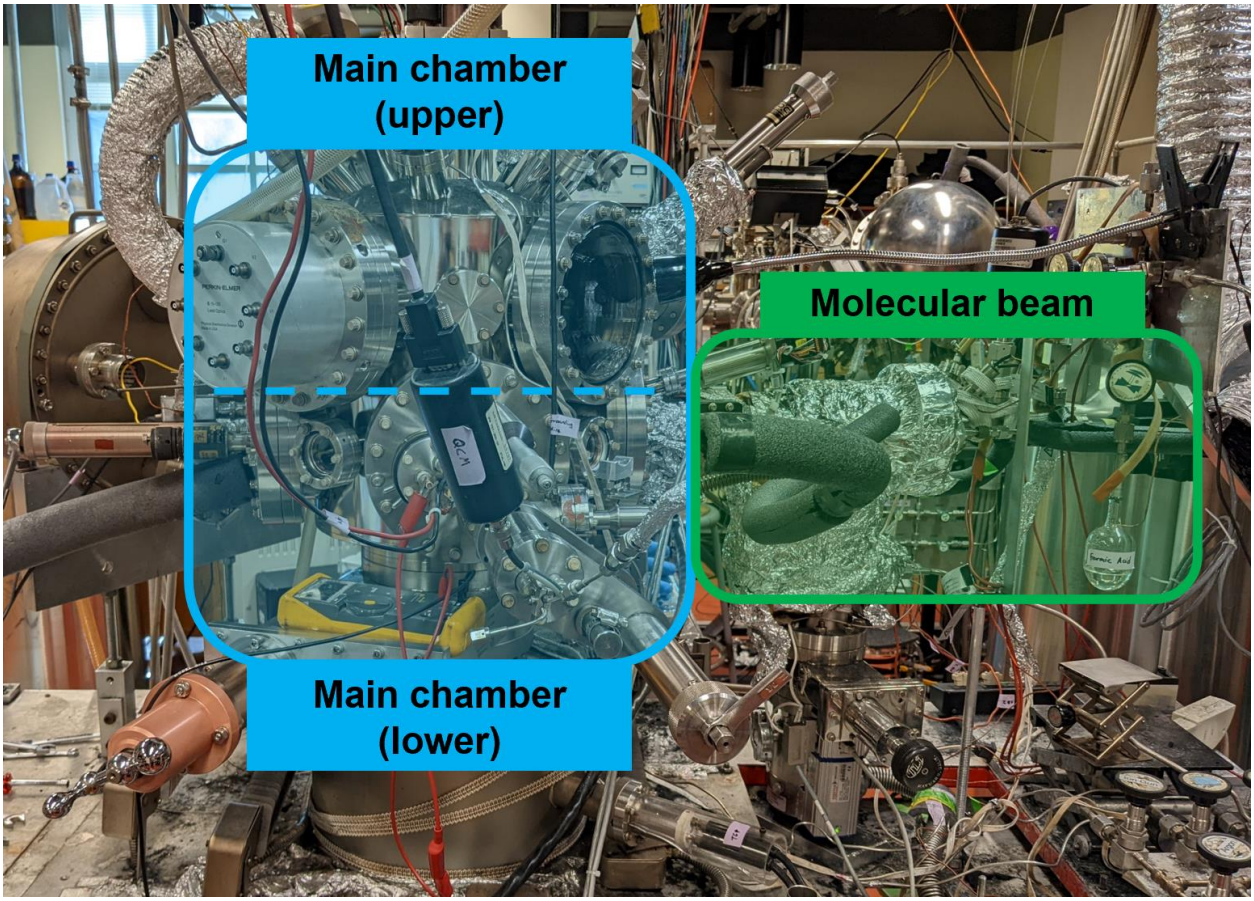

Figure 2.1 – External view of the Single-Crytal Adsorption Calorimeter, with main chamber sections and molecular beam highlighted.

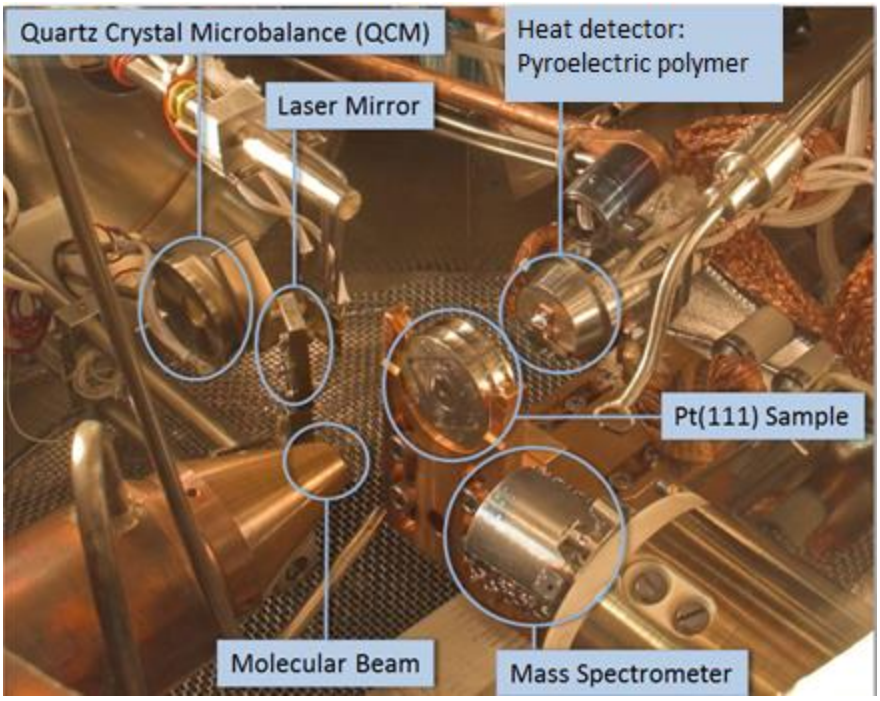

Figure 2.2 - An internal view of the Single-Crystal Adsorption Calorimeter. Molecular beam outlet, laser mirror, quartz crystal microbalance (QCM), heat detector, single-crystal sample and mass spectrometer are labeled.

Chapter 3 Energetics of Adsorbed Methanol and Methoxy on Ni(111): Comparison to Pt(111)

This chapter reprinted with permissions from Ref 34:

Carey, S.J., Zhao, W., Harman, S. E., Baumann, A.-K., Mao, Z., Zhang W., & Campbell, C. T. Energetics of Adsorbed Methanol and Methoxy on Ni (111) : Comparisons to Pt (111). *ACS Catalysis* **8** 10089-10095 (2018).

Chapter Abstract

The heats of adsorption of methanol molecularly adsorbed on clean Ni(111) and dissociatively adsorbed on oxygen-precovered Ni(111) were measured by single-crystal adsorption calorimetry (SCAC). The dissociative adsorption of methanol on oxygen-precovered Ni(111) produces adsorbed methoxy and hydroxyl, resulting in an integral heat of adsorption of -70. kJ/mol at a coverage of 0.25 ML. From this, the heat of formation of this adsorbed methoxy and the dissociation enthalpy of its bond to Ni(111) are estimated to be -233 and 250. kJ/mol, respectively. Analyzing previously measured bond enthalpies of monodentate formate and hydroxyl to Ni(111), we find a linear trend with a slope of 1 between the bond enthalpies of oxygenates to the Ni(111) surface and their corresponding gas-phase hydrogen-ligand bond dissociation enthalpies, similar to the trend for Pt(111) but ~69 kJ/mol stronger. We also compare our experimentally measured energetics for adsorbed methanol and adsorbed methoxy with density functional theory (DFT) calculations with periodic boundary conditions from previous literature. These energetic values and trends help clarify selectivity, reaction rate, and activity differences between metal surfaces in reactions involving adsorbed oxygenates.

3.1 Introduction

Surface methoxy is a key intermediate in many important catalytic reactions on Ni and other transition metal surfaces, such as steam reforming reactions, methanol synthesis, and direct alcohol fuel cell reactions. Critical catalytic properties, such as the activity, reaction rate, and selectivity, are determined by the energetics of adsorbed intermediates, and they are therefore important to know accurately. The adsorption and decomposition reactions of methanol on Ni(111) have been studied previously.[71–80] However, little is known about the energetics of adsorbed methanol and methoxy on this or any other Ni surfaces. So far, the heat of formation and bond enthalpy of adsorbed methoxy have been measured on only one metal surface, Pt(111), using single-crystal adsorption calorimetry (SCAC) by this group.[81] Here, we report the first calorimetric measurements of the energetics of adsorbed methanol and methoxy on the Ni(111) surface. These energetics are compared to adsorbed methoxy on Pt(111), helping clarify the different catalytic activities for these two transition metals in catalytic reactions involving methoxy intermediates. These experimental results also provide valuable benchmarks for validating the energy accuracy of density functional theory (DFT) methods.

In addition, we compare here the energetics of adsorbed hydroxyl and formate on Ni(111), reported by our group previously,[82,83] with the measurement of adsorbed methoxy here, and find the bond dissociation enthalpies of these three adsorbed oxygenates (hydroxyl, formate, and methoxy) to Ni(111) linearly track their corresponding gas-phase hydrogen–ligand bond dissociation enthalpies with a slope of 1. The same trend with unit slope was also discovered for these same three oxygenates on Pt(111) by this group previously.[84] The difference is that these three oxygenates bind to Ni(111) ~69 kJ/mol more strongly than Pt(111). These findings thus

provide a semiempirical method to predict the bond enthalpies and heats of formation of adsorbed oxygenates on these metal surfaces.

Previous studies have found that methanol adsorbs molecularly on Ni(111) below approximately 140 K.[75,80] Adsorbed methoxy has been observed on Ni(111) after dosing high coverages (possibly multilayers) of methanol at temperatures lower than 140 K and subsequently heating to 160–240 K.[73–75,78–80] Although not known from the literature, we show below that when methanol is dosed to Ni(111) precovered with oxygen adatoms, it dissociates to produce adsorbed methoxy plus −OH in the temperature range 100–190 K. This is based on the similarities of heats of reaction and sticking probabilities versus oxygen coverage to prior results for Pt(111), where this reaction is known to occur at similar temperatures.[82]

3.2 Experimental Section

Experiments were performed in a UHV chamber (base pressure $< 2 \times 10^{-10}$ mbar) designed for SCAC. It is equipped with X-ray photoelectron spectroscopy (XPS), Auger electron spectroscopy (AES), low-energy ion scattering spectroscopy (LEIS), and low-energy electron diffraction (LEED). The apparatus and procedures for SCAC have been described in extensive detail previously.[24,68,85] To summarize, the Ni(111) samples used in these experiments are 1 μm thick single-crystal foils and were provided by Jacques Chevallier at Aarhus University. The surface was cleaned by cycles of Ar^+ ion sputtering and annealing to 1120 K. The atomic oxygen-precovered surface was prepared by exposing the clean Ni(111) surface to O_2 at cryogenic temperatures (100–190 K) as described in the literature.[86–88] The heats of adsorption and sticking probability were measured simultaneously as a pulsed molecular beam of methanol was dosed onto the Ni surface. The molecular beam was created by expanding ∼2 mbar of

methanol through a glass capillary array and collimated through a series of five orifices that are cooled with liquid nitrogen, and then chopped into 102 ms pulses. The heats were measured with a pyroelectric ribbon gently pressed on the backside of the Ni crystal. The short-term and long-term sticking probabilities were measured with a quadrupole mass spectrometer (QMS) using the King and Wells method.[70]

In this Article, we report coverages in monolayers (ML), which are defined as the number of methanol molecules that adsorb to the surface irreversibly, normalized by the number of nickel surface atoms in the Ni(111) surface (1.86×10^{15} Ni atoms/cm^2). A typical molecular beam flux gives ~0.015 ML per pulse (~4.2×10^{12} molecules/pulse).

3.3 Results

3.3.1 Heat of Molecular Adsorption on Clean Ni(111)

In this Article, we define the term heat of adsorption as the negative of the differential standard molar enthalpy change for the adsorption reaction, $-\Delta H_{ad}$, with the gas and the metal surface being at the same temperature as the metal surface. ("Standard" here implies only that the gas is at 1 bar as a pure ideal gas.) As described previously, this requires a small enthalpy correction on the measured heat because the gas molecule's enthalpy at this temperature is slightly different from the actual experimental molecular beam conditions.[18]

According to the literature,[72,75] methanol molecularly adsorbs on Ni(111) below 160 K and forms multilayers below 140 K. Figure 3.1 shows the heat of adsorption of methanol on Ni(111) at 100 K. Initially, methanol adsorbs molecularly with a heat of adsorption of 63.2 ± 0.8 kJ/mol in the limit of low coverage. As coverage increases to 0.4 ML, the heat of adsorption decreases in two linear segments. For the first 0.3 ML, the heat of adsorption is well described by

a best fit line (63.2–23.9 θ) kJ/mol, where θ is coverage, in monolayers, yielding an average heat of 59.6 kJ/mol. The average (or integral) heat of adsorption up to 1/4 ML is 60.2 kJ/mol. Combined with the standard heat of formation of methanol gas of −202 kJ/mol,[89] this gives the standard heat of formation of adsorbed methanol on Ni(111) to be −262 kJ/mol. After 0.30 ML and up to 0.4 ML, the heats of adsorption decrease much more rapidly and are well described by the best-fit line (99.3–142.7 θ) kJ/mol. The sticking probability of methanol is always close to unity at all methanol coverages at 100 K; see Figure 3.6.

These changes in the heat of adsorption could be the result of a model suggested by scanning tunneling microscopy (STM) and DFT studies of methanol on Cu(111), Au(111), and Pt(111).[90–92] On these surfaces at cryogenic temperatures, the methanol molecules bind to the surface through their oxygen atom but with the methyl group near the surface, forming hydrogen bonds with their neighbors. This results in clusters of hydrogen-bonded hexamers at low coverages and long hydrogen-bonded chains at higher coverages with the methyl groups pointing outward. One STM study found that these methanol chains get closer to one another as coverage increases.[90] The decrease in heat with coverage in Figure 3.1 may be due to dipole–dipole and steric repulsions between chains and hexamers as they are forced closer together.

At coverages greater than 0.4 ML, the heat of adsorption becomes nearly constant, implying that additional methanol adsorbs on top of methanol adsorbates, forming multilayers. Above 1.0 ML, the multilayer adsorption energy is 44.0 ± 0.6 kJ/mol. This value is in agreement with the heat of sublimation of bulk methanol (solid) at 100 K, 45.3 kJ/mol, calculated from bulk thermodynamic data,[93,94] and with results from a detailed TPD study of multilayer methanol on Au(111) that employed leading edge analysis to determine a sublimation enthalpy of 42.1–44.6 kJ/mol[95] (after correction using bulk solid and gas-phase heat capacities from 150 to 100 K).

Previous literature reported that exposing a clean Ni(111) surface to a high coverage of methanol at a temperature lower than 140 K and subsequent heating to 180–240 K leads to adsorbed methoxy and hydrogen.[75,80] Amemiya and co-workers determined that methoxy could also be produced on Ni(111) by directly dosing methanol at 200 K.[80] Thus, we performed SCAC experiments of methanol adsorption on clean Ni(111) at temperatures ranging from 180–300 K in hopes to produce adsorbed methoxy. However, we observed an initial heat of adsorption that was very similar to that for molecular adsorption of methanol on Ni(111) at 100 K (~63 kJ/mol) and a maximum surface coverage of adsorbed methanol (regardless the products on surface) of ≤0.04 ML at 180–300 K. It indicates that methanol transiently adsorbs on Ni(111) at these temperatures, but then desorbs again before the next methanol pulse. Thus, we were unable to dissociate the methanol on clean Ni(111). In at least some of the prior studies mentioned above, it was possible that photon or electron beam damage (e.g., from X-rays in XPS or electrons from mass spectrometer filaments) may have facilitated dissociation.

3.3.2 Heat of Dissociative Adsorption of Methanol on Oxygen-Predosed Pt(111)

After predosing the Ni(111) surface with oxygen adatoms (by the dissociative adsorption of O_2 gas), the heat of adsorption of methanol at temperatures from 100 to 190 K is considerably higher than the heat of molecular adsorption (~25 kJ/mol higher initially), and the resulting coverage of permanently adsorbed methanol is much higher. According to the studies of methanol dissociatively adsorbing on O-precovered Pt(111)[81] and water dissociatively adsorbed on O-precovered Ni(111),[82] we thus conclude that reaction 3.1 occurs to produce adsorbed methoxy and hydroxyl, as

$$CH_3OH_g + O_{ad} \rightarrow CH_3O_{ad} + OH_{ad} \qquad (3.1)$$

Figure 3.2 shows the heat of adsorption of methanol on oxygen-precovered Ni(111) at 100 K with 0.25 ML of O_{ad} (red squares) and a low coverage of O_{ad} (black triangles). The heat of adsorption of molecular methanol on clean Ni(111) at 100 K is also reproduced from Figure 3.1 (blue circles), for comparison. When the Ni(111) surface is covered with 0.25 ML of O_{ad}, a significantly higher heat of adsorption is observed, ~88 kJ/mol in the limit of low coverage. This heat then decreases linearly with increasing coverage of adsorbed methanol. After ~0.25 ML, the heat of adsorption is the same as that of methanol molecularly adsorbed on clean, O-free Ni(111), suggesting that methanol molecularly adsorbs from 0.25 ML until saturation at ~0.3 ML. In the case of the low coverage of O_{ad}, the heat of adsorption of methanol starts high, close to the curve for 0.25 ML O_{ad}, and more quickly decreases to the same heat as that of molecular adsorption on O-free Ni(111) (the blue curve) at ~0.1 ML. This shows that the coverage dependence of the heats of adsorption of methanol on O-precovered Ni(111) significantly depends on the precoverage of O adatoms, again implying that methanol reacts with O adatoms to form adsorbed methoxy and hydroxyl until all of the O_{ad} is consumed. This same reaction was observed on Pt(111) with similar heats.[81]

The heats of adsorption observed at low coverage on the 0.25 ML O_{ad} surface are much higher than what would be expected for simple molecular adsorption. On both Pt(111) and Ni(111), water molecularly coadsorbed with oxygen adatoms releases only ~3 kJ/mol more heat as compared to the molecular adsorption of water on clean surfaces.[82,96] We would expect a similar marginal change in heat if methanol molecularly coadsorbed with O_{ad}. In contrast, here the heat is ~25 kJ/mol higher for methanol adsorbed on the O-precovered surface at the limit of low coverage as compared to the clean Ni(111), which indicates dissociative adsorption on O-precovered Ni(111). We attribute this much higher heat to methanol reacting with O_{ad} to form

adsorbed methoxy and hydroxyl following reaction 3.1. This reaction has also been unambiguously observed on O-precovered Pt(111).[81,97] We expect reaction 3.1 to proceed until all oxygen is titrated off the surface, after which methanol continues to adsorb molecularly and releases the same heat as on clean Ni(111). For the 0.25 ML O_{ad} precovered surface, this reaction completes at ~0.25 ML as expected; for the low coverage experiments, this higher-heat reaction completes at ~0.1 ML(Figure 3.2). We are unsure of the structure of the molecularly adsorbed methanol that populates after all 0.25 ML of the O_{ad} is consumed by reaction 3.1, but its heat quickly drops to that for multilayer methanol by 0.4 ML. It is not clear why the coverage dependence of the heat in this range from 0.25 to 0.4 ML is so similar to that without 0.25 ML of predosed oxygen adatoms.

Figure 3.3 shows the more direct comparison for methanol adsorbed on Ni(111) and Pt(111), dissociatively and molecularly. The red curves show SCAC results of methanol on both Ni(111) and Pt(111) predosed with 0.25 ML O_{ad}, and the blue curves show SCAC results of methanol on clean Ni(111) and Pt(111). The two curves shown for Pt(111) were published previously[81] and reproduced here for comparison. On Pt(111), a reaction scheme identical to that proposed here for Ni(111) is known to occur.[81] On clean Ni(111) at 155 K and clean Pt(111) at 150 K, methanol adsorbs molecularly and only forms a single layer, and the heats are consistent with the adsorption on clean surfaces at 100 K.[72,97] For the 0.25 ML O-precovered surfaces, methanol reacts with O_{ad} forming adsorbed methoxy and hydroxyl until the 0.25 ML of O_{ad} is titrated. After that, methanol continues to adsorb molecularly until the saturation coverage for that temperature is reached, releasing the same heat as observed on the clean surfaces at the same coverages. On the O-precovered surface on Ni(111), the heat of adsorption is initially 87 kJ/mol at the limit of low coverage. It decreases linearly until ~0.25 ML and is well described by the

linear fit (85.1–117.2 θ) kJ/mol. The vertical dashed line at 0.25 ML marks the expected coverage of O_{ad} and represents the point where reaction 3.1 completes. After this vertical dashed line, it is clearly observed that the heat of adsorption of methanol on the oxygen-precovered surface has decreased to be the same as that on clean Ni(111) at higher coverages. Methanol saturates at ~0.3 ML (see Figure 3.6 for related sticking probability data) for the single layer of adsorbates on Ni(111) at 155 K, smaller than Pt(111) at 150 K (~0.33 ML),[81] which is expected due to Pt(111) having a larger lattice parameter and 19% smaller density of surface atoms than Ni(111).

Further evidence for the formation of methoxy is shown in Figure 3.7, which shows the SCAC results for methanol adsorption onto O-precovered Ni(111) at 190 K. Here, we observe the same heats as the O-precovered Ni(111) surface at 100 and 155 K, but a lower final coverage of ~0.16 ML, due to a lower predosed coverage of O_{ad} (see also Figure 3.6).

3.4 Discussion

3.4.1 Energetics of Adsorbed Methoxy

From the heats of adsorption measured in this work by calorimetry and the available literature values for the heats of formation of adsorbed and gas-phase species, we may extract the heat of formation of methoxy on Ni(111) and its bond enthalpy to this surface. We attribute the integral heat of adsorption from 0–0.25 ML on the 0.25 ML oxygen-precovered Ni(111) surface at 155 K (Figure 3.3) of −70. kJ/mol to the heat of reaction 3.1. Figure 3.4 shows the thermodynamic cycle, which uses this integral heat to extract the heat of formation of adsorbed methoxy and the CH_3O–Ni(111) bond dissociation enthalpy, $D(CH_3O–Ni(111))$.

This thermodynamic cycle starts on the left-hand side with all atoms in their standard state, which therefore possesses an enthalpy of formation of 0 kJ/mol. Following the bottom path shows the formation of gaseous methanol and an adsorbed oxygen atom, which possess enthalpies of formation of −202 and −240. kJ/mol, respectively.[18,89] The bottom path then tracks the dissociative adsorption of methanol to make adsorbed methoxy plus adsorbed hydroxyl, the enthalpy of which we measured with calorimetry (−70. kJ/mol). This is an exothermic process and the enthalpy of reaction is a negative value, while the values shown in Figure 3.3 are the heats of adsorption, which, by convention, are shown as positive values. Combining the heats of formation and measured reaction enthalpy of the bottom path results in the total heat of formation of coadsorbed methoxy and hydroxyl, both at 0.25 ML coverage, a value of −512 kJ/mol.

The middle path in the thermodynamic cycle (Figure 3.4) shows this enthalpy change of converting all atoms in their standard states directly to coadsorbed methoxy and hydroxyl. Therefore, the sum of their enthalpies of formation must be equal to the total heat of formation (−512 kJ/mol). The enthalpy of formation of hydroxyl at 0.25 ML on Ni(111) was previously measured to be −279 kJ/mol.[82] Subtracting this enthalpy of formation of adsorbed hydroxyl from the total enthalpy of formation results in the enthalpy of formation of adsorbed methoxy at 0.25 ML coverage: −233 kJ/mol.

Following the top pathway on this thermodynamic cycle (Figure 3.4) shows the method to extract the bond enthalpy of methoxy to Ni(111). This top route starts by converting the standard state elements to a gaseous methoxy radical and an adsorbed hydroxyl, which possess an enthalpy of formation of +17 and −279 kJ/mol, respectively.[82,98] These two species have a total enthalpy of formation of −262 kJ/mol. The difference in enthalpies between these two

species and our final state on the far right is negative of the adiabatic CH_3O–Ni(111) bond dissociation enthalpy. Therefore, +250. kJ/mol is the enthalpy for breaking the CH_3O–Ni(111) bond at 0.25 ML coverage (when coadsorbed with 0.25 ML of hydroxyl).

3.4.2 Comparison to DFT Calculations

The bond energy of molecular methanol and methoxy to Ni(111) measured here may be compared to theoretical calculations. Table 3.1 compares computational values obtained by various DFT methods to the experimental values of this work. DFT calculations report integral bond energies of adsorbates at specific coverages. To calculate the bond energy of molecular methanol at a specific coverage, the best-fit line of the measured differential heats of methanol adsorption versus coverage from 0 to 0.30 ML at 100 K (Figure 3.1) was integrated up to the desired coverage. These integral heats (enthalpies) were then converted to bond energies by subtracting *RT*. The calorimetric bond enthalpies for methoxy at the different coverages in Table 3.1 were calculated from thermodynamic cycles similar to that in Figure 3.4 discussed above, but by integrating to different coverages to calculate the integral heat of reaction at that coverage, using the reported heat of formation of adsorbed hydroxyl at that coverage.[82] Again, bond enthalpies were converted to bond energies by subtracting *RT*.

For molecular methanol, all reported DFT calculations significantly underestimated the bond energy measured in this work. The weaker bond strength found in these DFT studies than by calorimetry could be due to methanol forming hydrogen-bonded structures, similar to what has been observed in Cu(111) and Au(111).[90,91] These intermolecular hydrogen bonds may not be properly accounted for as these chains would have significantly larger unit cells than what was used in these calculations. These underestimations in bond energy could also be due to

underestimating the magnitude of van der Waals and dipole interactions between the adsorbate and the surface. For adsorbed methoxy, PW-91 and PBE perform well, differing from the experimentally determined value by only 0–14 kJ/mol. However, RPBE underestimates the bond energy by 69 kJ/mol. This RPBE paper only reported their calculated results on top sites.[99] Their value of 180 kJ/mol is close to the reported energies of methoxy bound to top sites by another DFT functional, PW-91 (175 kJ/mol).[100]

3.4.3 Comparison to Pt(111)

Previous work[81] from this research group studied the adsorption of methanol and methoxy on Pt(111), allowing for a direct comparison between the two metal surfaces. These values are adjusted slightly (by a value of RT_{source}) from the literature to account for a systematic error as discussed elsewhere.[18] Methoxy on Pt(111) at 0.25 ML coverage coadsorbed with 0.25 ML of hydroxyl has a heat of formation of −168 kJ/mol (as compared to −233 kJ/mol on Ni(111) under the same conditions) and a bond enthalpy of −185 kJ/mol (as compared to −250. kJ/mol on Ni(111) under the same conditions). These much larger values on Ni(111) are to be expected as it is well-known that Ni is more oxophillic than Pt, so that Ni–O bonds should be stronger.

It is interesting to consider how these energetic differences between Ni and Pt manifest themselves in catalysis. Let us consider a simple reaction involving C–O bond cleavage:

$$CH_3O_{ad} \rightarrow CH_{3,ad} + O_{ad} \qquad (3.2)$$

Using the published heats of formation of $CH_{3,ad} + O_{ad}$ of −71 kJ/mol[104] and −240. kJ/mol,[18] respectively, together with the heat of formation of CH_3O_{ad} on Ni(111) of −233 kJ/mol found above gives a highly exothermic enthalpy for reaction 3.2 of −78 kJ/mol on Ni(111). In contrast, the heats of formation of these three species on Pt (111) of −168 kJ/mol for methoxy,[81] −99

kJ/mol for O_{ad},[105] and −50. kJ/mol for methyl[106] give an endothermic enthalpy for reaction 3.2 of +19 kJ/mol. Clearly, such simple C–O bond-cleavage reactions that produce O adatoms are much more exothermic (by almost 100 kJ/mol) on Ni than Pt catalysts, and thus should be much faster and have much larger equilibrium constants on Ni catalysts. Similarly, C–O bond forming reactions (like the reverse of reaction 3.2) should be much more facile on Pt than Ni catalysts. In contrast, C–O bond cleavage reactions that involve oxygen transfer to another surface fragment rather than to produce O_{ad} should be similar on Ni and Pt catalysts, as seen for the simple reaction:

$$CH_3O_{ad} + H_{ad} \rightarrow CH_{3,ad} + OH_{ad} \qquad (3.3)$$

The enthalpy for reaction 3.3 is −69 kJ/mol on Ni(111) and quite similar, −54 kJ/mol, on Pt(111). (The heat of formation of H_{ad} is −47 kJ/mol on Ni(111)[18] and −36 kJ/mol on Pt(111).[18] The heat of formation of OH_{ad} is −278 kJ/mol on Ni(111)[82] and −208 kJ/mol on Pt(111).[18,107])

3.4.4 Trends in Bond Enthalpies of Adsorbed Oxygenates

It has previously been shown that the ligand–metal σ-bond strengths found in organometallic complexes in liquid solutions strongly correlate with the corresponding gas-phase ligand–hydrogen bond strength.[108–110] Previously this research group found that this trend is also true for ligands (i.e., molecular fragments) bound to Pt(111).[84] Specifically, the adiabatic bond dissociation enthalpies of oxygenate adsorbates to Pt(111) (monodentate formate, hydroxyl, and methoxy) vary linearly with a slope of 1 with the corresponding gas-phase RO–H σ bond enthalpy but offset by −251 kJ/mol. Analyzing the bond enthalpy of methoxy measured in this work and the bond enthalpies of formate and hydroxyl measured previously[82,83] on Ni(111), we find this same trend, as shown in Figure 3.5, which shows the adiabatic bond dissociation

enthalpies of three oxygenate adsorbates, which we refer to here as "ligands" (or L), on both Ni(111) and Pt(111) versus their corresponding gas-phase hydrogen–ligand bond dissociation enthalpies. The data points and trendline for Pt(111) are recreated here from the literature[84] and adjusted slightly to account for systematic error equal to RT_{source}, as discussed elsewhere.[18] A linear trend with a slope of 1 ($y = x$ – 182 kJ/mol) is shown on Figure 3.5 to fit the data points for Ni(111) very well and possesses a standard deviation of 4.7 kJ/mol. The best-fit line of variable slope ($y = 1.05x$ – 207 kJ/mol) fits only slightly better, with a standard deviation of 4.6 kJ/mol. The strength of σ-bonds of adsorbed oxygen-bound molecular fragments to Ni(111) varies linearly with the strength of binding of those same fragments to H atoms in gas-phase molecules with a slope of 1.00, but offset by −182 kJ/mol. It is weaker than binding to a H atom, but ∼69 kJ/mol stronger than binding to Pt(111), which makes sense because Ni is known to be more oxophillic than Pt. Therefore, we are able to predict the bond enthalpies of other oxygen-bound molecular fragments to Ni or Pt through these trend lines. This will probably fail for larger adsorbates, because these will have strong van der Waals attractions to the surface as well, which are not accounted for in the trends in Figure 3.5. Given that these trends of Figure 3.5 hold for both Pt(111) and Ni(111), we expect that the bond enthalpies of small adsorbed oxygenates to other transition metal surfaces will follow a similar trend with a slope near 1.

3.5 Conclusions

The energetics of the molecular and dissociative adsorption of methanol on Ni(111) were measured by SCAC. At 100 K, the heat of adsorption is well fit by the curve (63.2–23.9 θ) kJ/mol from 0–0.30 ML and (99.3–142.7 θ) kJ/mol from 0.30–0.40 ML. The dissociative adsorption of methanol on O-precovered Ni(111) produces adsorbed methoxy and hydroxyl and

gives an integral heat of adsorption at 155 K of −70. kJ/mol at a coverage of 0.25 ML (of both products). This gives a heat of formation for adsorbed methoxy of −233 kJ/mol and a bond enthalpy of 250. kJ/mol. We find a linear trend with a slope of 1 between the bond enthalpies of small oxygenates to Ni(111) and Pt(111) and their corresponding gas-phase hydrogen–ligand bond dissociation enthalpies. These values and trends improve our ability to understand the selectivity, reaction rate, and activity differences between metal surfaces in reactions involving adsorbed oxygenates.

Acknowledgements

We acknowledge support for this work by the National Science Foundation under Grant no. CHE-1665077. We would like to thank Gregory Arps for his assistance in the laboratory.

3.6 Figures and Tables

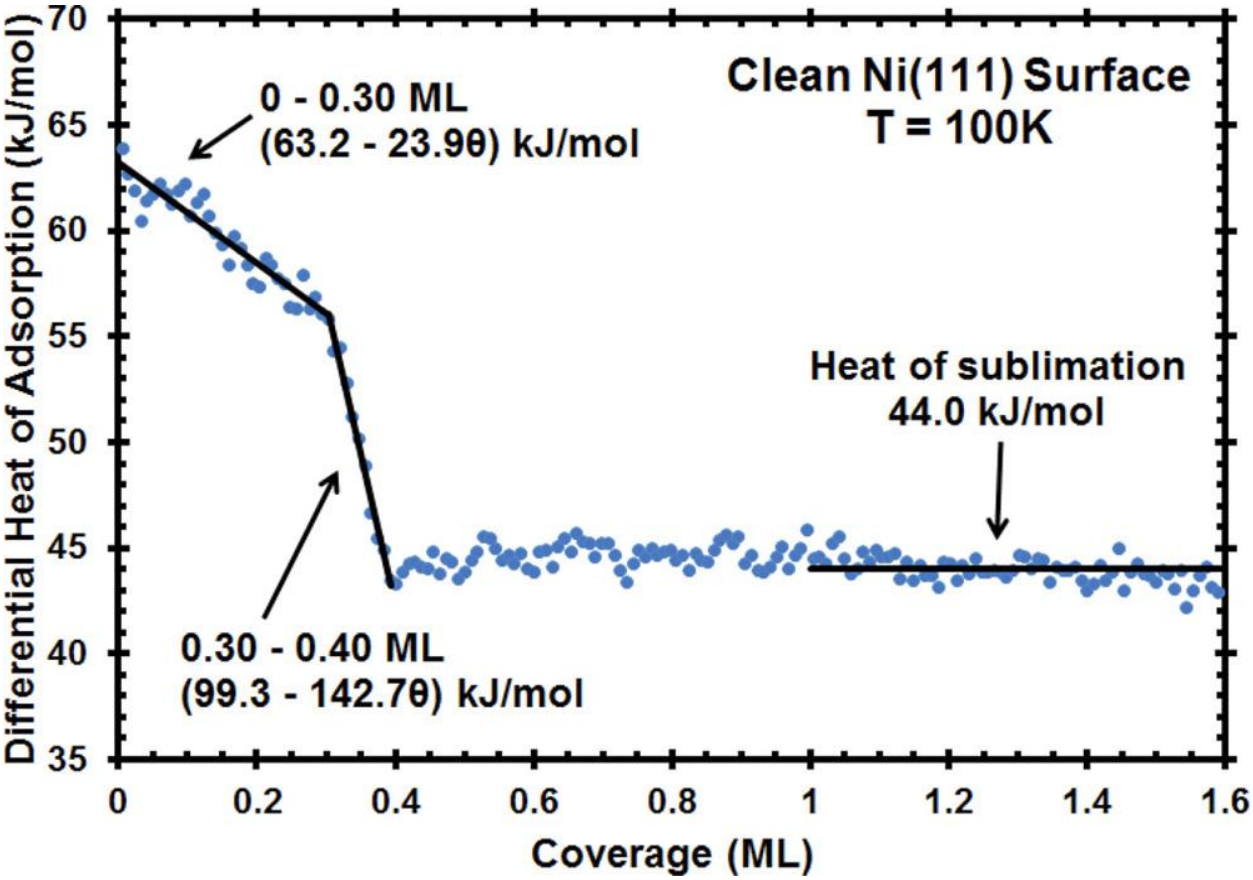

Figure 3.1 – Differential heat of adsorption of methanol on the clean Ni(111) surface as a function of methanol coverage at 100 K.

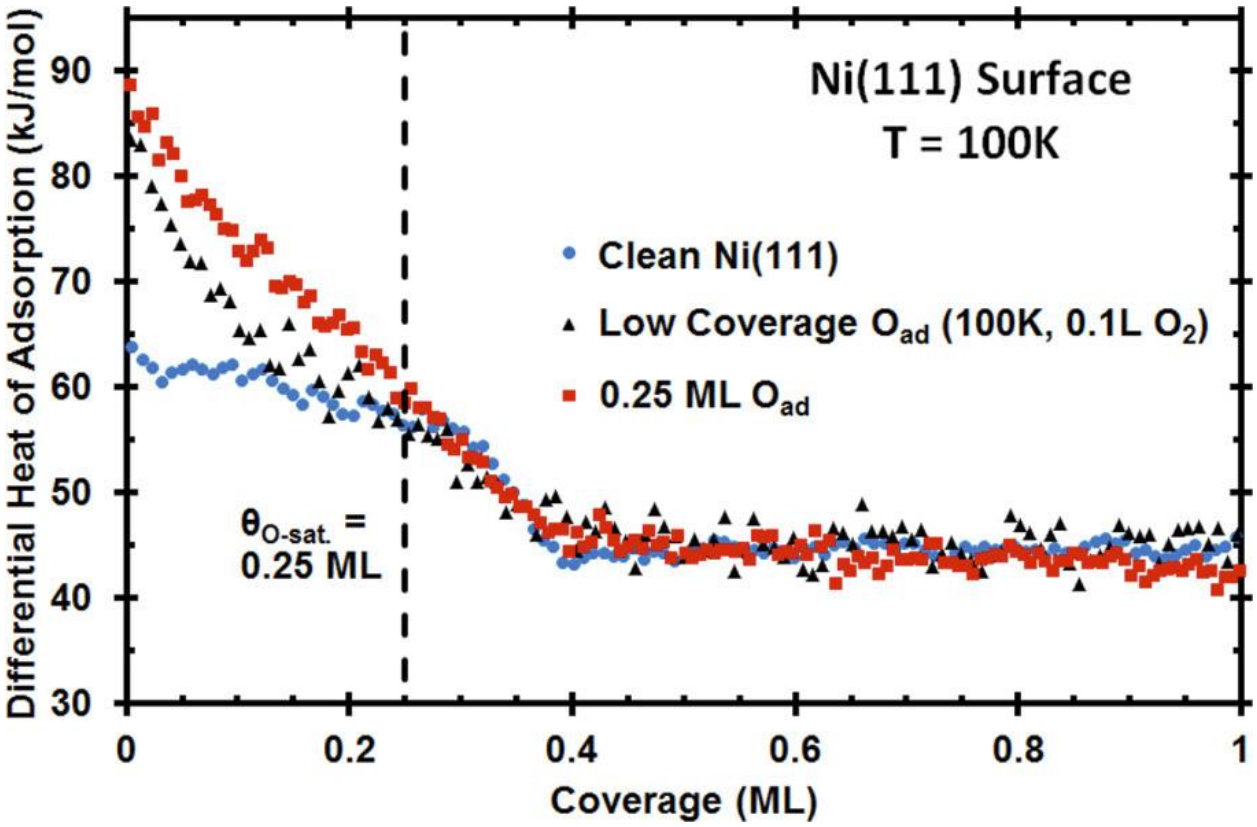

Figure 3.2 – Differential heat of adsorption of methanol on Ni(111) at 100 K versus total methanol coverage. Each curve represents a different coverage of predosed oxygen adatoms on the surface, including the clean, O-free surface, a low coverage of O_{ad}, and 0.25 ML of O_{ad}. The vertical dashed line at 0.25 ML is where the reaction of methanol with O_{ad} to produce CH_3O_{ad} + OH_{ad} is expected to finish for this highest predose of O_{ad}.

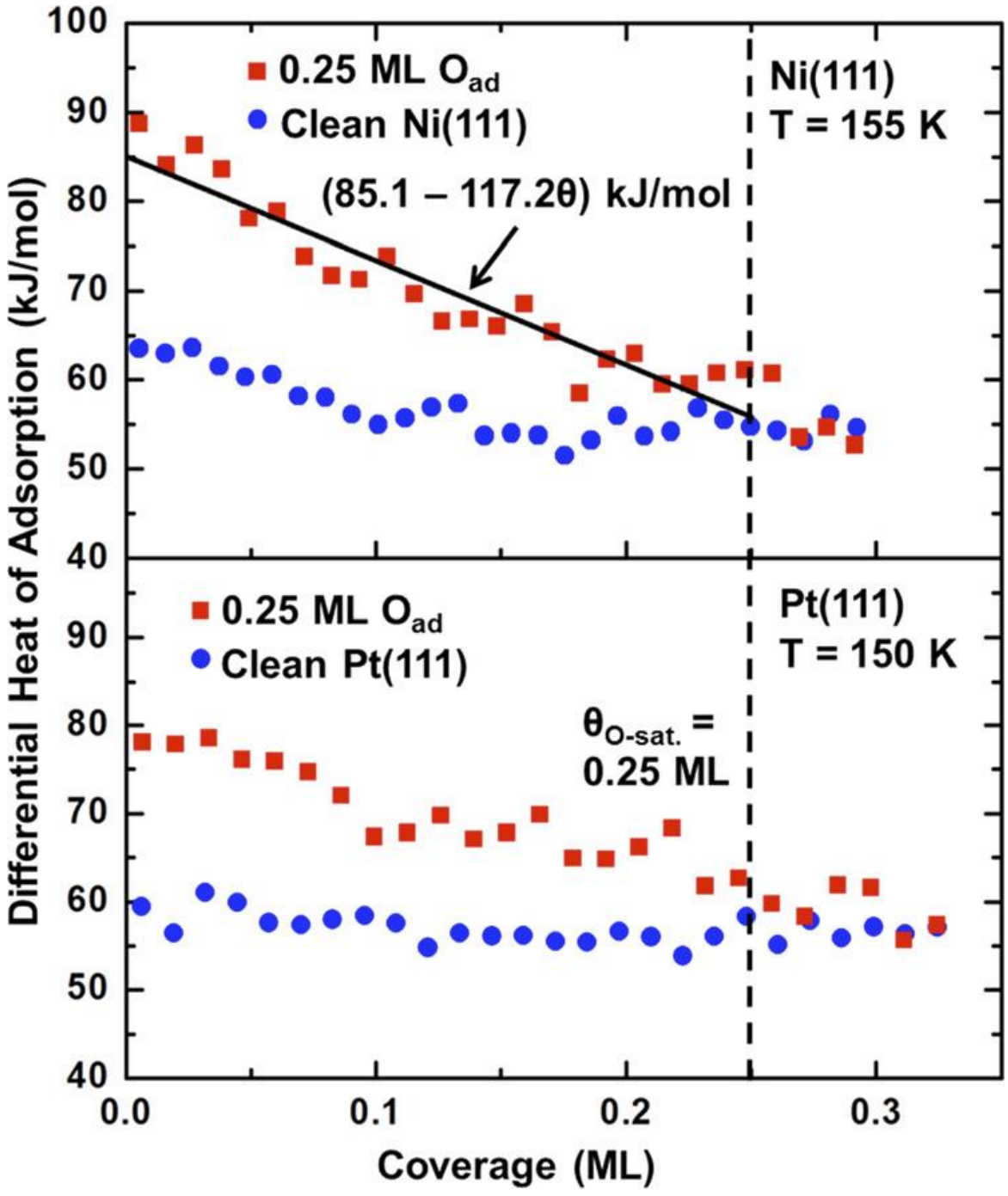

Figure 3.3 - Differential heat of adsorption of methanol versus total methanol coverage on Ni(111) at 155 K and on Pt(111) at 150 K at two surface conditions: the clean metal surface and with 0.25 ML precoverage of O_{ad}. The vertical dashed line at 0.25 ML is where the reaction of methanol with O_{ad} to produce CH_3O_{ad} + OH_{ad} is expected to finish.

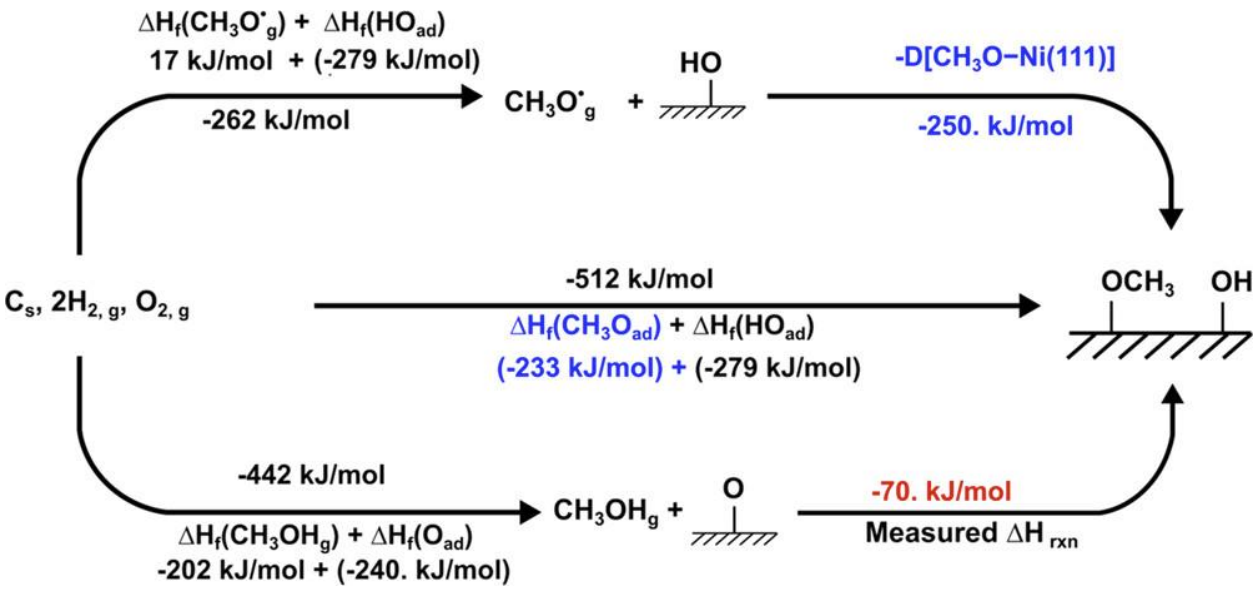

Figure 3.4 - Thermodynamic cycle used to calculate the heat of formation and bond dissociation enthalpy of adsorbed methoxy to the Ni(111) surface, which are shown in blue. The red value of −70. kJ/mol is the measured enthalpy of reaction of gaseous methanol onto the surface precovered with 0.25 ML of O_{ad} at 100 K producing adsorbed methoxy and hydroxyl. This is the integral or average reaction enthalpy from 0 to 0.25 ML of dissociatively adsorbed methanol. The other values shown in black are from the literature, as described in the text.

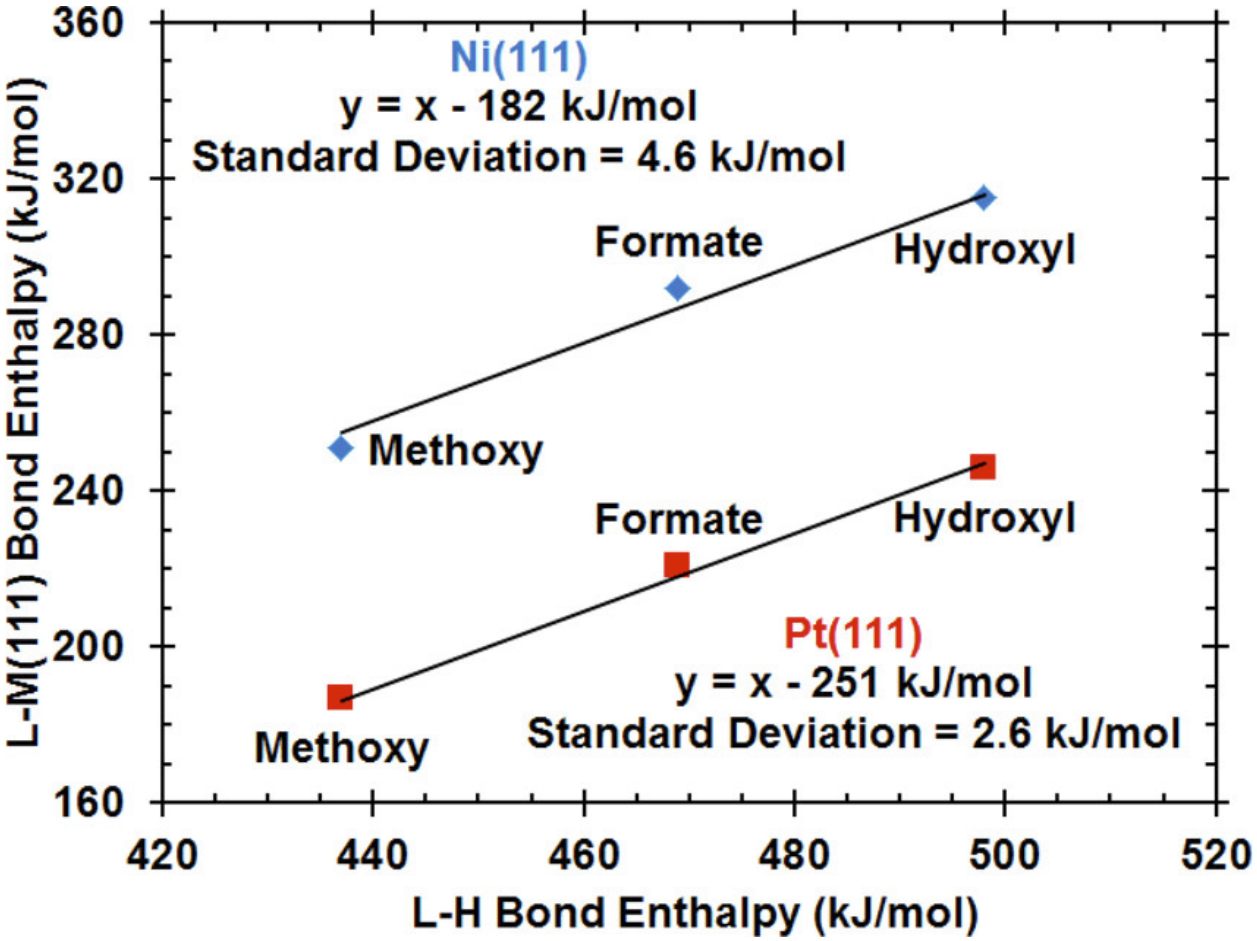

Figure 3.5 - Calorimetric bond dissociation enthalpies of three adsorbates (i.e., ligands, L) on both Ni(111) and Pt(111) versus their corresponding gas-phase hydrogen–ligand bond dissociation enthalpies. These data points are fitted with the linear trendlines shown, each with a slope of 1.

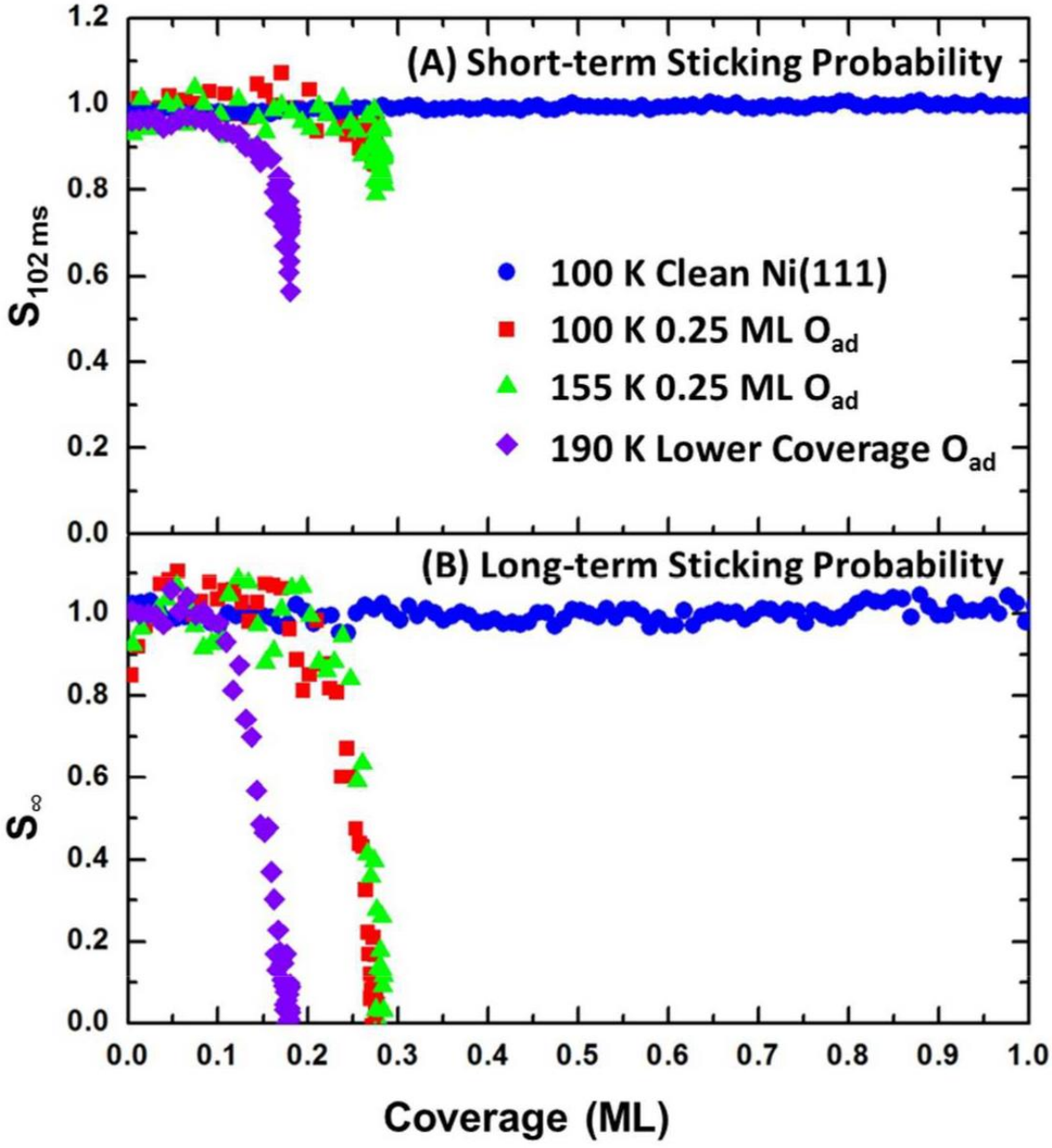

Figure 3.6 - Average short-term (A) and long-term (B) sticking probabilities of methanol as a function of total methanol coverage on Ni(111) at several temperatures and surface conditions. Note that the reaction completes at ~0.16 ML for the "lower coverage" of Oad, which we interpret to indicate that this coverage (from 5 L O2 at 190 K) is ~0.16 ML of Oad.

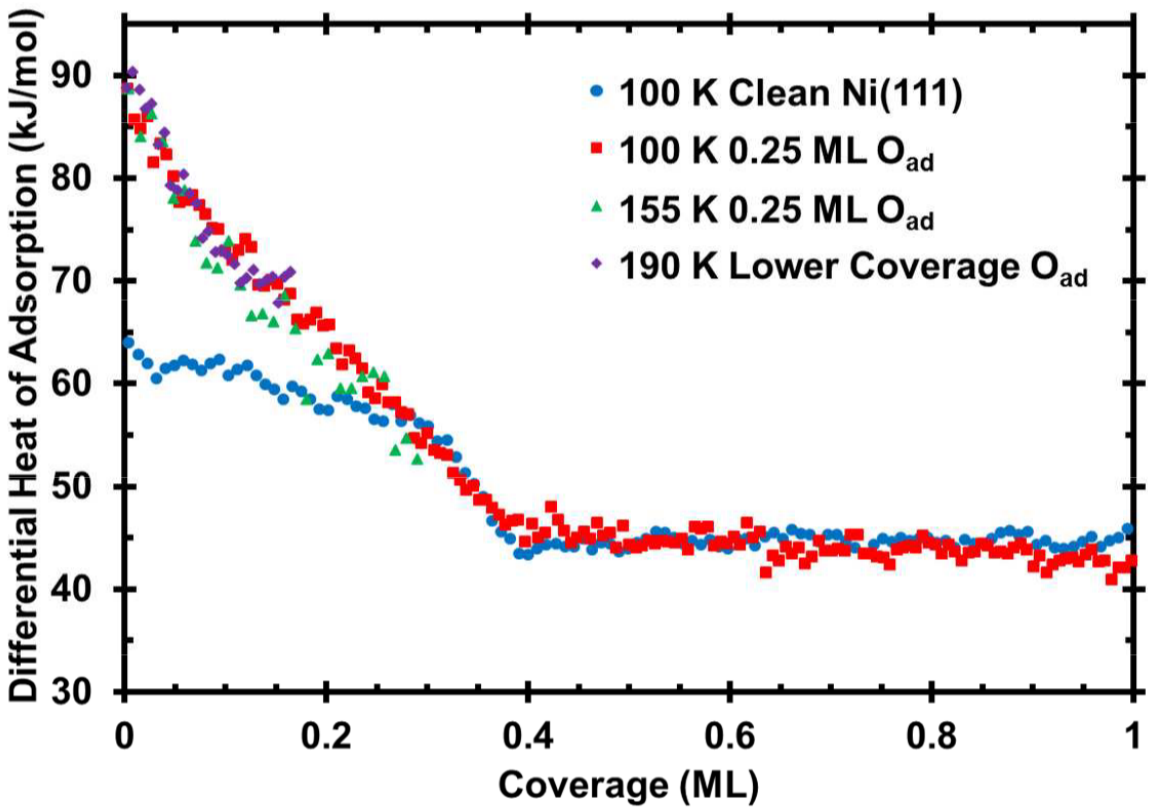

Figure 3.7 - Comparison of the differential heats of adsorption of methanol on Ni(111) at several different temperatures and surface conditions as a function of adsorbed methanol coverage. The methanol dissociates to make methoxy and –OH on the oxygen-predosed surfaces, until this titrates all the Oad.

Table 3.1 Comparison of the Present Calorimetric Integral Bond Energies of Methanol to the Ni(111) Surface with Calculated Values Using DFT with Periodic Boundary Conditions

Molecularly adsorbed methanol			**Bond energy (kJ/mol)**		**Ref**
Coverage	**DFT functional/method**	**DFT site**	**DFT**	**Calorimetry**	**DFT**
1/9 ML	PW-91	Top	24	61	101
1/9 ML	PW-91	Top	32	61	100
1/6 ML	PBE	Top	16	60	102
1/4 ML	RPBE	top	2	59	99
Methoxy			**Bond energy (kJ/mol)**		**Ref**
Coverage	**DFT functional/method**	**DFT site**	**DFT**	**Calorimetry**	**DFT**
1/9 ML	PW-91	Hollow	257	257	101
1/9 ML	PW-91	FCC hollow	243	257	100
1/6 ML	PBE	FCC hollow	249	254	102
1/6 ML	PW-91	FCC hollow	264	254	103
1/4 ML	RPBE	top	180	249	99

Chapter 4 Energetics of Adsorbed Formate and Formic Acid on Cu(111) by Calorimetry

This chapter reprinted with permissions from Ref 39:

Ruehl, G. and Harman, S. E., Gluth, O. M., Lavoy, D. H., & Campbell, C. T. Energetics of Adsorbed Formate and Formic Acid on Cu(111) by Calorimetry. *ACS Catalysis* (2022). https://doi.org/10.1021/acscatal.2c02608

Chapter Abstract

The heats of adsorption of formic acid molecularly adsorbed on clean Cu(111) and dissociatively adsorbed on oxygen-predosed Cu(111) were measured by adsorption calorimetry. The dissociative adsorption of formic acid on oxygen-predosed Cu(111) at 240 K produces adsorbed bidentate formate and gaseous water. For this, the differential heat of adsorption is initially 99 kJ/mol, decreasing to 80.4 kJ/mol by ~0.20 ML. This is (to our knowledge) the only experimental measurement of the energy of *any* molecular fragment bonded to *any* clean and well-ordered Cu single-crystal surface, making these results important benchmarks for validating the energy accuracy of computational models for a wide range of adsorbates on Cu catalysts. The integral (average) heat of adsorption at 240 K and 0.20 ML is 89.7 kJ/mol. From this, the heat of formation of bidentate formate and its bond enthalpy to Cu(111) were determined to be approximately -465 and 335 kJ/mol, respectively. Corresponding values were estimated for monodentate formate on Cu(111), giving -437 and 307 kJ/mol. Comparing to previous calorimetric results on Pt(111) and Ni(111) shows that the bond enthalpies and enthalpies of formation of formate on Cu(111) are similar to those on Ni(111), but ~75 kJ/mol stronger than

on Pt(111). Comparing these to reported DFT calculations shows that DFT systematically underestimated the stability of formate on these metals by ~50 kJ/mol. The differential heat of molecular adsorption of formic acid on clean Cu(111) at 120 K is initially 81 kJ/mol, dropping to ~70 kJ/mol by ~0.50 ML, before decreasing to a multilayer energy of 64.3 kJ/mol. Using this heat of adsorption through bulk-like multilayer coverages, we estimate the adhesion energy for liquid formic acid to Cu(111) to be 0.271 J/m^2.

4.1 Introduction

Understanding the energetics of small molecules and molecular fragments on transition metal surfaces is crucial for advancing fundamental insights into catalysis, the development of new catalysts and catalytic processes, and improving the energy accuracy of methods like density functional theory (DFT) used for computational modeling of these systems. Here, we expand upon the previous work of the Campbell group that measured the energetics of irreversible adsorption for molecular fragments on Pt(111) and Ni(111) to now include adsorption on the Cu(111) surface.[34,51,66,67,82,83,96,104–106,111–113] In this paper, we use calorimetry under ultrahigh vacuum conditions to directly measure the heat of molecular adsorption of formic acid onto clean Cu(111), and the heat of dissociative adsorption of formic acid onto oxygen-predosed Cu(111). We compare and contrast these heats on Cu(111) with those measured for the same adsorbates on Pt(111) and Ni(111), and with DFT predictions of these heats on Cu(111).

Formic acid and adsorbed formate are considered important intermediates for many reactions on late transition metal catalysts. This includes well-established industrial reactions such as methanol synthesis, water-gas shift, and steam reforming of methane,[35–38] as well as more emergent applications such as biomass reforming, fuel cell feeds, and a potential hydrogen carrier.[114–118] The surface interactions of organic molecules containing -COO^- or -COOH groups such as peptides, proteins, and amino acid residues are also important for a wide variety of applications ranging from medical implants[119,120] to the controlled synthesis of nanoparticles and nanostructures.[121,122] More recently, formate has emerged as an adsorbed intermediate of interest in thermal and electrocatalytic processes for the reduction of CO_2.[123–125] Thus, reaction pathways for these processes are the subject of intense study.[114,115,117,118,126–128] The results reported here

provide important benchmarks to improve the energy accuracy of computational models that seek to elucidate these processes.

Formate is the simplest example of a carboxylate adsorbate, and can consequently act as a prototype for understanding the bonding energetics for more complex examples of this class of adsorbates. However, since the dissociative adsorption of formic acid is an irreversible adsorption process, traditional methods for studying the energetics of surface adsorbates, such as Temperature Programmed Desorption (TPD), cannot be used. To date, the heat of formation of adsorbed formate has only been measured for two surfaces, Pt(111)[111] and Ni(111),[83] both previously reported by this group. This work not only expands these results to the Cu(111) surface, but constitutes (to our knowledge) the only measured heat of formation for *any* molecular fragment on *any* well-defined Cu surface (i.e. any clean and well-ordered single-crystalline Cu surface).

Copper is an important transition metal catalyst for a number of chemical applications where formate and more complex carboxylates are adsorbed intermediates, including water-gas shift, methanol synthesis, partial oxidation of methanol, and the conversion between esters and alcohols.[35–38,129] It has also garnered interest as the most promising monometallic catalyst for CO_2 reduction chemistry, particularly in electrocatalytic applications.[124,130–132] Formate is commonly seen in these reactions as an intermediate in either preferred or competing reaction pathways.[123–125] Additionally, Cu is predicted by DFT to show large differences in adsorbate bond energies in comparison to Ni and Pt. Thus in combination with previous studies from this group on Pt(111) and Ni(111), these measurements on Cu(111) provide a set of key experimental benchmarks on these three surfaces. As all three of these metals are widely used in industrial catalytic reactions, this suite of benchmarks can expand our fundamental understanding of

observed differences in catalytic activity between them. The (111) surface is chosen for all three metals as it is the most thermodynamically stable facet and thus is expected to dominate the surfaces of these metal catalysts, at least when particle size is large. Consequently, the (111) surface has been widely studied as a well-defined model for Cu, Ni, and Pt catalysts.

Here, we use calorimetry under ultra-high vacuum conditions to directly measure the heat of molecular adsorption of formic acid onto clean Cu(111), and the heat of dissociative adsorption of formic acid onto oxygen-predosed Cu(111). This allows for the extraction of the bond enthalpy and enthalpy of formation of adsorbed bidentate formate on Cu(111), along with estimates of the corresponding values for monodentate formate. These values not only serve as important benchmarks for computational models, but also clarify the energetics of important elementary reaction steps that occur in catalysis on Cu surfaces.

4.2 Experimental Methodology

The experiments were performed in an ultra-high vacuum (UHV) chamber (base pressure $<2 \times 10^{-10}$ mbar) designed for single-crystal adsorption calorimetry (SCAC). The chamber is also equipped with X-ray photoelectron spectroscopy (XPS), low-energy electron diffraction (LEED), Auger electron spectroscopy (AES), low-energy ion-scattering spectroscopy (LEIS), a quadrupole mass spectrometer (QMS), and a calibrated liquid-nitrogen-cooled quartz crystal microbalance (QCM), used to measure the absolute flux of the HCOOH molecular beam. The SCAC apparatus and experimental procedures for the molecular beam flux, sticking probability, and heat measurements have been described in depth previously.[24,67,68]

To briefly summarize, the Cu(111) sample used was a 2 μm thick single-crystal foil provided by Bine Hansen at Aarhus University. The surface was cleaned by repeated cycles of

Ar^+ ion sputtering and annealing until a well-ordered (111) LEED pattern was obtained. (Due to the high reflectivity of Cu, the exact annealing temperature of the sample surface could not be determined using an optical pyrometer.) The oxygen-predosed surface was prepared by exposing the clean Cu(111) surface at 240 K to 30 L of O_2 gas (1 L = 1 Langmuir = 10^{-6} torr sec), which we show below produces atomically-adsorbed oxygen at a coverage of ~0.10 ML O adatoms per Cu surface atom. The clean or O-predosed Cu(111) surface was exposed to a pulsed, collimated molecular beam of formic acid, and the heat of adsorption and sticking probability were recorded simultaneously. The purity of the HCOOH molecular beam generated in this way was verified with direct observation by the QMS, consistent with our earlier measurements.[83,111] The sticking probabilities (both long-term (S_∞) and short-term (S_{102ms})) were measured with a QMS using the King and Wells method,[70] and are as defined previously[67,68] to relate to the fraction of molecules in the gas pulse that stick to and remain on the surface until the start of the next pulse (S_∞), and those that stick long enough to contribute to the heat signal (S_{102ms}, which is measured only in the first 102 ms here). The heat of adsorption was measured by a pyroelectric ribbon pressed against the back of the Cu(111) crystal. The molecular beam was created by expanding approximately 4.0 mbar of formic acid through a glass capillary array held at 360 K and collimated through a series of orifices that are cooled with liquid nitrogen. The resulting molecular beam is then chopped into 102 ms pulses every 3 s.

Here, one monolayer of coverage is defined as the number of molecules of formic acid adsorbed to the surface per unit area, regardless of the product produced, normalized to the density of Cu atoms on the (111) surface (1.77×10^{19} atoms per m^2). A typical dose is 0.010 ML (~4.5×10^{12} molecules within the beam diameter of ~4 mm) per formic acid gas pulse.

Light pulses from a HeNe laser (632.8 nm) were used to calibrate the heat detector sensitivity, as described previously for studies on Pt(111)[51,66,67,105–107,111,112] and Ni(111).[34,82,83,104] Since Cu(111) has a much higher reported optical reflectivity for this wavelength (0.973)[133] than Pt (0.76) and Ni (0.65),[134] the accuracy of the laser calibration of the heat signal is less reliable than for Pt and Ni. (Any small relative difference between our samples' actual reflectivity and this literature value (which we assumed for calibration) leads to ~10-fold larger error in the heat adsorbed.) These SCAC experiments on Cu also had ~10-fold lower heat signal and poorer heat signal-to-noise ratio than was typical for experiments from this group on Pt and Ni. We think this may also be due at least partially to the much lower infrared optical emissivity (absorptivity) of Cu, which might make a large contribution to the heat transfer rate from the metal crystal to the heat detector. However, during the course of these measurement reported here, there was also an extra contribution to the heat signal's noise that was only discovered *after* the experiments reported here, so the signal to noise ratio on heats reported here is significantly lower than is in principle possible with the instrumentation used here even for Cu.

4.3 Results

4.3.1 Sticking Probabilities

Recent experiments have shown that formic acid will not dissociatively adsorb on clean Cu(111) except to a small extent attributed to the step edge defect density.[116,135] This produces low coverages of adsorbed formate, which takes on the monodentate structure ($HCOO_{mono,ad}$) at low temperatures but converts to bidentate ($HCOO_{bi,ad}$) at 200 K and above.[116,135] Higher coverages of monodentate formate can be formed by extended HCOOH gas dosing (10 to 30

minutes) at 150-160 K.[136] Early reports of rapid dissociative adsorption of HCOOH on Cu(111)[137,138] may have been due to X-ray beam damage.

Dissociative adsorption of HCOOH does occur rapidly on oxygen-predosed Cu(111), resulting in the formation of adsorbed formate in the bidentate structure, $HCOO_{bi,ad}$, with coverages up to 0.33 formate molecules per Cu surface atom.[139] That reaction was characterized at 330 K by the net stoichiometry:[139]

$$2\ HCOOH_g + O_{ad} \rightarrow 2\ HCOO_{bi,ad} + H_2O_g \quad . \qquad (4.1)$$

However, this probably involves the step:

$$HCOOH_g + O_{ad} \rightarrow HCOO_{bi,ad} + OH_{ad} \quad , \qquad (4.2)$$

which is known to occur on Cu(110) and Cu(111),[140,141] and then the two hydroxyls thus produced convert to water and O_{ad} via:

$$2\ OH_{ad} \rightarrow H_2O_g + O_{ad} \quad . \qquad (4.3)$$

Reaction 4.3 is known to occur on Cu(111) already at 160 K during TPD after producing OH_{ad} by dosing methanol to a surface at 110 K with pre-adsorbed O_{ad}.[142] Interestingly, Reaction 4.3 only occurs at much higher temperatures on the other widely-studied Cu faces: 220 K on Cu(100)[143] and 290 K on Cu(110).[144,145] We note that Reaction 4.2 above may occur in two steps, whereby the less stable monodentate formate forms first but converts to bidentate formate (as noted in literature cited farther above).

Given these results from the literature, one expects that when we dose HCOOH to O predosed Cu(111) at 240 K, we get the same net reaction as Reaction 4.1.

Figure 4.1 shows the average long-term (S_∞) and short-term (S_{102ms}) sticking probabilities versus coverage for formic acid adsorption on O-predosed Cu(111) at 240 K. The HCOOH-derived coverages reported throughout this paper represent the amount of formic acid adsorbed

for the entire duration of the experiment, regardless of the product produced (i.e., formate or molecularly adsorbed HCOOH). We will use "O-predosed Cu(111)" throughout to refer to a Cu(111) surface with ~0.10 ML of oxygen adatoms, obtained by predosing 30 L of O_2 at 240 K. The long-term sticking probability (S_∞) is the probability that a gas molecule strikes the sample surface, sticks, and remains until the next gas pulse starts 3 s later. This is used to calculate the adsorbate coverage at the start of the next gas pulse. The short-term sticking probability (S_{102ms}) is the probability that a gas molecule strikes the sample surface, sticks, and remains at least through the time window of the heat measurement (i.e., the first 102 ms). This is used to calculate the number of moles of gas-phase reactants that contribute to the measured heat signal for that gas pulse, and thus the heat of adsorption per mole adsorbed.

At 240 K, both the long-term and short-term sticking probabilities are initially high (>0.9) and remain at unity (within the noise) through a coverage of ~0.15 ML. Past this coverage, the long-term sticking probability drops off rapidly, reaching zero by 0.20 ML, while the short-term sticking probability remains high (>0.90). After this coverage, formic acid continues to transiently adsorb on the saturated adlayer with a high probability, as evidenced by the high short-term sticking probability, but desorbs again completely (but slowly) before the next pulse starts 3 s later. This suggests that the O adatoms are fully reacted in the dissociative adsorption reaction, and no further dissociative adsorption can occur. We note that the temperature here is above that necessary for multilayer adsorption (~150 K[135]), so no molecular adsorption beyond the first layer is expected.

The inset in Figure 4.1 shows the HCOOH coverage at which its long-term sticking probability at 240 K drops to 0.50 (which closely tracks the saturation coverage of dissociatively adsorbed HCOOH) as a function of the amount of pre-exposure of the clean Cu(111) surface at

240 K to O_2 gas. As seen, this HCOOH coverage increases steeply with O_2 pre-dose, from nearly zero with no predose of O_2, and quickly saturates at ~0.18 ML after ~20 L of O_2. Similarly, the HCOOH coverage at which its S_∞ dropped below 0.1 saturated at ~0.20 ML after ~20 L of predosed O_2 (not shown). Assuming a 2:1 stoichiometric ratio in Reaction 4.1 proposed above based on prior literature ($2\ HCOOH_g + O_{ad} \rightarrow 2\ HCOO_{bi,ad} + H_2O_g$), we take this to indicate that the 30 L O_2 pre-exposure at 240 K used in Figure 4.1, which gives a saturation formate coverage of 0.20 ML, corresponds to about 0.10 ML of O adatoms. This is about 10-fold smaller O_2 dose than was reported to produce this same coverage on Cu(111) at a higher temperature (296 K).[146] This coverage of O_{ad} is also smaller than the saturation coverage at 296 to 600 K (reported as ~0.44 ML[146]). Defects such as step edges may aid in O_2 dissociation, especially at the lower temperature used here.

Based on the prior literature summarized above, we concluded that when we dose HCOOH to O-predosed Cu(111) at 240 K, we get the same net reaction as Reaction 4.1. This also means that gaseous H_2O should have evolved simultaneously with the dissociation of HCOOH. We attempted to detect this H_2O_g by averaging the QMS signal at m/e = 18 for the pulses below 0.2 ML dose, but were unable to see signal above the noise due to H_2O evolution. However, given the high background signal of water in the chamber (and associated large noise at m/e = 18), the expected water peak intensity (~1/2 the QMS signal for formic acid at zero-sticking probability, according to the stoichiometry of Reaction 4.1) would not have been visible above the noise in the background signal. Thus, we still believe Reaction 4.1 dominates at 240 K.

At 120 K on clean Cu(111), where formic acid adsorbs molecularly, the short-term and long-term sticking probabilities are both unity (within the pulse-to-pulse noise similar to that in Figure 4.1) at all coverages, so they are not shown here. As this temperature is low enough to

form multilayers of formic acid on the Cu(111) surface, the sticking probability was found to remain at unity through at least five layers of coverage.

4.3.2 Heats of Adsorption

In this paper, the term "heat of adsorption" is defined at the negative of the standard molar enthalpy change for the adsorption reaction, with the gas and the sample surface being at the sample temperature. As explained in detail previously, this requires a small enthalpy correction on the measured heat since the gas molecule's enthalpy in the molecular beam is slightly higher than a Boltzmann distribution at the Cu(111) temperature due to the actual experimental molecular beam conditions.[67] The differential heat of adsorption is the heat released per mole when a small increment of adsorbate is added to the surface at nearly fixed coverage, as occurs in one of our molecular beam pulses during SCAC. The integral heat of adsorption is the integral of the differential heat versus coverage from zero up to the coverage of interest, divided by that coverage, and is thus the average heat for that coverage range.

Figure 4.2 shows the differential heats of adsorption for formic acid on clean Cu(111) at 120 K (blue) and on O-predosed Cu(111) at 240 K (red) (after this small correction to the raw heats noted above) as a function of adsorbate coverage. The integral heat of adsorption at 240 K is also shown in black from the low coverage limit. These are averages of three and nine runs at 120 K and 240 K, respectively. For both the 120 K and 240 K data, the first two data points are significantly higher than subsequent points and are attributed to adsorption on defect sites on the surface, likely at step edges. These two points are excluded from integral heat and initial heat determinations so that these values correspond to adsorption on terraces and are not inclusive of these defect sites that bind more strongly.

Previous results from literature show that formic acid molecularly adsorbs on clean Cu(111) below ~250 K, and multilayers will adsorb to the surface below 150 K.[135] Thus, calorimetric measurements at 120 K on clean Cu(111) correspond to molecular adsorption of formic acid in the first layer, with the formation of multilayers at higher coverages.

At 120 K, the initial heat of adsorption is 80.9 kJ/mol (excluding the first two points, which are higher, and may be due to adsorption at defects, likely step edges). The heat decreases approximately linearly with coverage until reaching ~70 kJ/mol by 0.50 ML, where the first adlayer of formic acid appears to be completed. A very similar decrease (~10 kJ/mol) in heat of HCOOH adsorption with coverage was reported on Pt(111) and Ni(111),[83,111] implying net repulsive adsorbate-adsorbate interactions. The HCOOH units are likely attached by hydrogen bonds, but groups of H-bonded HCOOHs must have group-group repulsions. This has been suggesting to occur for methanol on Pt, Au and Cu(111),[81] where H-bonded hexamers and/or/ chains have repulsive group-group interactions. Beyond 0.5 ML, the heat of adsorption stays constant at ~68.5 kJ/mol through ~1.5 ML, before decreasing to the multilayer energy value of 64.3 ± 2.9 kJ/mol. (This is the run-to-run average and standard deviation of the multilayer heats of the three runs.) Each run's multilayer heat is the pulse-to-pulse average heat for coverages above 1.75 ML. The heat of sublimation of bulk formic acid was estimated to be 61.9 kJ/mol at 120 K, using literature values for the enthalpies of phase transitions[147] along with heat capacities of solid, liquid, and gaseous formic acid,[148] as a heat of sublimation at 120 K was not available in literature. The bulk heat of sublimation at 120 K was also estimated using the same heat capacities but instead starting from a reported bulk heat of sublimation at 200 K (60.5 kJ/mol[149]), which gives a very similar value of 61.3 kJ/mol. The average of these two bulk literature values (61.3 and 61.9 kJ/mol) falls within the error bars of the multilayer heat measured here (61.4-67.2

kJ/mol). This close agreement provides an estimate of the absolute accuracy of the results in Figure 4.2. The ~2 kJ/mol higher heat of adsorption in the first monolayer after completion of the first adlayer (i.e., between 0.5 and 1.5 ML coverage) is possibly due to long-range attractive interactions between the HCOOH molecules and the underlying metal (e.g., dipole-induced dipole interactions). It is common to have higher heats than the true multilayer heats in the later after completion of the first adlayer.[51,150,151]

At 240 K, the initial heat of adsorption on the O-predosed Cu(111) surface is 99.1 kJ/mol (again excluding the first two points, which are higher, and may be due to adsorption at defects, likely step edges). The heat decreases approximately linearly with coverage until reaching 80.4 kJ/mol by a coverage of ~0.20 ML. Past this point, the long-term sticking probability has dropped to zero, indicating that surface O adatoms have been fully consumed by the dissociation reaction and the surface adlayer is saturated. Any additional formic acid molecules that impinge on the surface adsorb transiently (as indicated by the high short-term sticking probability), but fully desorb before the next pulse begins 3 s later. The integral heat of adsorption at 240 K is shown in black versus coverage up to saturation, and is well fit by (99.1-46.8θ) kJ/mol, where θ is coverage in ML, with an integral heat of 89.7 kJ/mol at saturation (0.20 ML).

Above saturation on O-predosed Cu(111) at 240 K, the transiently adsorbed HCOOH has a constant heat of adsorption at saturation ($\Delta H_{ad,sat}$) of 72.5 ± 3.3 kJ/mol. By averaging the mass spectrometry pulse line-shapes (signal versus time) after saturation and fitting an exponential decay function to the post-pulse signal decay, we obtained a decay constant, τ, which is equal to the reciprocal of the first-order desorption rate constant, k_{des}, given by:[20]

$$1/\tau = k_{des} = \nu_{des} \exp(-E_{des}/RT) \ , \qquad (4.4)$$

where ν_{des} is the prefactor for desorption, E_{des} is the activation energy of desorption, R is the gas constant, and T is the temperature. Using the values of τ = 0.85 s and k_{des} = 0.173 s^{-1} determined from this exponential decay fit, along with E_{des} = 71.5 kJ/mol determined from the measured heat after saturation ($E_{des} = \Delta H_{ad,sat} - 1/2RT$[18]), a prefactor for desorption can be calculated. In that way, we determined an experimental prefactor for HCOOH desorption of $\nu_{des} = 4.3 \times 10^{15}$ s^{-1}. This can be compared to the prefactor for desorption estimated by the method of Campbell & Sellers,[20] which gives $\nu_{des} = 2.4 \times 10^{15}$ s^{-1} for molecularly adsorbed HCOOH at 240 K. This good agreement indicates that the transiently adsorbed HCOOH is molecularly adsorbed and not, for example, transiently dissociated and then recombined.

4.4 Discussion

4.4.1 Energetics of adsorbed formate on Cu(111) at 240 K

As discussed above, our calorimetric measurements on the O-predosed Cu(111) surface at 240 K represent the heats of dissociative formic acid adsorption onto Cu(111), via Reaction 4.1 above: $2\ HCOOH_g + O_{ad} \rightarrow 2\ HCOO_{bi,ad} + H_2O_g$. By using available literature values for the heats of formation of various gas-phase and adsorbed molecules and the experimentally measured heat at 240 K, we can extract the bond enthalpy of bidentate formate to Cu(111) ($HCOO_{bi,ad}$=Cu(111)) and the enthalpy of formation of bidentate formate on the Cu(111) surface ($\Delta H_f(HCOO_{bi,ad})$). To do so, we construct the thermodynamic cycles shown in Figure 4.3 & Figure 4.4. Note that all positive heats of adsorption in Figure 4.2 represent exothermic processes, while here they have been converted to negative enthalpies of reaction for use in the thermodynamic cycles.

The cycle in Figure 4.3 begins on the left-hand side, starting with gas-phase formate and a surface-bound oxygen atom (but with only ½ mole of O_{ad}, for ½ of the stoichiometry of Reaction 4.1, which then corresponds to a single formate adsorbate). The bottom pathway represents our measurement at 240 K, and is quantified by the integral heat of adsorption at 0.20 ML. This must be energetically equivalent to the parallel pathway; therefore, the sum of the steps in the top pathway must equal -90. kJ/mol. The first step in the top pathway is to dissociate gas-phase formic acid into a gas-phase hydrogen atom and a gas-phase formate radical. The enthalpy of reaction for this step (+468 kJ/mol) is calculated using literature values for the enthalpies of formation for each of the three gas-phase species from elements in their standard states at 298 K ($HCOOH_g$ = -379.2, $HCOO_g$ = -129.7, and H_g = +218.0, in kJ/mol).[147]

In the second step of the top pathway, the ½ oxygen adatom is desorbed to form ¼ gaseous O_2, with the other species unchanged. In the absence of any reported value for the enthalpy of formation of adsorbed O on Cu(111), or the reverse of this step, the enthalpy of this reaction (+116 kJ/mol) is estimated from reported literature values for the enthalpy of dissociative adsorption of O_2 on polycrystalline Cu of 465 kJ per mole O_2.[152,153] Reported DFT calculations (summarized in Table 4.3 below) for the adsorption energy of O_{ad} on different Cu faces showed that O_{ad} is 21 to 36 kJ/mol less stable on Cu(111) than on the (110) and (100) faces.[154] This suggests that this calorimetric heat for ½ O_{ad} → ¼ $O_{2,g}$ of 116 kJ/mol in Figure 4.3 may be too large for Cu(111) by 10 to 18 kJ/mol. The third step in the top pathway is to combine O_2 gas and H gas to form gaseous water. The enthalpy of this step (-339 kJ/ml) was calculated using literature values for the enthalpies of formation for each of the three gas-phase species from elements in their standard states at 298 K.[147]

Finally, this leaves the top right step as the only unsolved value. This step represents the enthalpy to form bidentate formate from the gas-phase formate radical, which provides an estimate of the total bond enthalpy of bidentate formate to Cu(111), from both its O-Cu bonds. The extracted $HCOO_{bi,ad}$=Cu(111) bond enthalpy is 335 kJ/mol. Given that this value is very close to that of the bond enthalpy of bidentate formate to Ni(111) (320 kJ/mol[83]), we assume the same difference in bond enthalpies between mono- and bidentate formate on Cu(111) as previously measured on Ni(111) (28 kJ/mol[83,155]) in order to estimate the bond enthalpy of monodentate formate to Cu(111). This estimated bond enthalpy of monodentate formate to Cu(111), or $HCOO_{mono,ad}$-Cu(111), is thus 335 - 28 = 307 kJ/mol. This assumed difference between mono- and bidentate formate of 28 kJ/mol is also close to that calculated on Cu(111) by DFT (42 kJ/mol[36]) and that measured on Pt(111) (33 kJ/mol[111,155]). Since the ½ O_{ad} species on Cu(111) may be up to 18 kJ/mol less stable than the enthalpy value used for ½ O_{ad} in this cycle of Figure 4.3 (which is for polycrystalline Cu instead of Cu(111), see above), these bond enthalpies of both bi- and monodentate formate to Cu(111) may be smaller by up to 18 kJ/mol, placing them very close to their values to Ni(111).

Figure 4.4 shows how this extracted $HCOO_{bi,ad}$=Cu(111) bond enthalpy can be used in another thermodynamic cycle to extract the enthalpy of formation of bidentate formate on Cu(111). In this case the cycle starts on the left-hand side with the elements in their standard states. The top pathway uses first the literature value for the enthalpy of formation of gas-phase formate,[156] followed by the extracted bond enthalpy of bidentate formate from Figure 4.3. This results in the formation of surface-bound bidentate formate. The bottom pathway then represents the enthalpy of formation for bidentate formate on Cu(111), and again must be energetically equivalent to the parallel pathway. The resulting extracted value for the enthalpy of formation of

bidentate formate, or $\Delta H_f(HCOO_{bi,ad})$, on Cu(111) is -465 kJ/mol. Using the same method as discussed above, the estimated corresponding enthalpy of formation for monodentate formate, or $\Delta H_f(HCOO_{mono,ad})$, on Cu(111) is -465 + 28 = -437 kJ/mol. Again, these heats of formation of both bi- and mono-dentate formate to Cu(111) may be smaller in magnitude (less stable) by up to 18 kJ/mol.

4.4.2 Comparison of calorimetric energy of adsorbed formate and HCOOH to DFT

The bond energies of bidentate and monodentate formate to Cu(111) measured in this work are compared to theoretical values obtained by DFT in Table 4.1. DFT calculations report integral bond energies of adsorbates at specific coverages. Bond enthalpies were converted to bond energies by subtracting RT (2 kJ/mol at 240 K). The bidentate bond enthalpies at 0.20 ML were calculated from the thermodynamic cycle in Figure 4.3. In order to match the reported coverage of most of the DFT values, equivalent values at 0.11 ML were calculated in an identical manner to that at 0.20 ML, but using the integral heat value at 240 K and 0.11 ML of 94 kJ/mol. All of these values in Table 4.1 for Cu(111) show a range that extends to lower adsorbed formate stability by 18 kJ/mol to allow for the uncertainty in the calorimetric heat of formation of O_{ad} mentioned above.

As can be seen, all of the reported DFT calculations significantly underestimate the measured bond energies of bidentate and monodentate formate to the Cu(111) surface. On average, the DFT values are ~80 to 62 kJ/mol lower than the experimentally determined bond energy of bidentate formate, and ~95 to 77 kJ/mol lower than that for monodentate formate. While larger in magnitude for Cu(111), this underestimation of the formate bond energy by DFT is also seen when comparing the experimental and theoretical values for Ni(111). For example,

prior DFT calculations had underestimated the bond energy of bidentate formate to Ni(111) by 26 to 58 kJ/mol compared to calorimetry.[83] Both of these margins of error are supported by the fact that it is well known that DFT has substantial errors in energy accuracy.[17] Since prior to this present work, there had not been experimentally determined bond energies reported for *any* molecular fragment on *any* well-defined Cu surface, this work provides an important benchmark for comparison to computational studies of small molecular fragments on Cu(111). However future experimental results beyond the formate/Cu(111) system will be important for extending these benchmarks to Cu systems more widely.

A PW91 DFT study calculated the adsorption energy of HCOOH on Cu(111) to be 15 kJ/mol,[115] compared to the integral heat of molecular adsorption of ~80 kJ/mol found here by calorimetry.

4.4.3 Comparison of adsorbed formate energy on Cu(111) to Pt(111) and Ni(111)

Previous calorimetric measurements by this group studied the adsorption of formic acid on Pt(111) & Ni(111), allowing for a direct comparison between the three metal surfaces.[83,111] The values of the bond enthalpies and enthalpies of formation for both mono- and bidentate formate to Pt(111), Ni(111), & Cu(111) are summarized in Table 4.2. When possible, coverages as close to the saturation coverage of 0.20 ML in this work have been reported, but that is not available for all values. The bidentate formate bond enthalpies are 251, 320, and 335 to 317 kJ/mol on Pt(111), Ni(111), and Cu(111), respectively. The enthalpies of formation of bidentate formate are -381, -449, and –(465 to 447) kJ/mol on Pt(111), Ni(111), and Cu(111), respectively. Thus, the formate bond energies to Cu(111) are experimentally indistinguishable from those to Ni(111) but 68 to 84 kJ/mol stronger than to Pt(111).

These calorimetric bond energies for monodentate formate to Pt(111) and Ni(111) were well fitted based on a model previously developed by Carey and Campbell that is based on Pauling's equation and uses only known parameters (gas-phase ligand-hydrogen bond enthalpies, bond enthalpies of adsorbed H atoms to the surface, electronegativities of the elements, and group electronegativities).[155] That model explained well the much stronger formate bond energies to Ni(111) compared to Pt(111), mainly associated with their differences in electronegativity. The electronegativity of Cu is much closer to that for Ni than Pt, suggesting that formate could have bond energy on Cu(111) similar to Ni(111). However, that model also includes a term for the H atom's bond energy to the surface, which is much stronger for Ni(111) than Cu(111) and would predict formate to bind more strongly to Ni than Cu. Indeed, that model was also used to predict formate bond energies to surfaces for which experimental measurements had not yet been reported, including Cu(111). The model's predicted bond enthalpy of monodentate formate to Cu(111) was 228 kJ/mol,[155] versus the estimated experimental value of 307 to 289 kJ/mol reported here. This is a large error, but slightly smaller than DFT errors (see above). This model also predicted the bond enthalpy of monodentate formate to Ni(111) (275 kJ/mol) to be a lot stronger than to Cu(111) (228 kJ/mol), whereas the experiments show these to be similar or with Cu(111) slightly stronger.

Table 4.2 also lists the bond energies for bidentate formate to these three metal surfaces as reported from DFT calculations (using the same version of PW91 at the same coverage by the same group in all cases).[128,157] (These DFT energies are without ZPE correction, but that correction would lower these bond energies by nearly the same ~14 kJ/mol on all three metals.) As seen, DFT has reproduced the experimental observations that formate binds much more weakly to Pt(111) than to Ni(111) or Cu(111), while the bond energies to Ni(111) and Cu(111)

are much closer to each other. Still, the errors in DFT relative to SCAC are rather large (-24, -50 and –(69 to 51) kJ/mol for Pt, Ni and Cu(111), respectively.) It is well known that DFT has substantial errors in energy accuracy in comparison to experimental energies, but these present errors are somewhat larger than the mean absolute error of 28 kJ/mol reported for PW91 on a group of 25 such 'strongly covalently adsorbed' systems, which showed a mean signed error of -20 kJ/mol.[17] If one adds 48 kJ/mol uniformly to all three of these PW91 bond energies, their errors relative to experiments drop to only +24, -2, and –(21 to 3) kJ/mol for Pt, Ni and Cu(111), respectively. This suggests there might be some large (~48 kJ/mol) error in DFT for the energy of the reference state for all of these bond energies: gaseous formate radical. In addition, it is known that PW91 underestimates adsorption energies by ~40 kJ/mol on average for systems where van der Waals interactions are thought to contribute a large amount of the adsorption energy.[17] Again, this present work on Cu(111) provides an important benchmark to aid future efforts to improve computational accuracy for adsorbate energies on late transition metals.

Further experimental measurements of molecular fragments on Cu(111) will be important to validate this observed difference between the experimental values measured here and those predicted by DFT or the electronegativity-based model of Carey & Campbell. At this point the basis for this difference is unclear, and the study of additional oxygenates on Cu might further elucidate the underlying reasons.

4.4.4 Adhesion energy of liquid formic acid to Cu(111)

Solvent/metal adhesion energies are crucial to understanding solvent effects on adsorption energies, which is increasingly critical as catalytic and electrocatalytic reactions occurring at solid surfaces in liquid solvents become more important. The determination of the

adhesion energy for liquid formic acid on Cu(111) can provide valuable insight into the energetics of this liquid-solid interface. However, there is currently no way to directly measure the adhesion energy of a liquid solvent to a clean metal surface. To estimate this adhesion energy, we will employ a recently developed method from this group that allows for an estimate of the adhesion energy from experimentally determined differential heat of adsorption data like that in Figure 4.2.[28,30] See refs.[28,30,51] for an in-depth derivation and discussion of this model.

This model results in the following equation for the determination of adhesion energy from calorimetric data:

$$E_{adh,S(liq)/M(s)} = [Q_{adsorption} - n \cdot \Delta H_{vap,S}]/A + 2\gamma_{S(liq)} \quad (4.5)$$

where $E_{adh,S(liq)/M(s)}$ is the adhesion energy of the liquid solvent (formic acid) to the solid metal surface (Cu(111)), $\gamma_{S(liq)}$ is the surface energy per unit area of bulk, liquid formic acid, and the term $[Q_{adsorption} - n \cdot \Delta H_{vap,S}]/A$ is equal to the numerically integrated area from zero coverage up to a (bulklike) multilayer coverage (with n moles adsorbed per area A) of the heat versus coverage curve ($Q_{adsorption}$) minus n/A times the molar heat of vaporization of the liquid solvent ($\Delta H_{vap,S}$). Ideally, these values would all be measured at room temperature to provide the adhesion energy at room temperature. Since $Q_{adsorption}$ can only be measured on a clean metal surface in ultra-high vacuum, which is only possible for formic acid at temperatures where the solvent grows as solid films rather than liquid films, the assumption was made that the term $[Q_{adsorption} - n \cdot \Delta H_{vap,S}]/A$ at room temperature is approximately equal to the analogous quantity at experimental temperatures where the solvent is a solid, or $[Q_{adsorption} - n \cdot \Delta H_{sub,S}]/A$, where $\Delta H_{sub,S}$ is the heat of sublimation of bulk formic acid.

Using this method and the reported surface energy of bulk, liquid formic acid of $\gamma_{S(liq)} = 0.0377$ J/m^2,[30,158] we calculate the adhesion energy of liquid formic acid to the Cu(111) surface

at 120 K to be E_{adh} = 0.271 J/m^2. Comparatively, this value is slightly less than the adhesion energy of formic acid to Ni(111) (0.279 J/m^2), but greater than that to Pt(111) (0.162 J/m^2).[30]

Understanding this adhesion energy, and particularly how it compares to other common solvents, could enable the intelligent selection among these solvents to tune reaction environments to have more desirable energetics for surface adsorption or desorption for catalytic reactants and intermediates. Unfortunately, there is currently no other reported solvent adhesion energies to the Cu(111) surface for comparison. However, these values are reported for multiple solvents on Pt(111) and Ni(111) and follow the trend of methanol < formic acid < water < benzene ≈ phenol.[30] This indicates that solvents with higher heats of adsorption per unit area in the first adsorbed layer have higher adhesion energies to a given metal surface. We note that these adhesion energies were all estimated using the same assumption of a negligible difference in heat capacities (including the heat of fusion) between the first and subsequent layers, and the errors associated with this assumption are possibly large (~25%). However, all of these errors are likely qualitatively similar, so these trends in E_{adh} values will remain. The close alignment of the adhesion energy of liquid formic acid to Cu(111) with the equivalent values to Pt(111) and Ni(111) suggests that these energetic trends will extend to the Cu(111) surface as well. However further experimentally determined solvent/metal adhesion energy values on Cu(111), along with computational approaches, will provide valuable comparison to support or refute the extension of these trends to Cu(111).

4.4.5 Formic acid multilayer structure on Cu(111)

The multilayer heat of adsorption obtained in this work on Cu(111) (64.3 ± 2.9 kJ/mol) is in close agreement with the estimated range for the heat of sublimation of bulk formic acid of

61.3-61.9 kJ/mol at 120 K, estimated from literature values as noted above. However, this is different than those heats previously reported by this group for multilayer adsorption of formic acid on Pt(111) and Ni(111) (49.9 and 52.8 kJ/mol, respectively).[83,111] Previous literature results show that below 143 K, adsorption of formic acid on Pt(111) results in the formation of an amorphous multilayer rather than the more stable crystalline (also referred to as polymeric) phase.[159,160] Therefore, Silbaugh *et al.* attributed the observed multilayer heat of 49.9 kJ/mol measured at 100 K to amorphous multilayer adsorption on Pt(111).[111] However, infrared adsorption reflection spectroscopy studies of formic acid multiplayers on Cu(111) at 100 K indicate polymeric (crystalline) phase when grown instead on Cu(111).[116] This crystalline phase is expected to be more stable than the amorphous phase seen on Pt(111), as supported by the higher multilayer heat of adsorption seen here on Cu(111). Therefore, this multilayer heat measured at 120 K in Figure 4.2 is assigned to the crystalline phase. Imaging with STM of monolayer formic acid molecularly adsorbed on Cu(111) also shows a crystalline phase in the first layer between 80 and 120 K,[135] which may act as a template to enable crystalline grown in the multilayer. This first-layer polymeric phase on Cu(111) is composed of hydrogen-bonded chains that align in a β configuration on the surface (roughly a zig-zag structure) that minimizes repulsive forces,[135] and is consequently likely to be more energetically favorable than amorphous adsorption.

4.4.6 Stability of OH_{ad} & energetics of H_2O desorption on Cu(111), Cu(100) & Cu(110)

In analyzing the heat measurements above when making bidentate formate, we used the fact that the desorption temperature for H_2O_g from $2\ OH_{ad} \rightarrow H_2O_g + O_{ad}$ (Reaction 4.3) was reported in a study of the dissociative adsorption of methanol on O-dosed Cu(111)[142] to be 160

K, so that this process was fast at our measurement temperature of 240 K. However, this temperature of 160 K is much lower than that known for this same reaction on Cu(110) (290 K[144,145]). To our knowledge, such a large percentage change in desorption temperatures between low-index faces of the same metal has not been reported for any reaction. As this value of 160 K for Cu(111) was only reported by one group, we wanted to verify that it is reasonable. To do this, we next compare this experimental difference to predicted results extracted from adsorption energies for O_{ad}, OH_{ad}, & H_2O_{ad} on Cu(111), Cu(100), & Cu(110) calculated by DFT.[154] The DFT adsorption energies used for these calculations, along with resulting enthalpies of reaction and predicted desorption temperatures are summarized in Table 4.3. To get these, we used the energy for the gas-phase Reaction 4.2 $OH_g \rightarrow H_2O_g + O_g$ to be -70.7 kJ/mol as calculated from the experimental standard heats of formation of O_g, OH_g, and H_2O_g reported at 298 K (249.1, 39.0 and -241.8 kJ/mol, respectively).[147]

The listed adsorption energies were first used to calculate the enthalpy of reaction for Reaction 4.3 (the desorption of gaseous water via $2\ OH_{ad} \rightarrow H_2O_g + O_{ad}$). This resulting reaction enthalpy was converted to an activation energy for water desorption by this reaction, E_{des}, by subtracting 1/2 RT. We made the assumption that this net reaction's enthalpy was equal to its activation energy (after converting from enthalpy to energy) based on computational results in literature that predict that the energetic barrier for desorption of molecularly adsorbed water is far larger than the energetic barrier for the reaction of two surface-bound hydroxyls to form adsorbed water plus O_{ad} on Cu(111).[36] Table 4.3 also shows the DFT energy for Reaction 4.3 is considerably more endothermic than that for the Reaction 4.2 $OH_{ad} \rightarrow H_2O_{ad} + O_{ad}$. Thus, we assume that $2\ OH_{ad} \rightarrow H_2O_{ad} + O_{ad}$ is fast to equilibrium, followed by the slow step $H_2O_{ad} \rightarrow$

H_2O_g, so that the net Reaction 4.3 has an activation energy equal to the sum of the reaction energies of those two elementary steps.

A prefactor for desorption of $\nu_{des} = 5 \times 10^{14}$ s^{-1} was estimated using the method of Campbell & Sellers.[20] Together, these E_{des} and ν_{des} values can be used to estimate a temperature for the desorption of H_2O via the reaction $2\ OH_{ad} \rightarrow H_2O_g + O_{ad}$ from each of the three surfaces, using the first-order Readhead equation:[19]

$$E_{des} = RT_m\ [\ln(\nu_{des} T_m/\beta) - \ln(-E_{des}/RT_m)] \qquad (4.6)$$

where R is the gas constant, T_m is temperature corresponding to the maximum of the desorption peak in TPD, and β is the heating rate. Using an assumed $\beta = 5$ K/s, the resulting estimated T_m values for Cu(111), Cu(100), & Cu(110) are 244, 286, and 407 K, respectively. In comparison, the values obtained in the TPD study of methanol by Pöllmann *et al.* are 160, 220, & 290 K, respectively.[142] As seen, the extremely wide range of the temperatures of desorption is reflected in the predicted temperatures, but the accuracy of the values are not well aligned with the experimental results. However, if we scale the DFT-derived reaction enthalpies by 0.70, equivalent to assuming an over-estimation of the reaction enthalpy of ~50% by DFT, we obtain desorption temperatures of 173, 202, and 287 K for Cu(111), Cu(100), & Cu(110). These values are now in very close agreement to the results of Pöllmann *et al.*, and provide a verification of both the experimentally determined desorption temperatures and the extreme dependence of this temperature on the crystal face of Cu.

4.5 Conclusions

The energetics of the molecular and dissociative adsorption of formic acid on Cu(111) were measured by SCAC. The enthalpy of formation and bond enthalpy of bidentate formate to

Cu(111) are -465 kJ/mol and 335 kJ/mol, respectively, at 240 K and 0.20 ML. Corresponding enthalpies are estimated for monodentate formate on Cu(111), which give an enthalpy of formation of -437 kJ/mol and a bond enthalpy of 307 kJ/mol. A comparison to DFT calculations in the literature shows that DFT systematically underestimated the bond enthalpies of mono- and bidentate formate to Cu(111). In comparison to experimental measurements on Pt(111) and Ni(111), these enthalpy values indicate that formate binds ~15 kJ/mol more strongly to Cu(111) than to Ni(111), and ~85 kJ/mol more strongly than to Pt(111).

At 240 K, the integral heat of the dissociative adsorption of formic acid on oxygen-predosed Cu(111) is well fit by $(99.1 - 46.8\theta)$ kJ/mol, which gives an integral (average) heat of 89.7 kJ/mol at 0.20 ML. The initial differential heat of adsorption is 99.1, which decreases linearly to 80.4 kJ/mol by 0.20 ML. At 120 K, the molecular adsorption of formic acid on clean Cu(111) has an initial differential heat of adsorption of 80.9 kJ/mol, which decreases to ~70 kJ/mol by 0.50 ML. Past that coverage, the heat remains at ~70 kJ/mol through 1.5 ML, after which it drops to a multilayer energy of 64.3 kJ/mol by 1.75 ML. Using the 120 K heat of adsorption curve measured out to multilayer coverages, we estimate the adhesion energy for liquid formic acid to Cu(111) to be 0.271 J/m^2.

These results can serve as important experimental benchmarks for DFT calculations and efforts to improve the energy accuracy of computational models. As formate is the simplest example of a carboxylate adsorbate, these results are applicable not only for systems with formate, but as well as other carboxylates and, more broadly, other oxygenates on Cu surfaces. These results further our understanding of fundamental energetic differences on catalyst surfaces, and can help explain differences in catalytic activity between late transition metal catalysts and guide the development of new catalysts and catalytic pathways.

Acknowledgements

The authors acknowledge support for this work by the National Science Foundation under grant number CBET-2004757.

4.6 Figures and Tables

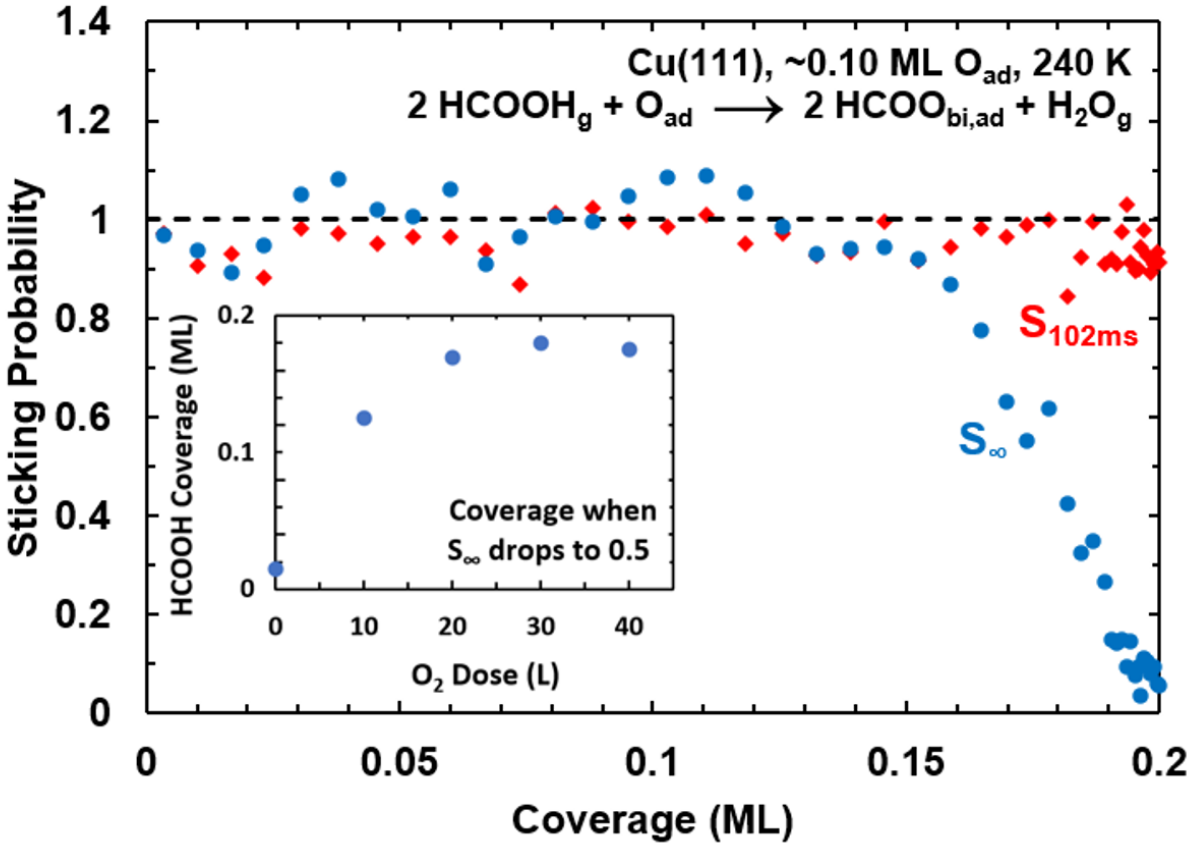

Figure 4.1 - Average short-term (red diamonds, S_{102ms}) and long-term (blue circles, S_∞) sticking probabilities of formic acid dissociatively adsorbing on Cu(111) at 240 K, predosed with 0.10 ML O_{ad}, as a function of the HCOOH-derived adsorbate coverage. Note that the first red diamond with S_{102ms} = 0.98 is nearly completed hidden under the first blue circle. A coverage of 1 ML is defined as one adsorbate per Cu(111) surface atom or 1.77×10^{19} $HCOO_{bi,ad}$ per m^2.

Inset: The HCOOH-derived adsorbate coverage at which S_∞ at 240 K drops to 0.50 (which closely tracks its saturation coverage) versus the pre-exposure of O_2 gas to clean Cu(111) at 240 K.

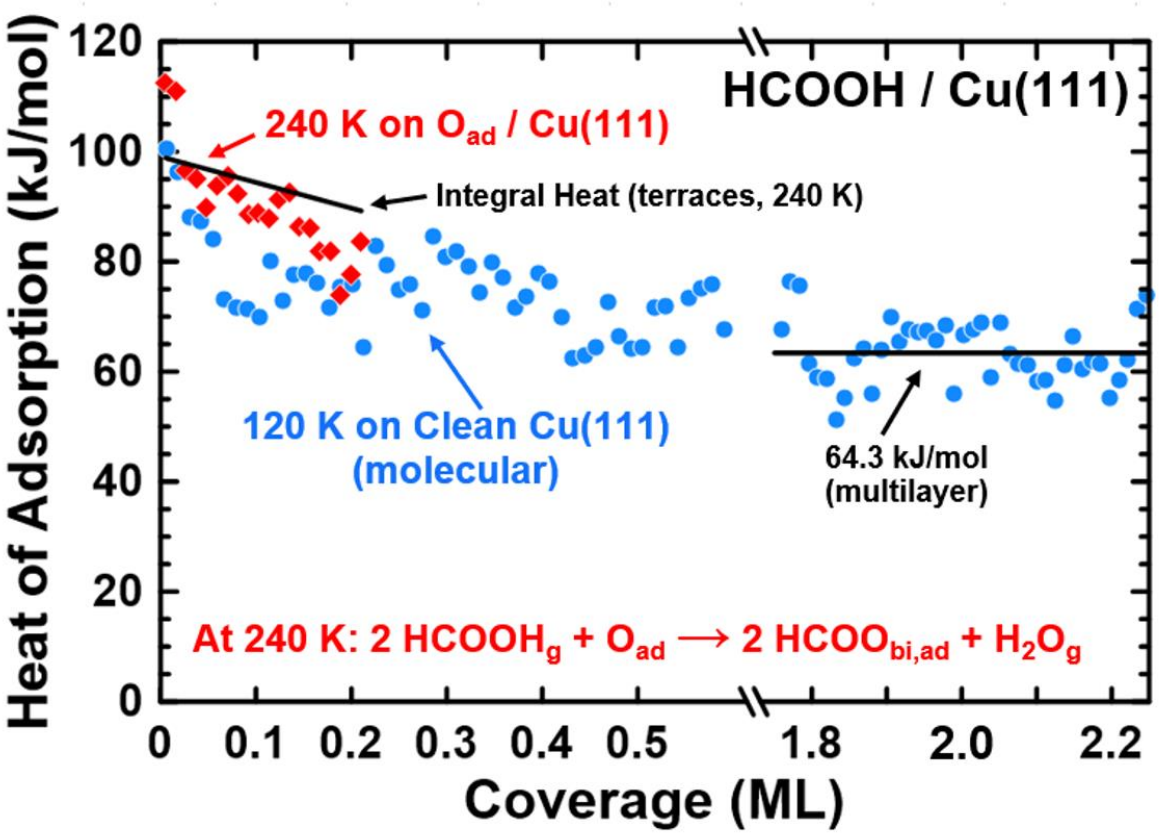

Figure 4.2 - Differential heats of adsorption of formic acid on clean Cu(111) at 120 K (blue circles) and O-predosed Cu(111) at 240 K (red diamonds) as a function of the HCOOH-derived adsorbate coverage. The average heat of molecular adsorption at the multilayer limit is shown by the black line through the 120 K data, giving 64.3 ± 2.9 kJ/mol. The integral heat of adsorption for 240 K is shown from the low coverage limit as the black line fit, (99.1−46.8θ) kJ/mol, giving 89.7 kJ/mol at saturation (θ = 0.20 ML). 1 ML = 1.77 × 1019 adsorbates per m^2.

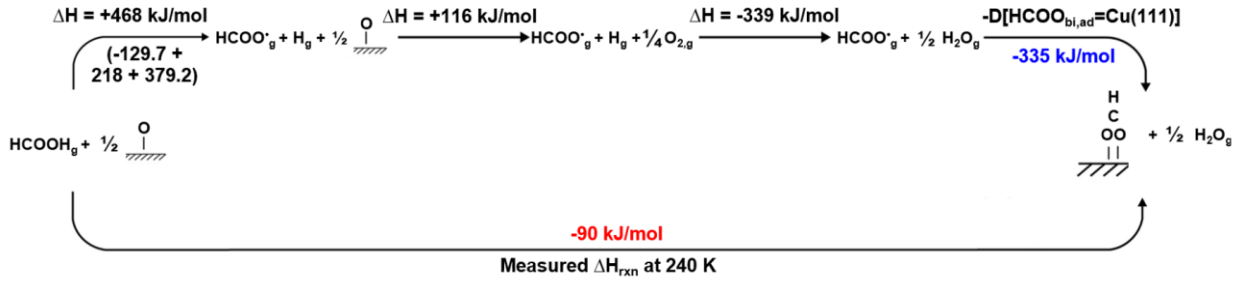

Figure 4.3 - Thermodynamic cycle used to determine the total bond enthalpy of bidentate formate to Cu(111) (formate gas to surface-bound bidentate formate) from the integral heat of dissociative formic acid adsorption at 240 K and 0.20 ML of formate (90 kJ/mol, shown in red). The top right-hand step shows the enthalpy to form bidentate formate from gas-phase formate radical, which provides an estimate of the total bond enthalpy of bidentate formate to Cu(111), from both its O-Cu bonds. Values in red are experimental values from this study, black are taken from literature as described in the text, and blue values are values that were extracted using this cycle.

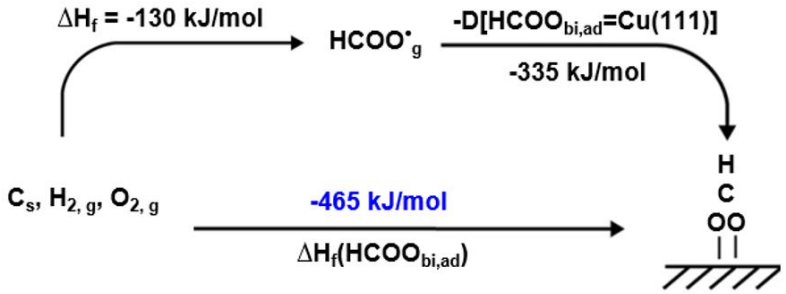

Figure 4.4 - Thermodynamic cycle used to determine the total enthalpy of formation of bidentate formate on Cu(111) using the total bond enthalpy extracted from the thermodynamic cycle above (Figure 4.3). The bottom pathway shows the total enthalpy to form surface-bound bidentate formate from elements in their standard states. Values in black are previously extracted values or tabulated enthalpies of formation as referenced in the text, and blue values are values that were extracted using this cycle.

Table 4.1 Comparison of the present calorimetric bond energies of bidentate and monodentate formate to the Cu(111) surface with calculated values using DFT.

Coverage	DFT Functional or method	$HCOO_{bi,ad}$ bond energy (kJ/mol)	$HCOO_{mono,ad}$ bond energy (kJ/mol)	Ref.
0.20 ML (1/5 ML)	Calorimetry	333-315	305-287	This paper
0.11 ML (1/9 ML)[a]	Calorimetry	337-319	309-291	This paper
DFT:	--	--	--	--
0.11 ML (1/9 ML)	RPBE	242	200	127
0.11 ML (1/9 ML)	PBE-DFT-D2	253	218	126
0.11 ML (1/9 ML)	PW91 / (PW91 with ZPE)	268, 266 / (253)	217 / (206)	38, 128
0.25 ML (1/4 ML)	GGA-PW91 / (GGA-PW91 with ZPE)	267 / (253)	224 / (210)	36

[a] As many DFT values reported here are calculated at 0.11 ML coverage, the experimentally determined bond enthalpy values of bidentate and monodentate formate to Cu(111) were also calculated at 0.11 ML in an identical manner to that at 0.20 ML but using the integral heat value at 240 K and 0.11 ML of 94 kJ/mol.

Table 4.2 Comparison of calorimetrically measured enthalpies of formation and bond enthalpies of monodentate and bidentate formate on Pt(111), Ni(111) and Cu(111). Also listed are DFT (PW91) bond energies for bidentate formate at 1/9 ML.

	Coverage (ML)	ΔH_f $HCOO_{mono,ad}$ (kJ/mol)	ΔH_f $HCOO_{bi,ad}$ (kJ/mol)	Bond enthalpy $HCOO_{mono,ad}$ (kJ/mol)	Bond enthalpy $HCOO_{bi,ad}$ (kJ/mol)	Bond enthalpy $HCOO_{bi,ad}$ (by DFT, kJ/mol)
Pt(111)	0.25	-345 (ref.[18])	-381 (ref.[18])	221 (ref.[155])	251 (ref.[18]) [a]	227 (ref.[128,157])
Ni(111)	0.143[b]	-422 (ref.[83])[c]	-449 (ref.[83])	292 (ref.[155])	320 (ref.[83])	270 (ref.[128])
Cu(111)	0.20	-(437-419)	-(465-447)	307-289	335-317	266 (ref.[128])

[a] The bond enthalpy of bidentate formate to Ni(111) was calculated from this listed enthalpy of formation of bidentate formate on Ni(111) using the known heat of formation of formate gas (-129.7 kJ/mol[147]). [b] Values for monodentate formate on Ni(111) were reported at 0.20 ML, while the other values are at 0.143 ML. [c] This enthalpy of formation of monodentate formate on Ni(111) was calculated from this listed bond enthalpy of monodentate formate to Ni(111) (292 kJ/mol[155], estimated from the calorimetry date measured previously[83]), using the known heat of formation of formate gas (-129.7 kJ/mol[147]).

Table 4.3 Summary of adsorption energies taken from DFT,[154] and the resulting calculated reaction enthalpies and predicted TPD desorption peak temperatures for H2O desorption from Cu(111), Cu(100), & Cu(110), compared to published TPD results.[142]

Crystal Surface:	**Cu(111)**	**Cu(100)**	**Cu(110)**
$\Delta E_{ads,DFT}$ of OH_{ad} (kJ/mol) (ref.[154])	-315	-389	-349
$\Delta E_{ads,DFT}$ of O_{ad} (kJ/mol) (ref.[154])	-488	-524	-509
$\Delta E_{ads,DFT}$ of H_2O_{ad} (kJ/mol) (ref.[154])	-21	-24	-37
$\Delta H_{rxn,DFT}$ for: $2\ OH_{ad} \rightarrow H_2O_g + O_{ad}$ (kJ/mol)	70	83	119
$\Delta H_{rxn,DFT}$ for: $2\ OH_{ad} \rightarrow H_2O_{ad} + O_{ad}$ (kJ/mol)	49	59	82
Predicted T_{max} for H_2O desorption (K)	244	286	407
Predicted T_{max} if $\Delta H_{rxn} = (0.70*\Delta H_{rxn,DFT})$ (K)	173	202	287
T_{max} from TPD (K) (ref.[142])	160	220	290

Chapter 5 Acetonitrile Adsorption and Adhesion Energies onto the Pt(111) Surface by Calorimetry

This chapter has been reprinted with permission from Ref 50:

Ruehl, G., Harman, S. E., Arnadottir, L., & Campbell, C. T. Acetonitrile Adsorption and Adhesion Energies onto the Pt (111) Surface by Calorimetry. *ACS Catalysis* **12,** 156-163 (2002).

Chapter Abstract

Acetonitrile is a common solvent for heterogeneous catalysis and electrochemical applications, as well as the simplest example of an organic nitrile. Understanding the energetics and nature of its interactions with Pt(111) is of interest for a wide array of applications, especially for estimating the effect of acetonitrile as a solvent on the adsorption energies of catalytic and electrocatalytic reaction intermediates on Pt-group metals. Here, the heat of adsorption of molecular acetonitrile on clean Pt(111) was measured by single-crystal adsorption calorimetry (SCAC) as a function of coverage, and from that, the adhesion energy of liquid acetonitrile to Pt(111) was estimated. At 180 K, the differential heat of adsorption is initially 82.9 kJ/mol, decreasing to 63.2 kJ/mol by a saturation coverage of 0.25 ML. The integral (average) heat of adsorption at 180 K is 74.3 kJ/mol at a saturation coverage of 0.25 ML. At 100 K, the heat of adsorption is 84.5 kJ/mol initially, decreases to ~45 kJ/mol after the completion of the first layer (0.35 ML), and finally reaches a constant multilayer heat of 43.4 kJ/mol at coverages higher than 0.7 ML. (Errors bars on all heats are ±4%.) The saturation coverage is higher at 100 K than 180 K, attributed to the formation of a less stable adsorbate configuration at

100 K due to lower surface mobility. Using the heats of adsorption at 100 K up to bulklike multilayer coverages, we estimate the adhesion energy for liquid acetonitrile to Pt(111) to be 0.198 J/m^2, which can be used to estimate the effect of acetonitrile as a solvent on the adsorption energies of catalytic reactants relative to the gas phase. This adhesion energy is considerably lower than those for water, benzene, and phenol on Pt(111) but slightly greater than those for methanol and formic acid.

5.1 Introduction

Due to its wide use as a solvent, the interactions of acetonitrile with Pt surfaces are important in electrochemistry and electrocatalysis. As the simplest example of an organic nitrile, a fundamental understanding of its interactions with Pt(111) is also of general interest to surface chemistry and catalysis. Here, we report calorimetric measurements of adsorption energies versus coverage of molecularly adsorbed acetonitrile on clean Pt(111) at 100 and 180 K and estimate from these the adhesion energy of liquid acetonitrile to Pt(111) at room temperature. Most importantly, this adhesion energy can be used to estimate the adsorption energies of catalytic reaction intermediates on Pt(111) in an acetonitrile solvent based on energies measured (or calculated) in the gas phase. This is done using an equation we recently developed that shows that the difference in adsorption energy in a liquid solvent relative to the gas phase is dominated by the product of this solvent adhesion energy times the footprint area of the adsorbed intermediate on the surface.[28,29] Since there is vast knowledge already of adsorption energies on Pt-group metals in the gas phase, but very few such energies are known in liquid solvents, this opens up important new opportunities to gain fundamental insights into catalysis in liquid solvents and electrocatalysis.

Acetonitrile is a polar, organic solvent commonly used in a number of chemical reactions and synthesis processes. Its high dielectric constant and aprotic nature make it an attractive electrolyte solvent in electrochemical reactions and electrocatalysis,[40–45] as well as in batteries and capacitors.[46–49] Its low viscosity and high miscibility with a wide variety of polar solvents and solutes makes it promising for applications in many other areas of heterogeneous catalysis including biofuels synthesis and biomass-based chemical upgrading, as well as the engineering of optimal mixed solvent environments.[50,161–165] The measurement here of its adhesion energy to

a Pt-group metal, and the use of that value to estimate the adsorption energies of catalytic and electrocatalytic reaction intermediates on that and other Pt-group metal surfaces, which generally have similar molecular adsorption and adhesion energies to Pt,[30,166,167] will aid in developing a basic understanding of those important reactions, their mechanisms, and their reaction energy diagrams.

Platinum, in addition to its widespread use as a heterogeneous catalyst in numerous industrial processes, is a common electrode material for electrochemical applications. Therefore, elucidating the energetics and nature of the interaction between acetonitrile and the Pt surface is of great interest. Pt(111) is the most thermodynamically stable face of platinum and is consequently commonly used as a model catalyst. Previously, experimental results from temperature-programmed desorption (TPD) and vibrational spectroscopy (RAIRS) studies have shown that acetonitrile will form multilayers at low temperatures (<150 K) but only forms a single, molecularly adsorbed adlayer from 150 to ∼200 K.[168] The adsorption of acetonitrile on Pt(111) has also been studied by density functional theory (DFT).[169–171] Here, we report the enthalpies of adsorption for acetonitrile to clean Pt(111) at 100 and 180 K, determined in ultrahigh vacuum conditions using single-crystal adsorption calorimetry (SCAC). These results, when combined with those recent RAIRS, TPD, and DFT studies, provide detailed insight into the nature and energy of surface adsorption and interaction of acetonitrile with Pt(111). Enthalpies of adsorption for acetonitrile to clean Pt(111) have also been studied by SCAC previously, but only at 298 K,[170] where later TPD studies show that the first layer is already desorbed almost completely.[168] The highly accurate adsorption energy and estimated adhesion energy of acetonitrile on Pt(111) reported here are the first such values reported for any nitrile-containing molecule on any Pt-group metal surface, and as such, they serve as important

benchmarks for validating the energy accuracy of computational methods (like density functional theory) used to estimate these energies when nitrile groups are involved. In addition, a recently developed method by this group has enabled the extraction of solvent adhesion energies from SCAC measurements of adsorption energies in ultrahigh vacuum (UHV).[30] Below, we use this method to extract and report the adhesion energy of liquid acetonitrile to the Pt(111) surface. This adhesion energy can in turn be used to quantitatively estimate the effect of this important solvent on the adsorption energies of catalytic reaction intermediates, as described previously.[28,29] This knowledge is of interest for efforts to utilize solvent properties to tune intermediate energetics and interactions with the catalyst surface and consequently affect reaction rates and selectivities in liquid solvents.

5.2 Experimental Methodology

The experiments were performed in an ultrahigh vacuum (UHV) chamber (base pressure $<2 \times 10^{-10}$ mbar) designed for single-crystal adsorption calorimetry (SCAC). The chamber is also equipped with X-ray photoelectron spectroscopy (XPS), low-energy electron diffraction (LEED), Auger electron spectroscopy (AES), low-energy ion-scattering spectroscopy (LEIS), a quadrupole mass spectrometer (QMS), and a liquid-nitrogen-cooled quartz crystal microbalance (QCM). The SCAC apparatus and experimental procedures for the molecular beam flux, sticking probability, and heat measurements have been described in depth previously.[24,68,85]

To briefly summarize, the Pt(111) sample used was a 1 μm thick single-crystal foil provided by Bine Hansen at Aarhus University. The surface was cleaned by repeated cycles of Ar^+ ion sputtering and annealing to 1120 K. The Pt(111) surface was exposed to a pulsed, collimated molecular beam of acetonitrile, and the heat of adsorption and sticking probability

were recorded simultaneously. The sticking probability was measured with a QMS using the King and Wells method,[70] and the heat of adsorption was measured by a pyroelectric ribbon pressed against the back of the Pt(111) crystal. The molecular beam was created by expanding approximately 1.5 mbar of acetonitrile through a glass capillary array and collimated through a series of orifices that are cooled with liquid nitrogen. The resulting molecular beam is then chopped into 102 ms pulses every 3 s.

Here, one monolayer of coverage is defined as the number of molecules of acetonitrile adsorbed to the surface per unit area, normalized to the density of Pt atoms on the (111) surface (1.50×10^{19} atoms/m^2). A typical dose is 0.005 ML ($\sim 1.0 \times 10^{12}$ molecules within the beam diameter of ~4 mm) per acetonitrile gas pulse.

5.3 Results

5.3.1 Sticking Probabilities

Figure 5.1 shows the average long-term (S_∞) and short-term (S_{102ms}) sticking probabilities versus coverage for acetonitrile adsorption on clean Pt(111) at 180 K. The long-term sticking probability is the probability that a gas molecule strikes the sample surface, sticks, and remains until the next gas pulse starts 3 s later. This is used to calculate the adsorbate coverage remaining at the start of the next gas pulse. The short-term sticking probability is the probability that a gas molecule strikes the sample surface, sticks, and remains at least throughout the time window of the heat measurement (i.e., the first 102 ms). This is used to calculate the number of moles of gas-phase reactants that contribute to the measured heat of adsorption.

At 180 K, the long-term and short-term sticking probabilities were indistinguishable below 0.23 ML. They both start at a probability of ~0.98 and decrease with coverage to ~0.88

by 0.23 ML. Past this coverage, the long-term sticking probability drops off rapidly, reaching zero by 0.25 ML, while the short-term sticking probability remains high (>0.80). This indicates that the adsorption of acetonitrile on Pt(111) saturates by a coverage of 0.25 ML at 180 K; however, acetonitrile continues to transiently adsorb on that adlayer with a high probability but desorbs again completely (but slowly) before the next pulse starts 3 s later.

Accurate determination of the long-term sticking probabilities at 180 K and high coverage was complicated by adsorption and desorption of acetonitrile on the walls of the vacuum chamber. Molecules that did not adsorb left the Pt surface and adsorbed transiently on the chamber walls, with a residence time on the same scale of the 3 s pulse period. This resulted in a mass spectrometer signal that was a combination of the "real" signal coming from molecules directly leaving the Pt surface and the "background" signal of molecules desorbing from the chamber walls. Accurately distinguishing between these two signals was impossible without using a simple assumption based on previous TPD measurements. Those TPD results showed that more than a single layer will not build up at 180 K,[168] and therefore the long-term sticking probability must drop to zero upon saturation of the first layer at 180 K. We used this to more accurately estimate the background signal of the mass spectrometer, chosen such that the long-term sticking probability decreases to zero after saturation at 180 K. As seen in Figure 5.1,this steep drop occurs at a coverage of ~0.25 ML. This measured long-term sticking probability was then applied to the heat measurements to calculate accurate coverages.

At 100 K, the short-term sticking probability starts at 0.98 and increases to unity within <1% by 0.15 ML. The long-term sticking probability is the same as the short-term sticking probability within error bars (~1%) at all coverages. As this temperature is cold enough to form

multilayers of acetonitrile on the Pt(111) surface, the sticking probabilities remain at unity through the formation of at least five multilayers.

5.3.2 Heats of Adsorption

In this paper, the term "heat of adsorption" is defined as the negative of the standard molar enthalpy change for the adsorption reaction, with the gas and the sample surface being at the same temperature. As explained in detail previously, this requires a small enthalpy correction on the measured heat since the gas molecule's enthalpy at this temperature is slightly different than a Boltzmann distribution at the sample temperature due to the actual experimental molecular beam conditions.[85] The differential heat of adsorption is the heat released per mole when a small increment of adsorbate is added to the surface at nearly fixed coverage, as occurs in one of our molecular beam pulses during SCAC. The integral heat of adsorption is the integral of the differential heat versus coverage from zero up to the coverage of interest, divided by that coverage, and is thus the average heat for that coverage range.

Figure 5.2 shows the differential heat of adsorption for acetonitrile on Pt(111) at 180 K (red) and 100 K (blue) (after this small correction to the raw heats) as a function of total acetonitrile coverage, along with the integral heat of adsorption at 180 K (black). These are the averages of eight and six runs at 100 and 180 K, respectively.

Previous results from literature show that acetonitrile molecularly adsorbs on Pt(111) below ~250 K, and multilayers will adsorb to the surface below 150 K.[168] Thus, calorimetric measurements here correspond to molecular adsorption on Pt(111), with multilayers of acetonitrile forming during the 100 K experiments but not at 180 K. The initial heat of adsorption at 100 K is 84.5 kJ/mol, which decreases until reaching ~45 kJ/mol by ~0.35 ML.

The heat then remains constant through ~0.7 ML, before dropping slightly to a final multilayer heat of 43.4 ± 1.7 kJ/mol. (This is the run-to-run average and standard deviation of the multilayer heats of the eight runs.) Each run's multilayer heat is the pulse-to-pulse average heat for coverages above 0.8 ML. This average multilayer heat is close to the heat of sublimation of bulk acetonitrile of 46.8 kJ/mol at 100 K, estimated from literature values for the enthalpies of phase transitions[147,172] along with heat capacities of solid, liquid, and gaseous acetonitrile,[173] as a heat of sublimation at 100 K was not available in literature. Given the error bars in this estimate, the measured heat is probably within the combined error bars. This multilayer heat is also within the error bars of the value from the activation energy of desorption of 44 ± 3 kJ/mol calculated from TPD (discussed further below).[168] The agreement with these values provides some estimation of the absolute accuracy of the results in Figure 5.2. This is consistent with our previous estimate of the accuracy of the absolute calibration of this calorimeter's heat measurement of 3%.[166]

The heat of adsorption at 180 K is initially 82.9 kJ/mol, decreasing to 63.2 kJ/mol by a coverage of ~0.25 ML. After this point, the long-term sticking probability has dropped to zero, indicating that the monolayer of adsorbed acetonitrile has become saturated. Any additional molecules that impinge on the surface adsorb transiently (as indicated by the high short-term sticking probability) but fully desorb before the start of the next pulse 3 s later. The integral heat of adsorption at 180 K is shown in black versus coverage, as fit by (82.9–34.4θ) kJ/mol, where θ is coverage in ML, with a heat of 74.3 kJ/mol at saturation (0.25 ML).

We estimate the saturation coverage of the adsorbate layer at 180 K to be 0.25 ML. (The midpoint of the steep drop off in the long-term sticking probability in Figure 5.1 occurs at 0.248 ML.) This is in excellent agreement with the coverage of one-fourth that corresponds to an ideal (2 × 2) overlayer with one acetonitrile molecule for every four Pt surface atoms. This is

supported by a previous study that used low-energy electron diffraction (LEED) and found the presence of a (2 × 2) overlayer for acetonitrile adsorbed on Pt(111) up through the coverages of 0.19 ML, though this pattern was replaced by the absence of long-range order by the next coverage studied of 0.36 ML and the experimental temperature was not reported.[174] Additionally, the Somorjai group found the acetonitrile saturation coverage on Ni(111) at 190 K to also be a (2 × 2) overlayer using LEED.[175] As seen in Figure 5.1, the first layer seems to complete at 100 K at a higher coverage, or ~0.35 ML.

Although the initial heat of adsorption is slightly higher at 100 K than at 180 K (84.5 vs 82.9 kJ/mol), the difference is within the error bars associated with absolute heat calibration (<±4%), and thus, the heat capacity is too small to measure accurately.

5.4 Discussion

5.4.1 Comparison to Temperature Programmed Desorption

Figure 5.3 compares the activation energy for desorption (E_{des}) of acetonitrile from Pt(111) versus acetonitrile coverage as determined from the heats measured here at 180 K from Figure 5.2 (black dots, corrected as needed by subtracting 1/2RT[22]) to that from the TPD study of Tylinski et al.[168] (The temperature *T* we used for this 1/2RT correction was 220 K, the midpoint of the monolayer TPD peak.) The smooth curve was determined by Tylinski et al. from the inversion of their TPD spectra for acetonitrile desorption from Pt(111) at different coverages, assuming the Polanyi–Wigner rate equation with a prefactor of $\nu = 10^{16}$ s^{-1} (which they assumed to be the same as that obtained from the Arrhenius fit of their multilayer desorption rates in TPD).

The bottom *x*-axis coverage (per Pt surface atom) here is defined relative to the surface density of Pt atoms on the (111) surface (1.50×10^{19} atoms/m^2), as in Figure 5.1 and Figure 5.2. The top *x*-axis coverage ($ML_{Tylinski}$) was defined by Tylinski et al. such that 1.0 $ML_{Tylinski}$ is the highest coverage of acetonitrile before the multilayer peak first appears in the TPD spectra after dosing at 20 K. (One can see this was their definition of "ML" by inspection of the TPD spectra in Figure 2 of their paper.) Even though the submonolayer peak is near saturation at that coverage, it is clear from careful inspection that it continues to grow at higher coverages, so that the first layer is not complete until a higher coverage than 1.0 $ML_{Tylinski}$. Instead, it seems more logical that in that study, the first layer was completed at the midpoint of the 10–15 kJ/mol drop in E_{des} with coverage they reported at 1.2–1.5 $ML_{Tylinski}$. As shown above, the first layer completes at a coverage of ~0.25 acetonitrile molecules per Pt surface atom. We have thus adjusted the coverage axes in the two curves in Figure 5.3 such that 1.28 $ML_{Tylinski}$ corresponds to 0.25 acetonitrile molecules per Pt surface atom.

As seen, with this adjustment, desorption energies versus coverage from the calorimetry results are in excellent agreement with those determined by TPD. The discrepancy at very low coverages is likely due to a higher concentration of surface defects (step sites) for the Pt(111) surface used for TPD than that used for calorimetry. Further, the multilayer heat of 43.4 ± 1.7 kJ/mol obtained from calorimetry is within the error bars of the activation energy of 44 ± 3 kJ/mol determined by Tylinski et al. from leading-edge analysis of the multilayer desorption peak (which can be corrected to a heat of adsorption by adding 1/2RT = 0.47 kJ/mol with T = 140 K). The strong agreement of these results provides a convincing confirmation of each study. Collectively, the combination of energetic data from calorimetry and structural information from

RAIRS performed by Tylinski et al. provides detailed insight into the nature and energy of surface adsorption and interaction of acetonitrile with Pt(111).

The adsorption of acetonitrile on Pt(111) was studied previously by SCAC but only at 298 K by Shayegi et al.[170] The initial heat of adsorption reported there at 298 K (87 kJ/mol) is very close to that measured here at 100 and 180 K in Figure 5.2 (83–85 kJ/mol). However, the heat drops much more rapidly with coverage in those results at 298 K, and the saturation coverage (~0.18 ML) is lower. It is very clear from looking at the TPD spectra for acetonitrile on Pt(111) presented in Tylinski et al.[168] that most of the first layer of molecularly adsorbed acetonitrile desorbs well below 298 K, so it is not clear what species Shayegi et al. were producing above ~0.05 ML. That SCAC study at 298 K[170] did not present the long-term and short-term sticking probabilities versus coverage, so it is difficult to assess how to interpret those data.

5.4.2 Monolayer Saturation Coverage

In the heats of Figure 5.2, saturation of the first layer appears to occur much later in the 100 K data, at a coverage of ~0.35 ML, than at 180 K (0.25 ML). This can be explained by a closer analysis of acetonitrile adsorbate configurations, along with the lower surface mobility at 100 K which limits the ability for adsorbed molecules to arrange themselves in the most energetically stable configurations compared to those at 180 K. This also explains why the heat from ~0.2 to 0.25 ML is lower at 100 K than at 180 K in Figure 5.2.

Previous work using RAIRS,[40,168,176] EELS,[177] and computational methods[169–171] showed that the most stable orientation of the adsorbed acetonitrile molecule on Pt(111) is a bridged structure, referred to as the μ-configuration. This configuration was observed at temperatures as

low as 60 K but is the dominant surface configuration observed above 110 K in vacuum.[168] In this configuration, the C≡N triple bond becomes a C═N double bond, and new C–Pt and N–Pt bonds are formed, leaving the methyl group oriented away from the surface. Further, DFT calculations[169–171] suggest that the second most stable orientation, referred to as the N-top configuration, is bound to a single Pt surface atom via the lone pair on the N atom, with the acetonitrile molecule oriented perpendicularly to the plane of the surface. The N-top configuration thus requires a smaller area on the surface than the μ-configuration. The N-top configuration was observed from 60 to 110 K by RAIRS but was only present above 110 K in vacuum at coverages nearing and above saturation of the first layer (above 1 $ML_{Tylinski}$ or 0.19 ML per Pt surface atom).[168] At the highest temperature, they studied by RAIRS below 110 K (i.e., 60 K), there is not enough thermal energy for the adsorbates to overcome the activation barrier for the formation of the μ-configuration, and by coverages nearing the completion of the first layer, stearic constraints are present.[168] Additionally, SFG measurements for acetonitrile in the liquid phase at a Pt electrode interface also observed the formation of the N-top configuration due to stearic constraints introduced by the presence of solvents (ethanol, methanol, or water).[41,178]

At 100 K in UHV, all incoming acetonitrile molecules adsorb when they hit the surface, regardless of the local surface coverage where they hit, as evidenced by the unity sticking probability at high coverage. The heat stays much higher than in the second layer up to at least 0.25 ML (Figure 5.2), implying that they transiently adsorb when landing on top of preexisting adsorbates and diffuse rapidly to find an adsorbate-free site to bind strongly to the Pt atoms below, as commonly occurs when organic molecules adsorb on late transition-metal surfaces.[3] As the first adsorbate layer nears saturation, stearic constraints arise which inhibit the formation

of the μ-configuration, which requires multiple adjacent, unoccupied Pt surface atoms. This surface temperature is apparently cold enough to both prevent desorption as well as prevent μ-bonded molecules from moving apart to create larger free metal sites to accommodate the more favorable μ-configuration. So, some molecules only have enough space to form the N-top configuration. The resulting surface adlayer is a combination of μ and N-top configurations, enabling the formation of a higher-density first layer that saturates by ~0.35 ML. This is consistent with RAIRS data showing the presence of both configurations on Pt(111) at 120 K at coverages near and above saturation of the first layer.[168]

In contrast, the saturation coverage at 180 K is only 0.25 ML. As the first layer nears saturation at 180 K, any incoming adsorbate molecules that land at a less favorable site can migrate to a more favorable site or wait until thermal fluctuations create more open space to allow it to convert to the most stable μ-configuration. Again, RAIRS data observed the formation of the N-top configuration only below 110 K or at coverages higher than a single layer, but never at 180 K, which is too hot to form more than a single layer.[168] Thus, thermal motion at 180 K enables the formation of an adsorbate layer dominated by the more stable μ-configuration, as seen in literature for adlayers deposited over the range of 120–140 K.[168] This results in a less densely packed first layer that not only saturates by 0.25 ML but also makes the higher temperature (180 K) results in Figure 5.2 a more accurate approximation of the most stable structure of the first layer and its heat versus coverage. DFT calculations have shown that the μ-configuration is stable at a coverage of 0.25 ML (i.e., one per 2 × 2 unit cell),[169–171] consistent with the saturation coverage we measure here at 180 K of 0.25 ML. This is further supported by LEED studies that have observed a (2 × 2) overlayer structure for acetonitrile adsorbed on Pt(111) and Ni(111). On Pt(111), the (2 × 2) overlayer was observed up through coverages of

0.19 ML but was no longer present by a coverage of 0.36 ML.[174] For Ni(111), the acetonitrile saturation coverage at 190 K was found to be a (2 × 2) overlayer.[175]

5.4.3 Adhesion Energy

Given how commonly acetonitrile is used as a solvent, determination of the adhesion energy of liquid acetonitrile on Pt(111) can provide valuable insight into the energetics of the liquid–solid interface. It has been shown that solvent–metal adhesion energies are the dominating factor that determines differences in reactant adsorption energies in different solvents or in any solvent relative to gas-phase adsorption energy measurements.[28,30] Solvent adhesion energies allow one to quantitatively estimate the effects of different solvents on the adsorption energies of catalytic reaction intermediates.[28] Thus, it is highly desirable to measure the adhesion energy of acetonitrile to Pt(111) to enable the prediction of adsorption energies of molecules to Pt(111) in an acetonitrile solvent. However, there is currently no way to directly measure the adhesion energy of a liquid solvent to a clean metal surface.

To estimate this adhesion energy, we will employ a recently developed method from this group.[28,30] This method used a standard thermodynamic cycle to derive a relationship between the adhesion energy of a solvent and the experimentally determined differential heat of adsorption data like that in Figure 5.2. Notably, this requires heat versus coverage measurements out to multilayer coverages of the solid solvent and that the coverage has known absolute units. This derived relationship is presented in equation 5.1, where $E_{adh,S(liq)/M(s)}$ is the adhesion energy of the liquid solvent to the solid metal and $\gamma_{S(liq)}$ is the surface energy of the liquid solvent at its gas or vacuum interface[30]

$$E_{adh,S(liq)/M(s)} = [Q_{adsorption} - n \cdot \Delta H_{vap,S}]/A + 2\gamma_{S(liq)} \quad (5.1)$$

As shown in this derivation,[30] $\gamma_{S(liq)}$ is multiplied by 2 here because, in the thermodynamic cycle used there, the first step is to produce (from gas molecules) a free-standing liquid slab, whose energy is higher than bulklike liquid by $\gamma_{S(liq)}$ times the area of *both* the top and the bottom surfaces of the slab. The term $[Q_{adsorption} - n \cdot \Delta H_{vap,S}]/A$ here is equal to the integrated area from zero coverage up to a (bulklike) multilayer coverage (with n moles adsorbed per area A) of the heat-versus-coverage curve ($Q_{adsorption}$) minus n/A times the molar heat of vaporization of the liquid solvent ($\Delta H_{vap,S}$). Ideally, these values would all be measured at room temperature to provide the adhesion energy at room temperature. Since $Q_{adsorption}$ can only be measured on a clean metal surface in ultrahigh vacuum, which is only possible for acetonitrile at temperatures where the solvent grows as solid films rather than liquid films, the assumption was made that the term $[Q_{adsorption} - n \cdot \Delta H_{vap,S}]/A$ at room temperature is approximately equal to the analogous quantity at experimental temperatures where the solvent is a solid, or $[Q_{adsorption} - n \cdot \Delta H_{sub,S}]/A$, where $\Delta H_{sub,S}$ is the heat of sublimation of bulk acetonitrile (see references[28,30] for justification of this assumption). We evaluate this quantity from the heat data in Figure 5.2 at 100 K as its integrated area above the solid horizontal line shown (at the bulk heat of sublimation). This is equivalent to assuming that the difference in the heat capacities (including the heat of fusion) between the first and subsequent layers of acetonitrile is negligible when heating from 100 to 300 K.

Using this method and the reported surface tension of bulk, liquid acetonitrile of $\gamma_{S(liq)}$ = 0.02866 J/m^2,[158] we calculate the adhesion energy of liquid acetonitrile to the Pt(111) surface at 100 K to be E_{adh} = 0.198 J/m^2. Comparatively, this value is slightly greater than the adhesion energies of formic acid and methanol to Pt(111) (0.162 and 0.168 J/m^2, respectively) but considerably below that of water, benzene, and phenol (0.273, 0.447, and 0.468 J/m^2,

respectively).[30] Understanding this adhesion energy, and particularly how it compares to other common solvents, could enable the intelligent selection among these solvents, or mixtures thereof, to tune reaction environments to have more desirable energetics for surface adsorption or desorption for catalytic reactants and intermediates. We note that these adhesion energies were all estimated using the same assumption of a negligible difference in heat capacities (including the heat of fusion) between the first and subsequent layers, and the errors associated with this assumption are possibly large (~25%). However, all of these errors are probably qualitatively similar, so these trends in E_{adh} values will remain. It is expected that computational approaches could provide estimates of the corrections needed for this heat capacity approximation.

We next show that this acetonitrile/Pt(111) adhesion energy can be used to estimate the adsorption energy of uncharged adsorbed catalytic reaction intermediates on Pt(111) in liquid acetonitrile solvent based on their far better-known values in the gas phase. The adsorption energy in acetonitrile is approximately equal to the gas-phase adsorption energy minus this adhesion energy times the area occupied on the surface per mole of the adsorbate. This is based on a bond-additivity type model which was used recently to derive a relationship between the adsorption energy of an adsorbate in a gas phase and the adsorption energy of that adsorbate in a liquid solvent.[28] Utilizing a thermodynamic cycle, a constant was derived to quantify the difference in these adsorption energies as a result of the presence of a solvent. This model was originally only for flat adsorbates (like benzene and phenol), but it was recently extended to adsorbates of arbitrary shape.[29] This relationship is presented below in equation 5.2, where $\Delta U_{ads,R(solvent)}$ is the adsorption energy of the adsorbate in a solvent, $\Delta U_{ads,R(gas)}$ is its adsorption energy in a gas phase, and the remaining bracketed term is the constant[29]

$$\Delta U_{ads,R(solvent)} = \Delta U_{ads,R(gas)} + \left[E_{ads,S/M} + \frac{\Delta U_{solvation,R(gas)}}{\sigma_{tot}} - \gamma_{S(liq)}\right]\sigma_R \qquad (5.2)$$

The difference in adsorption energy is composed of the adhesion energy of the solvent to the surface ($E_{adh,S/M}$), the gaseous adsorbate's solvation energy per unit molecular area ($\Delta U_{solvation,R(gas)}/\sigma_{tot}$), and the solvent's surface energy ($\gamma_{S(liq)}$), all multiplied by the footprint area of the adsorbate on the surface (σ_R). This equation is independent of the shape of the adsorbate other than the fact that the shape determines the ratio of the total outer surface area of the adsorbate (σ_{tot}) and the footprint of the adsorbate on the surface upon adsorption (σ_R). This constant is dominated by the solvent adhesion energy term, as the remaining terms are smaller, opposite in sign, and nearly cancel. The errors on this estimated constant are probably rather large (up to 30%), but we expect that it will capture the trends with changing solvents and adsorbates reasonably well. The determination of the adhesion energy of acetonitrile on Pt(111) therefore allows for the quantification of this constant and consequently the effect of acetonitrile as a solvent on the adsorption energy of any adsorbing species on Pt(111) for which the gas-phase adsorption energy is known. This model, combined with this adhesion energy, provides a powerful tool for improving the understanding and computational models for liquid-phase reactions on Pt(111) that use acetonitrile as a solvent, and in combination with previously published values for other solvents and catalyst surfaces,[29,30] liquid-phase heterogeneous catalysis in general.

5.5 Conclusions

The energetics of molecular adsorption of acetonitrile on Pt(111) were measured by SCAC, as a function of coverage. At 180 K, the integral heat of adsorption is 74.3 kJ/mol at a saturation coverage of 0.25 ML and well fit at lower coverages by (82.9–34.4θ) kJ/mol. At 180 K, the initial differential heat of adsorption is 82.9 kJ/mol, which decreases to 63.2 kJ/mol by 0.25 ML. At 100 K, the initial heat of adsorption is 84.5 kJ/mol, which decreases to ~45 kJ/mol

at the completion of the first layer (0.35 ML), and finally drops to a multilayer heat of 43.4 kJ/mol above coverages of 0.7 ML. This difference in saturation coverage of the first layer at 100 versus 180 K is a result of the formation of two different surface adsorbate configurations, μ and N-top, with the former being more energetically favorable but the latter arising in the presence of stearic constraints, which are present at 100 K due to lower adsorbate mobility across the surface. These present results agree well with recent TPD and RAIRS studies, and collectively these results provide a clear understanding of the nature of the interaction between acetonitrile, the simplest organic nitrile, and Pt(111).

Using the 100 K heat of adsorption curve measured out to multilayer coverages, we estimate the adhesion energy for liquid acetonitrile to Pt(111) to be 0.198 J/m^2. This is slightly higher than that of formic acid and methanol to Pt(111) but considerably lower than that of water, benzene, and phenol. This adhesion energy is useful for estimating the effects of acetonitrile as a solvent on the adsorption energies of catalytic reaction intermediates of interest in liquid-phase catalytic and electrocatalytic reactions.

Acknowledgements

The authors acknowledge support for this work by the National Science Foundation under grant number CBET-2004757.

5.6 Figures

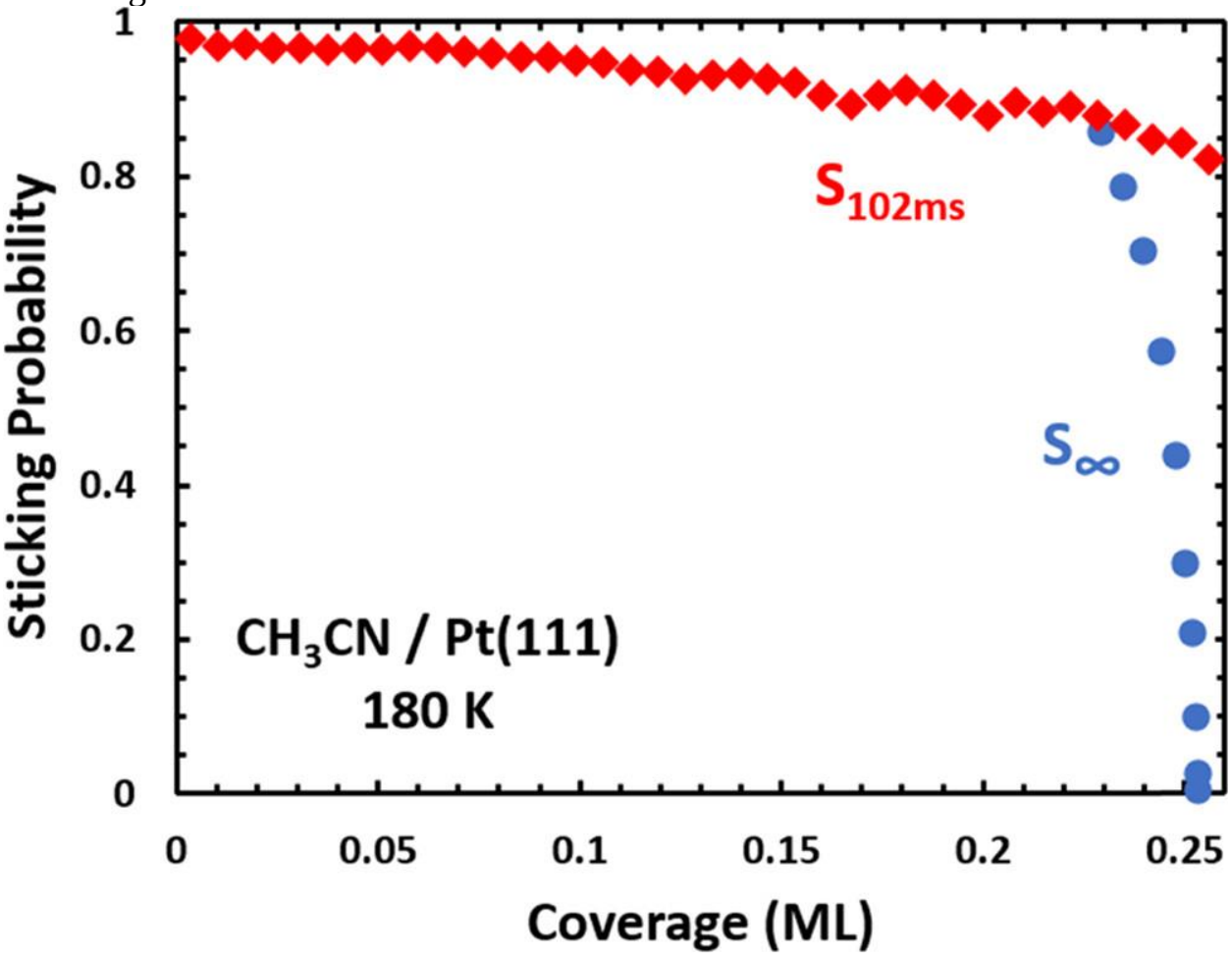

Figure 5.1 - Average short-term (red, S_{102ms}) and long-term (blue, S_{∞}) sticking probabilities of acetonitrile on Pt(111) at 180 K as a function of acetonitrile coverage. A coverage of 1 ML is defined as one adsorbate per Pt(111) surface atom or 1.50 × 1019 adsorbates/m^2. The short-term and long-term sticking probabilities were indistinguishable (within the noise) below 0.23 ML, so only one is shown.

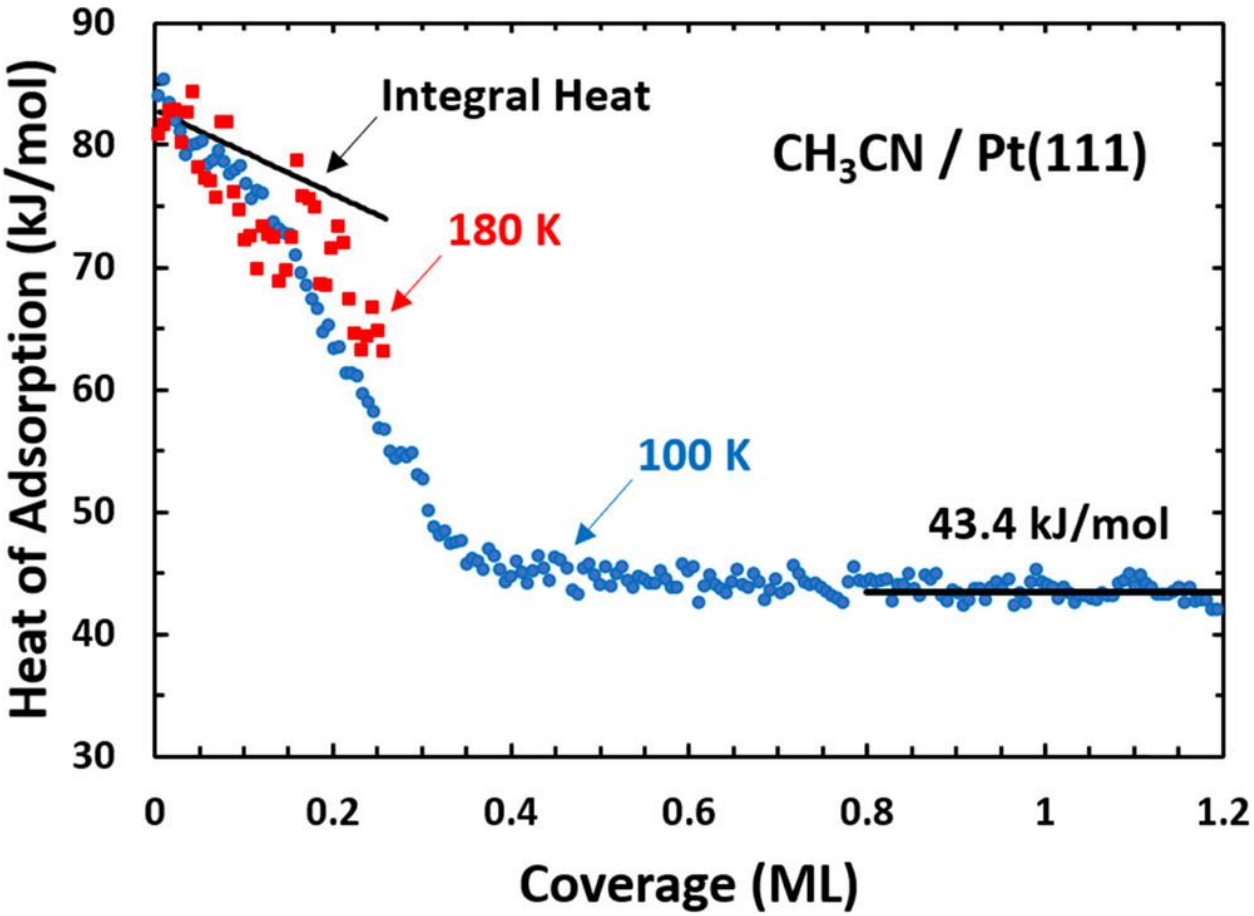

Figure 5.2 - Differential heats of adsorption of acetonitrile on Pt(111) at 100 K (blue circles) and 180 K (red squares) as a function acetonitrile coverage. The average heat of adsorption reached at the multilayer limit is shown by the black line through the 100 K data. The integral heat of adsorption for 180 K is shown in black from the low coverage limit, fit by (82.9–34.4θ) kJ/mol and giving 74.3 kJ/mol at saturation (θ = 0.25 ML). 1 ML = 1.50 × 1019 molecules/m^2.

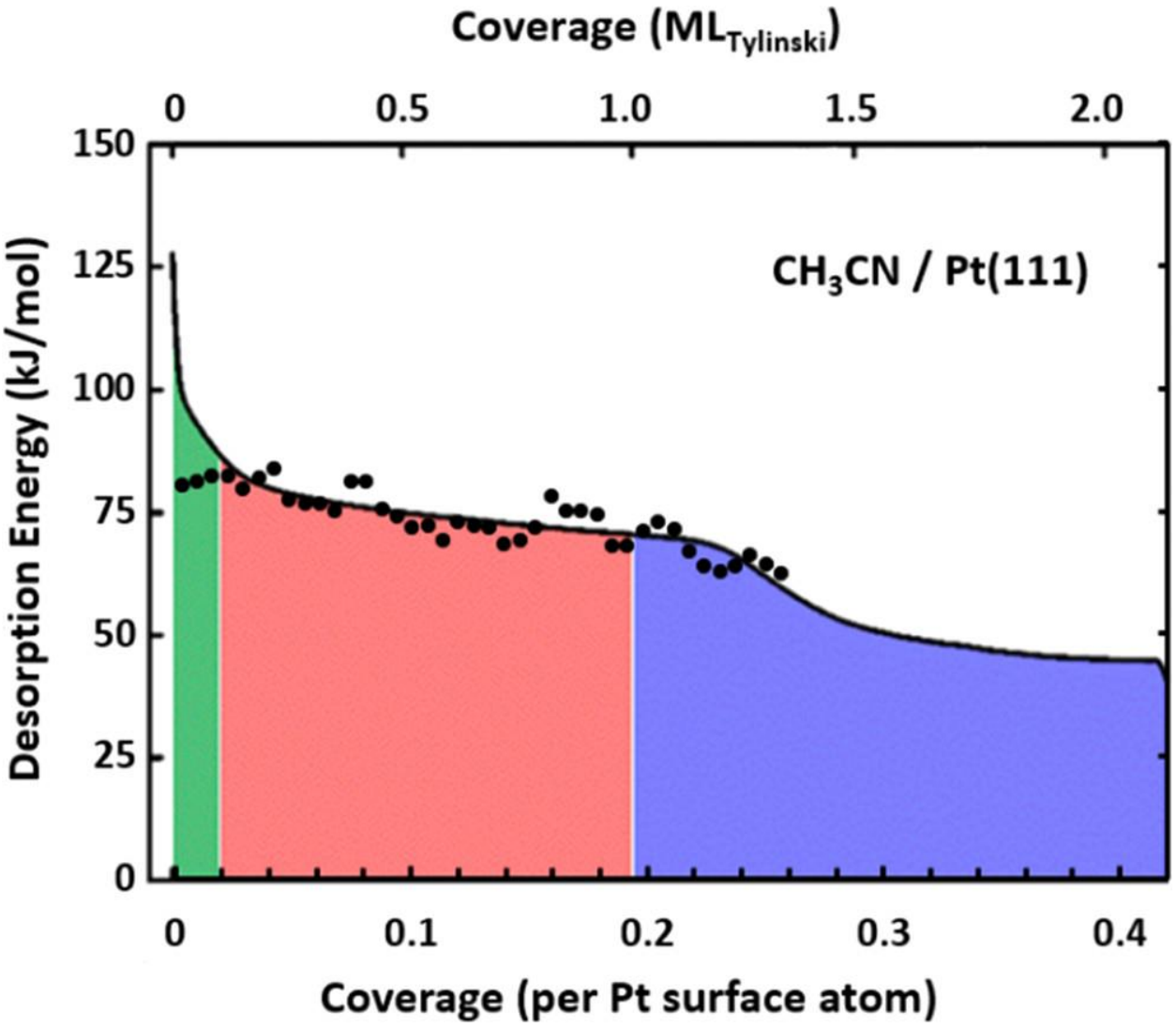

Figure 5.3 - Comparison of the desorption energy of acetonitrile from Pt(111) as a function of acetonitrile coverage as determined from the differential heats measured in this work (black points) to the values determined by Tylinski et al.[168] in a very careful TPD study (solid curve). The bottom x-axis coverage is defined as in Figure 5.1 and Figure 5.2, i.e., relative to the density of Pt atoms on the (111) surface (1.50×1019 atoms/m^2), while the top x-axis is in units as defined by Tylinski et al., where 1 ML$_{Tylinski}$ was the highest coverage of acetonitrile that showed no multilayer desorption peak in TPD. In this plot, we adjusted 1.0 ML$_{Tylinski}$ to correspond to 0.195 ML (per Pt surface atom) to align the steepest (broadened steplike) drop in desorption

energy versus coverage in Tylinski's data with the saturation coverage at 180 K (black points), which we assumed here to correspond to completion of the first layer of adsorbed acetonitrile at 0.25 ML (see text). The green, red, and blue shadings are from Tylinski et al. and were intended to separate the regions where TPD features were seen associated with step sites, (111) terraces in the first layer, and coverages where the multilayer TPD peak was also seen, respectively. We note that the TPD peak area associated with terrace sites continued to grow considerably in this blue region, which explains why 1.0 $ML_{Tylinski}$ corresponds to a lower coverage than 0.25 ML.

Chapter 6 Adsorption and Adhesion Energies of *n*-Decane on the Pt(111) Surface by Calorimetry

This chapter reprinted with permissions from Ref 53:

Harman, S. E. and Ruehl, G., & Campbell, C. T. Adsorption and Adhesion Energies of *n*-Decane on the Pt(111) Surface by Calorimetry. *Surface Science* (2022).

https://doi.org/10.1016/j.susc.2022.122166

Chapter Abstract

The heat of adsorption of *n*-decane molecularly adsorbed on Pt(111) at 150 K was measured by single-crystal adsorption calorimetry (SCAC). The heat of adsorption was initially ~152 kJ/mol on terrace sites up to a coverage of $\Theta = 0.045$ ML . Previous TPD measurements of the desorption energies of shorter n-alkanes (C_1 to C_6) on Pt(111) terraces showed a linear increase with chain length which predicts a desorption energy for n-decane in very good agreement with this new result. A heat of 169 kJ/mol was measured below 0.004 ML and attributed to defect sites, probably step edges. At coverages above $\Theta = 0.27$ ML (~3 molecular layers), the multilayer heat of adsorption was constant at ~85 kJ/mol. Using the heat of adsorption versus coverage at 150 K up through this bulk-like multilayer, the adhesion energy per unit area of liquid *n*-decane on Pt(111) terraces at room temperature was estimated to be 0.148 J/m^2. This is very similar to the value estimated for liquid *n*-hexane on Pt(111) from TPD energies, which shows that while adsorption energy increases nearly proportional to the number of CH_2 plus CH_3 groups, as the adhesion energy is a per unit area value, it remains nearly constant (0.15 J/m^2) between hexane and decane.

6.1 Introduction

The choice of solvent is known to have a dramatic effect on solid-catalyzed reaction rates and selectivities,[162–164,179–183] and understanding these effects is important for tuning catalyst performance. It is of great interest to understand the energetics of solvent bonding to catalytically relevant materials, since these energetics to a large extent determine how different solvents affect the heats of adsorption of catalytic reaction intermediates to the catalyst surface, and their differences with respect to heats of adsorption in the gas phase (which are much easier to measure and much easier to computationally estimate, and thus are much more widely known). Specifically, it has been shown theoretically that the heat of adsorption of neutral reaction intermediates decreases in a particular solvent (relative to the gas phase) by an amount approximately equal to the adhesion energy per unit area (E_{adh}) of that liquid solvent to the surface times the area on the surface occupied by that adsorbed intermediate (i.e., the area where solvent can no longer bind to the surface due to blocking by the adsorbate).[28–30,54] Since the energies of adsorbed intermediates and transition states determine catalytic reaction rates, understanding how different solvents affect adsorption energies of intermediates aids in our fundamental understanding of solvent effects on catalytic activity and selectivity, and in the improvement and design of catalytic processes. Here we report calorimetric measurements of adsorption energy versus coverage for *n*-decane on Pt(111) at 150 K, and use these gas phase measurements to estimate the adhesion energy of liquid *n*-decane on Pt(111) at room temperature. We compare this adhesion energy to the estimated energies of other linear alkanes on the Pt(111) surface to examine the relationships between adsorption energy, adhesion energy and size of these linear alkanes. The adsorption energy is found to be nearly proportional to chain length, whereas E_{adh} is nearly independent of chain length.

The adsorption energy of *n*-decane on Pt(111) is also of fundamental interest since hydrocarbon conversion reactions on Pt catalysts are ubiquitous in petroleum and biomass catalysis, decane is a common component in these reaction mixtures, and the Pt(111) surface is the most widely studied model of Pt catalyst surfaces. Due to the growing need to convert polymer waste to valuable products, the reactions of very long alkanes (polyolefins) on Pt and similar metal catalysts have recently become a subject of great interest. Thus, it is important to understand the relationship between alkane chain length and adsorption strength of linear alkane systems. Neither the adsorption energy nor desorption activation energy of *n*-decane were previously known. While the desorption energies of shorter linear alkanes (C_6 and smaller) on Pt(111) were previously measured using temperature programmed desorption (TPD), *n*-octane and *n*-decane did not desorb completely reversibly (they partially dissociated instead), and thus their desorption energies could not be measured using TPD.[52] As for other alkanes on Pt(111),[184,185] this dissociation occurs in competition with desorption during TPD near the desorption peak temperature. Single crystal adsorption calorimetry (SCAC) allows for the direct measurement of the heat of adsorption versus coverage of molecules that do not desorb reversibly.[186] This paper thus reports the heat of adsorption versus coverage of *n*-decane, the largest alkane that has been studied on Pt(111). We study it here at 150 K, well below the desorption temperature of *n*-hexane in those TPD studies (225 K),[52] so that negligible dissociation is expected to occur. With a small correction, this heat of adsorption can be converted to the desorption activation energy like that measured by TPD.[22]

6.2 Experimental

The experiments were conducted in an ultrahigh vacuum (UHV) chamber (base pressure $<2 \times 10^{-10}$ mbar) designed for single-crystal adsorption calorimetry (SCAC). The chamber also has in-situ instrumentation for X-ray photoelectron spectroscopy (XPS), low-energy electron diffraction (LEED), Auger electron spectroscopy (AES), low-energy ion-scattering spectroscopy (LEIS), a quadrupole mass spectrometer (QMS), and a liquid-nitrogen cooled quartz crystal microbalance (QCM). The SCAC apparatus and experimental procedures for the molecular beam flux, sticking probability, and heat measurements have been described in detail previously.[24,68,85]

In brief, the 1μm thick Pt(111) single crystal sample was purchased from Bine Hansen at Aarhus University. The crystal surface was cleaned by repeated cycles of Ar^+ ion sputtering and annealing to 1120 K, which was proven in earlier studies with this same apparatus to give a clean and well-ordered Pt(111) surface.[67] The Pt(111) surface was exposed to a pulsed, collimated molecular beam of *n*-decane, and the heat of adsorption and sticking probability were recorded simultaneously. The sticking probability was measured by the King and Wells method with a QMS, and the heat of adsorption was measured using a pyroelectric polymer ribbon in contact with the back of the Pt(111) crystal. The molecular beam was created by expanding 1.0 mbar of *n*-decane through a glass capillary array heated to 335 K and collimated via a series of liquid-nitrogen cooled orifices. This beam was then chopped into 102 ms pulses every 3 s. During the course of these measurements, these was an extra contribution to the heat signal's noise that was only discovered after the experiments reported here, so the signal-to-noise ratio on heats reported here is significantly lower than is typical for this calorimeter.

Here, one monolayer (ML) of coverage is defined as the number of molecules of *n*-decane adsorbed to the surface per unit area, normalized to the surface density of Pt(111) atoms

(1.50×10^{19} molecules/m^2). A typical beam pulse consists of approximately 0.002 ML (~4.7 x 10^{11} molecules within the beam diameter of ~4 mm) per *n*-decane gas pulse.

6.3 Results

6.3.1 Sticking Probabilities

Sticking probabilities were measured by comparing the time-integrated QMS signal for *n*-decane when the molecular beam scatters from the Pt(111) surface to that from a gold surface (after a saturation dose), which is known to have zero sticking probability for *n*-decane. When the signals are the same, the sticking probability is zero. Long-term and short-term sticking probabilities of *n*-decane on Pt(111) were found to be unity at 150 K. The long-term sticking probability refers to molecules that initially adsorb and remain adsorbed for the entire duration of the 3 s pulse window and contribute to the build-up of coverage of *n*-decane on the surface. The short-term sticking probability refers to the molecules that initially adsorb and contribute to the measured heat of adsorption during the 102 ms pulse, but then might desorb again before the next pulse and not add to the coverage. When both sticking probabilities are unity, as with *n*-decane on Pt(111) at 150 K here, all incoming molecules adsorb to the surface and remain adsorbed until the next pulse, fully contributing to the both the measured heat and coverage increase.

6.3.2 Heat of Adsorption

We define here the "heat of adsorption" as the negative of the standard molar enthalpy change for the adsorption reaction, with the gaseous molecules and single crystal surface being the same temperature. As explained in detail in previous papers, this requires a small enthalpy

correction on the measured heat as the gas molecule's enthalpy at this temperature is slightly different than a Boltzmann distribution at the sample temperature due to the actual molecular beam conditions.[85] The differential heat of adsorption measured is the heat released per mole when a pulse from the molecular beam is dosed onto the crystal surface at nearly fixed coverage, as is the case during our SCAC experiments here since the gas pulses contain only ~0.2 % of a ML. Figure 6.1 shows the differential heat of adsorption of *n*-decane on Pt(111) at 150 K as a function of *n*-decane coverage. This is the average of 6 experimental runs. After the first two gas pulses, the heat of adsorption at 150 K is nearly constant at 151.8 ± 5.4 kJ/mol up to 0.045 ML. The heat is slightly higher in the first two points (~169 kJ/mol), which has often been seen in SCAC measurements on the Pt(111) surfaces previously studied in this apparatus. This has been attributed to defect sites on the surface, likely step edges.[104] Above 0.06 ML, the heat of adsorption drops rapidly to ~90 kJ/mol at ~0.09 ML. It stays near 90 kJ/mol until above ~0.20 ML, then decreases to a constant multilayer heat of 84.9 kJ/mol above 0.27 ML which corresponds to coverage of more than three layers of *n*-decane on the Pt(111) surface.[167] The run-to-run standard deviation on this multilayer heat was 5.5 kJ/mol. Since there were six runs, the error bar on the *average* multilayer heat is smaller (~± (5.5 kJ/mol)/$(6-1)^{1/2}$ = ± 2.5 kJ/mol). This average multilayer heat is 2.5 kJ/mol below (but within this error bar of) the heat of sublimation of bulk n-decane(solid) at this temperature, which we estimate to be 87.4 kJ/mol at 150 K based on literature values for the heat capacities of solid, liquid and gaseous *n*-decane, and the enthalpies of vaporization and fusion.[147,148]

Linear n-alkanes on Pt(111) have first-layer packing densities that depend on the number of carbons per alkane, n, whereby 1/(n + 1) is the coverage (per Pt surface atom) of the first layer of adsorbate.[167] For *n*-decane, where n = 10, this predicts a coverage of 1/11= 0.091 ML for

completion of the first layer. This is in excellent agreement with the abrupt change in the slope of heat versus coverage, where the high heat measured in the first layer has deceased rapidly to 90 kJ/mol (at completion of the first layer), and then quickly becomes nearly constant with coverage at ~90 kJ/mol (within the second layer).

6.4 Discussion

6.4.1 Comparison to Temperature Programmed Desorption

Previously Tait et.al.[52] measured the desorption energies of various *n*-alkanes on Pt(111), C(0001)/Pt(111) and MgO(100). However, on Pt(111) the longest alkane that reversibly desorbed without significant dissociation was *n*-hexane, so desorption energies for longer alkanes were not studied there. Here, measuring the heat of adsorption of *n*-decane on Pt(111), and correcting for comparison to desorption energy values measured from TPD by subtracting ½ RT, we can compare these experimental results to the value predicted in that work. Taking the linear (near proportional) trend line reported by Tait et al. for the desorption energies for *n*-alkanes versus chain length (from C_1 to C_6) on Pt(111) terraces at a coverage of 0.5 "ML", we predict a desorption energy of *n*-decane on Pt(111) of 129.5 kJ/mol. It's important to note that Tait et al. defined 1 "ML" as their highest measured coverage where they saw only the monolayer desorption peak with no multilayer peak visible, which is close to one complete layer of *n*-alkanes adsorbed on the surface. We define 1 ML here differently, as one molecule of *n*-decane adsorbed to the surface per surface Pt atom (or 1.50×10^{19} molecules/m^2). As Tait et al. measured desorption energies at 0.5 "ML" by their definition, this corresponds to 0.5 x 0.091 ML = 0.0455 ML of decane in our ML units here.

We measured a differential heat of adsorption at 0.0455 ML of 151.8 kJ/mol, which corresponds to a desorption energy of 151.2 kJ/mol after applying the -1/2RT correction for direct comparison to TPD measurements.[22] This is 21.7 kJ/mol higher than the desorption energy of 129.5 kJ/mol predicted above at this coverage (i.e., half the coverage which completes the first layer) based on those TPD studies of shorter alkanes by Tait et al.. Those TPD studies indicate that, near the peak temperature for desorption, these alkanes make close-packed 2D islands over nearly the full first-layer coverage range, where their desorption energy remains nearly constant with coverage. Our measured integral heat at completion of the first layer (0.091 ML) is 132.7 kJ/mol, which corresponds to a desorption energy of 132.1 kJ/mol. This average heat of adsorption for the first layer is very close to the average value of 129.5 kJ/mol predicted by TPD measurements of shorter alkanes (see above).

The nearly constant heat of adsorption observed up to 0.045 ML (except at defects) seen in Figure 6.1 suggests adsorbed *n*-decane forms 2D islands, which was observed for the other shorter *n*-alkanes studied on Pt(111), and also for linear alkanes up to decane on MgO(100) and graphene, by Tait et al.[52] The decrease in heat seen here above 0.06 ML (~2/3 of the first layer completion) may be due to the lower temperature studied here (150 K, versus 200 and 250 K for MgO and graphene, respectively). Decane molecules on Pt(111) at 150 K here may not be mobile enough at high coverages to achieve their optimum packing configuration to maximize decane-decane attractions. Note too that decane's higher heat of adsorption on Pt(111) suggests that it will have higher surface diffusion barriers than on MgO and graphene, making it even slower to find the minimum-energy packing.

6.4.2 Adhesion Energy

There is great interest in understanding the energetics of solvents at the liquid-solid interface. The adhesion energy at the solvent-metal interface is the controlling factor in the differences between reactant adsorption energies in various solvents relative to its gas-phase adsorption energy.[28–30,54] Using the method previously described by Rumptz et al.,[30] we can estimate the adhesion energy of bulk liquid *n*-decane to Pt(111) at room temperature from the heats of adsorption in Figure 6.1 at 150 K. Equation 6.1 shows how the adhesion energy per unit area (E_{adh}) is estimated in that method from the integrated heat of adsorption of the solvent (S), here *n*-decane on the Pt(111) surface:

$$E_{adh} = \frac{[Q_{adsorption} - n\Delta H_{vap,S}]}{A} + 2\gamma_{S,liq} \quad (6.1)$$

In the first term, the integrated heat of adsorption at a thick multilayer coverage ($Q_{adsoprtion}$) minus the number of moles adsorbed (n) times the molar heat of vaporization of the liquid solvent ($\Delta H_{vap,S}$) is divided by area covered by the adsorbed film (A). The second term is twice the surface energy of the solvent (decane here) as a bulk liquid ($\gamma_{S,liq}$). For this, we use the reported surface tension of bulk, liquid decane at 298 K, $\gamma_{S,liq} = 0.02383$ J/m^2.[54] It is only possible to form multilayers of *n*-decane on Pt(111) in ultrahigh vacuum at low temperatures (here 150 K), where the incoming molecules adsorb to form a solid instead of a liquid. We make the assumption that $[Q_{adsorption} - n\Delta H_{vap,S}]$ at room temperature is approximately equal to $[Q_{adsorption} - n\Delta H_{sub,S}]$ measured at our lower experimental temperature of Figure 6.1 (150 K), where $\Delta H_{sub,S}$ is the heat of sublimation of bulk *n*-decane at this same temperature (taken to equal the limiting multilayer differential heat measured in Figure 6.1 at thick multilayer coverages, 84.9 kJ/mol). This assumes that the molar heat capacity of the solvent molecules in the first adsorbed layer equals that in the bulk multilayer at all temperatures between 150 K and 298 K (including the

contributions from their heats of fusion).[30,54] In this way, we estimate from the data in Figure 6.1 that the adhesion energy of *n*-decane on Pt(111) is 0.148 J/m^2.

In Figure 6.2 we plot the adhesion energies of various *n*-alkanes on Pt(111), graphene on Pt(111), and MgO(100) surfaces versus chain length, n. Except for decane on Pt(111), these points are all taken from Rumptz et al.,[54] who extracted them from TPD measurements[52] also using Equation 6.1.

Based on the trends seen in Figure 6.2 for MgO and graphene and as discussed by Rumptz et al.,[54] we expected that the adhesion energy of linear alkanes would be approximately constant as chain length increases. Although the molar adsorption energy of *n*-decane is higher than that of the shorter alkanes (and nearly proportional to chain length),[52] adhesion energy is a per area value (J/m^2), and the adhesion energy does indeed remain the nearly the same for decane as seen for *n*-hexane on Pt(111), since each CH_2 and CH_3 group adds nearly the same area per adsorbed alkane molecule.

This work now extends this understanding to systems that desorb irreversibly, by filling in the missing *n*-decane on Pt(111) adhesion energy. Not only do we see the expected independence of adhesion energy from chain length, but we also confirm that both TPD and experimental heats of adsorption can be used to determine the adhesion energies of bulk liquids on a surface. As there is no way to currently directly measure adhesion energies on clean metal surfaces, this indirect technique used in Figure 6.2 has great value in providing new insights using previously measured heats of adsorption, or desorption energies, of solvent molecules at lower temperature.

6.5 Conclusions

The heat of adsorption of *n*-decane on Pt(111) versus coverage was measured using SCAC at 150 K. The initial heat of adsorption was nearly constant at 152 kJ/mol though 0.0455 ML (except for the first two points below 0.004 ML, which were ~17 kJ/mol higher and attributed to defect sites). The heat then dropped to ~90 kJ/mol by 0.091 ML, then decreased to the multilayer heat of adsorption of 84.9 kJ/mol above 0.27 ML. The integral heat of adsorption at the saturation coverage of the first layer of adsorbed *n*-decane (0.091 ML) was 132.7 kJ/mol. This was close to that predicted based on desorption energies measured by TPD for shorter *n*-alkane on Pt(111) (C_1-C_6), which were found by Tait et al.[52] to increase nearly proportional to carbon number.

Using the experimentally measured heat of adsorption versus coverage out to a bulk-like multilayer coverage, we estimate the adhesion energy of liquid *n*-decane on Pt(111) at room temperature to be 0.148 J/m^2. This is very close to the adhesion energy per unit area of *n*-hexane on Pt(111) estimated based on TPD desorption energies. Thus, linear alkanes have average heats of adsorption in close-packed islands on Pt(111) which approximately equal to a constant (13.3 kJ/mol per C atom) times their total number of CH_2 plus CH_3 groups, but because each CH_2 and CH_3 group occupies nearly the same area on the surface, the adhesion energy per unit area is also nearly a constant (0.15 J/m^2).

Acknowledgements

The authors acknowledge support for this work by the National Science Foundation under grant number CBET-2004757.

6.6 Figures

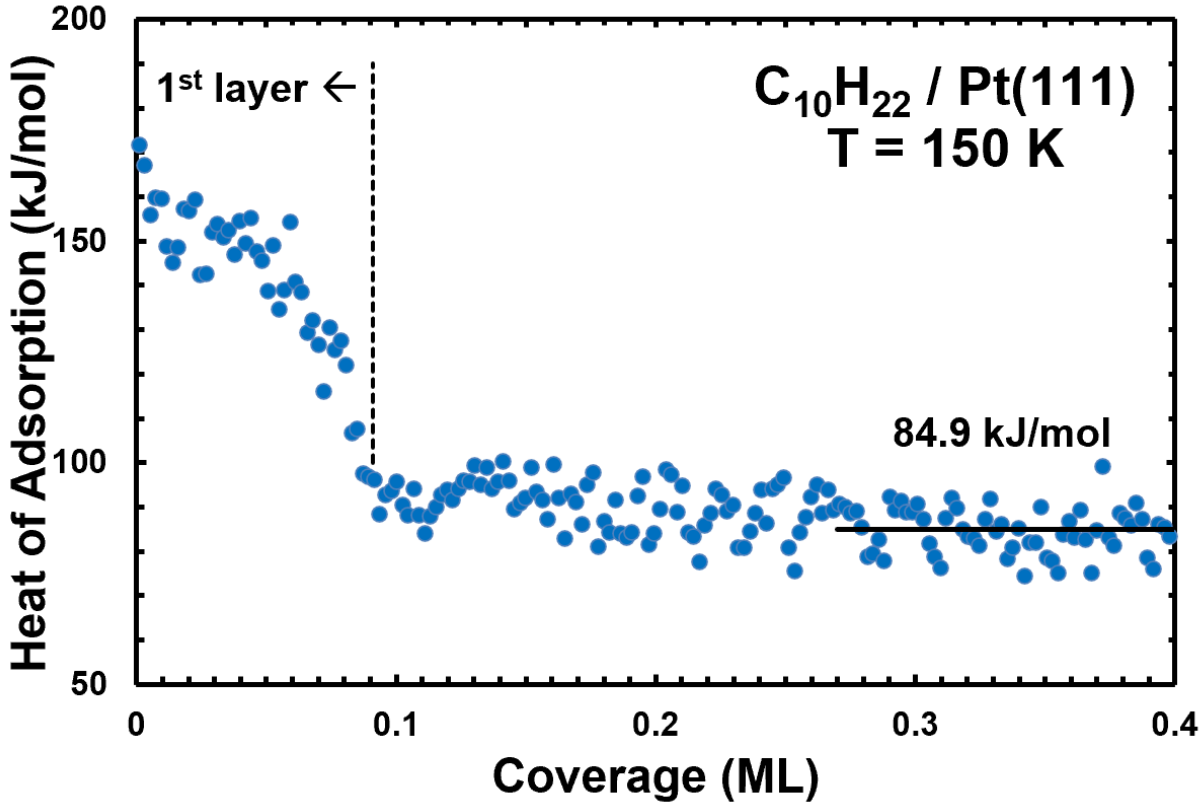

Figure 6.1 - Differential heat of adsorption of n-decane on Pt(111) at 150 K as a function of n-decane coverage. The average heat of adsorption reached at the thick multilayer limit is shown by the black line. (1 ML = 1 molecule per Pt surface atom, or 1.50 X 10^{19} molecules / m^2.

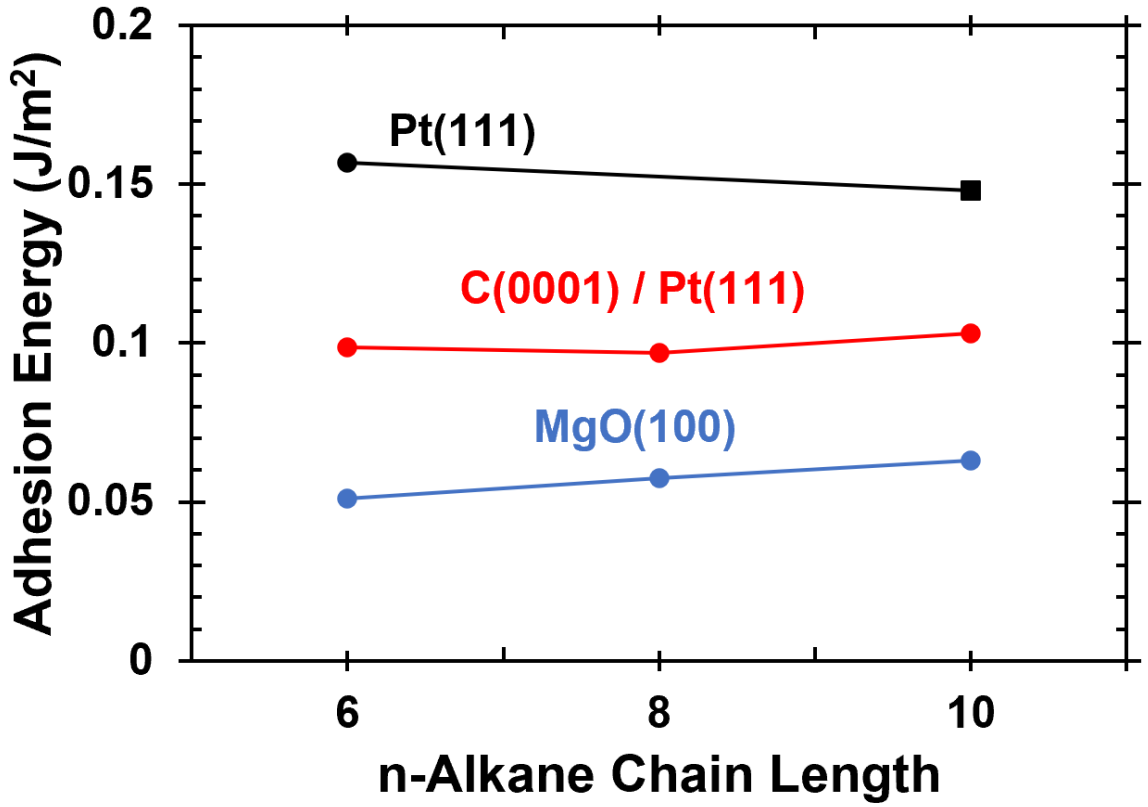

Figure 6.2 - Adhesion energies of liquid n-alkanes versus chain length on three surfaces, estimated from low-temperature measurements of heats of adsorption versus coverage using Equation 6.1. Circular points were determined previously[54] using published TPD desorption energies,[52] while the square point is determined from the calorimetrically measured heat of adsorption of *n*-decane on Pt(111) using Eq. (6.1) in this work. The potential error bars on these points are estimated to be less than ~15% based on a complex set of contributions from both assumptions in Eq. (6.1) and experimental error bars in absolute heat and coverage calibration.

Chapter 7 Energetics of Adsorbed Azulene on Pt(111) by Calorimetry

This chapter has been reprinted with permission from Ref 63:

Klein, B. P., Harman, S. E., Ruppenthal, L., Ruehl, G., Hall, S. J., Carey, S. J., Herritsch, J., Schmid, M., Maurer, R. J., Tonner, R., Campbell, C. T., & Gottfried, J. M. Enhanced Bonding of Pentagon − Heptagon Defects in Graphene to Metal Surfaces: Insights from the Adsorption of Azulene and Naphthalene to Pt(111). *Chemistry of Materials* **32**, 1041–1053 (2020).

Chapter Abstract

The performance of graphene-based (opto)electronic devices depends critically on the graphene/metal interface formed at the metal contacts. We show here that the interface properties may be controlled by topological defects, such as the pentagon−heptagon (5−7) pairs, because of their strongly enhanced bonding to the metal. To measure the bond energy and other key properties not accessible for the embedded defects, we use azulene as a molecular model for the 5−7 defect. Comparison to its isomer naphthalene, which represents the regular graphene structure, reveals that azulene interacts more strongly with a Pt(111) surface. Its adsorption energy, as measured by single-crystal adsorption calorimetry (SCAC), exceeds that of naphthalene by up to 116 kJ/mol (or up to 50%). Both isomers undergo hybridization of their frontier orbitals with metal states, as indicated by X-ray and ultraviolet photoelectron spectroscopy (XPS/UPS) and near-edge X-ray absorption fine structure (NEXAFS) spectroscopy combined with molecular orbital (MO) projection analysis through dispersion-corrected, periodic density functional theory (DFT) calculations. Based on the NEXAFS/DFT analysis, the stronger

bond of the 5−7 system is attributed to the different energetic response of its unoccupied frontier orbitals to adsorption. Adsorption-induced bond-length changes show substantial topology-related differences between the isomers. Electron transfer occurs in both directions through donation/back-donation, resulting in the partial occupation (deoccupation) of formerly unoccupied (occupied) orbitals, as revealed by periodic energy decomposition analysis (pEDA) for extended systems. Our model study shows that the topology of the π-electron system strongly affects its bonding to a transition metal and thus can be utilized to tailor interface properties.

It should be noted that I did not perform any of the DFT work or analysis, and that my contribution was that of the heat of adsorption measurements and comparison to the heat of adsorption of naphthalene. This is an excerpt of the full publication, focusing on my calorimetric research.

7.1 Introduction

Graphene as one of the most prominent two-dimensional (2D) materials is known for the exceptional electronic and mechanical properties of its ideal lattice.[187] Large-scale graphene samples, however, are typically polycrystalline and contain topological defects, such as pentagons, heptagons, and pentagon−heptagon (5−7) pairs (Figure 7.1 a),[188] especially at grain boundaries.[55,56,58,59,189,190] These defects, which are induced by rearrangement of carbon−carbon (C−C) bonds, strongly influence the chemical and physical properties of graphene, including chemical reactivity,[60,61] mechanical strength,[58,59,63,191] electron transport,[55,189] and magnetism.[64] Their utilization for tailoring the properties of graphene through topological design has been proposed.[192]

Interfaces between graphene and metals are formed during the epitaxial growth of the 2D material on metallic substrates.[193] They also play a prominent role in graphene-based electronic devices, where metal contacts are necessary.[194] The properties of the resulting graphene/metal interfaces control important performance-determining parameters such as the contact resistance.[195] Considering the substantial influences of defects on the properties of graphene, it is likely that they also affect the interfacial interaction, as indicated by the reduced resistances observed for contacts to graphene edges.[194] However, the bonding of intrinsic graphene defects to metals is largely unexplored, mainly due to the experimental challenges arising from the investigations of embedded defects in low concentrations. Expanding on a recently introduced approach,[196] we use here a molecular model system to study the bonding of 5−7 graphene defects to the reactive Pt(111) surface. In this model, azulene with its 5−7 ring structure represents the defect, whereas its isomer naphthalene is the reference molecule representing the hexagonal rings of defect-free graphene (Figure 7.1 b, c). The 5−7 motif was chosen because it is the most

abundant building block for topological defects. It occurs in isolated 5−7 defects, in pairs as Stone−Wales defects, or in chains at grain boundaries. In addition, the 5−7 motif represents a class of defects for which a molecular model can be contrived, unlike vacancies. The model system approach allows for the application of laterally integrating techniques and thus provides unique access to parameters that cannot be measured for the real embedded defects, such as bond energies. Even though naphthalene is strongly chemisorbed on Pt(111),[66] we find here that azulene binds even stronger with adsorption energies that are up to 50% higher.

To concisely describe the topological properties of the defect, we use here the established concept of alternant versus nonalternant topology.[197] In the alternant conjugated system of naphthalene (and regular graphene), the carbon atoms can be labeled in an alternating fashion (e.g., red and green as in Figure 7.1 b, c), while this is not possible for a nonalternant system like azulene (or the 5−7 defect). The nonalternant topology leads to the violation of the Coulson−Rushbrook pairing theorem and thus to a distinctly different valence electronic structure.[198] In our model molecules, this electronic difference is manifested in the large dipole moment (0.8 D)[199] and intense blue color of azulene, whereas naphthalene has no dipole moment and is colorless.

The importance of nonalternant aromatic structures extends far beyond their role as graphene defects. Recently, they have found attention for application as molecular or polymeric organic semiconductors in organic (opto)electronic devices because of their low band gaps and high charge carrier mobilities.[200] Their interfaces to metal electrodes, which are known to strongly influence the properties of the device,[201,202] have only rarely been studied, unlike interfaces to alternant aromatic systems.[203] Comparative studies of azulene and naphthalene on Pt(111) have not been reported. Limited work for the isolated systems was done with low-energy

electron diffraction (LEED),[204–207] temperature-programmed desorption (TPD),[205,206] and scanning tunneling microscopy (STM).[208–210] Work function (WF) measurements,[207] adsorption calorimetry,[66] and density functional theory (DFT) calculations[211,212] were until now only performed for naphthalene on Pt(111). For the more weakly interacting Cu(111) surface, it was recently shown that naphthalene is physisorbed, while azulene is chemisorbed,[196] raising the question whether differences in the interaction strength persist when both molecules are strongly chemisorbed.

In this study, we present a comprehensive multimethod comparison of the bonding of naphthalene and azulene to Pt(111). Using single−crystal adsorption calorimetry (SCAC), we measure the first reliable adsorption energies for any nonalternant aromatic molecule on any metal surface and show that it bonds stronger than its alternant isomer. Temperature-programmed desorption (TPD) cannot be applied here because the molecules do not desorb intact from Pt(111). Details of the chemical bond and the electronic structure are clarified using X-ray and ultraviolet photoelectron spectroscopy (XPS/UPS), near-edge X-ray absorption fine structure (NEXAFS) spectroscopy, and WF measurements. DFT calculations including a dispersion-correction scheme (PBE-D3) and applying periodic boundary conditions are used to interpret the experimental data and to gain detailed insight into the underlying mechanisms of the enhanced bonding at the defect/metal interface.

7.2 Experimental Methodology

The adsorption of azulene and naphthalene on Pt(111) was studied under ultrahigh vacuum (UHV) conditions at base pressures below 2×10^{-10} mbar. Coverages are given in the unit monolayer (ML) defined as the number of molecules per platinum atom in the Pt(111)

surface [atomic density of the Pt(111) surface: 1.50×10^{19} m^{-2}]. If a "full monolayer" is mentioned, this corresponds to one complete layer of molecules on the surface (which corresponds to 0.111 ML for azulene).

The SCAC experiments were performed in a UHV chamber equipped with facilities for XPS, LEED, Auger electron spectroscopy (AES), and low-energy ion scattering spectroscopy (LEIS). The apparatus and procedures for SCAC have been described in extensive detail previously.[24,68,85] Briefly, the Pt(111) samples used in the SCAC experiments were 1 μm thick single-crystal foils and were provided by Jacques Chevallier at Aarhus University. The sample was cleaned by gentle Ar^+ sputtering, followed by repeated cycles of O2 treatment at 10^{-6} mbar and 873 K and annealing at 1123 K in UHV. After this treatment, impurities were below the Auger and XPS detection limits, and LEED showed the spots expected for Pt(111). The heats of adsorption and sticking probability were measured simultaneously as a pulsed molecular beam of azulene was dosed onto the Pt surface. The molecular beam was created by expanding azulene vapor (0.2−0.9 mbar) through a glass capillary array, collimating it through a series of five orifices that were cooled with liquid nitrogen, and then chopping into 102 ms pulses. The heats were measured with a pyroelectric ribbon gently pressed on the backside of the Pt crystal. The sticking probabilities were measured with a quadrupole mass spectrometer (QMS) using the King and Wells method.[70]

7.3 Results and Discussion

7.3.1 Heat of Adsorption Measurements

The most important single parameter in this study is the heat of adsorption as a direct quantitative measure for the strength of the adsorbate−substrate bond. It is defined here as the

negative of the differential standard molar enthalpy change for the adsorption reaction, $-\Delta H$ ads, with the gas having the same temperature as the surface. "Standard" here implies only an ideal gas at 1 bar pressure. Figure 7.2 shows the molar heat of adsorption of azulene on Pt(111) at 150 K as a function of coverage. These heats were calculated from the measured absolute calorimetric heats by averaging over five individual measurements, dividing by the number of moles adsorbed in each pulse (given by flux times pulse duration times sticking probability) and adding $RT_{source}/2$, as described previously.[213] No detectable mass spectrometer signal was present due to any nonsticking fraction of the azulene molecular beam, indicating that its sticking probability is always ≥ 0.995. Consequently, both the short- and long-term sticking probabilities were concluded to be unity.

As described previously, a small enthalpy correction on the measured heat is necessary because the standard enthalpy of a gas at the temperature of the surface differs slightly from that of the actual experimental molecular beam's gas at this surface temperature.[18] Specifically, the temperature of the source, T_{source}, and thus the temperature of the molecules impinging on the sample, is 382 K, which deviates from the sample temperature of 150 K. Therefore, we had to take the additional contribution from the extra thermal energy of the gas molecules into account. We estimated this heat contribution by integrating the experimental heat capacity of the gas (C_p) vs T curve[85] between the sample and source temperature. The resulting heat, 29 kJ/mol, was subtracted from the directly measured heat. The thus corrected heat of adsorption is plotted vs coverage in Figure 7.2. It is equal to the standard (1 bar) molar enthalpy of adsorption and the isosteric differential heat of adsorption. Figure 7.2 shows that the heat of adsorption decreases with coverage. We attribute this decrease to repulsive lateral interactions among the adsorbed

azulene molecules. The solid line is a second-order polynomial fit of the experimental data and is described by the equation

$$-\Delta H_{ads} = \ (416 - 1370\Theta - \ 13100\Theta^2)\ kJ/mol \qquad (7.1)$$

where Θ is the coverage in monolayer (ML, given as molecules per surface atom; see the Methods section for a detailed explanation).

The heat of adsorption of naphthalene on Pt(111) was already measured in previous work with the same instrument.[66] For a direct comparison with the new data, the old measurements for naphthalene were also fitted with a second-order polynomial and follow the equation

$$-\Delta H_{ads} = \ (300 - 330\Theta - \ 18758\Theta^2)\ kJ/mol \qquad (7.2)$$

As can be seen, azulene has a substantially higher heat of adsorption than naphthalene over the whole coverage range, close to that expected for the larger anthracene.[66]

Also shown in Figure 7.2 is the heat of sublimation of bulk azulene at 150 K. The literature value for the sublimation enthalpy of azulene is 74.2 ± 2.2 kJ/mol at 298 K.[214] This was adjusted to account for the lower temperature of the Pt(111) sample at 150 K by integrating the heat capacities (C_p) for gaseous and solid azulene over this temperature range. For gaseous azulene, values are available between 200 and 1000 K.[215] The third-order polynomial fit relating C_p to temperature was extrapolated to 150 K and integrated between 150 and 298 K. The only available value for C_p of solid azulene is given at 298 K.[216] To determine the C_p of solid azulene at a lower temperature, we assessed the solid C_p values for the similar molecules naphthalene and benzene. The heat capacities for each molecule showed a linear relationship for the entire temperature range of interest, with an average decrease of 50 ± 5% from 298 to 150 K. Consequently, the heat capacity of solid azulene at 298 K was assumed to decrease by 50% between 298 and 150 K. The resulting linear relationship was integrated over this range. The

correction to the sublimation enthalpy of azulene between 150 and 298 K is +3.92 kJ/mol, resulting in a sublimation enthalpy of 78.1 ± 2.2 kJ/mol at 150 K.

The heat of adsorption of azulene on Pt(111) at 150 K decreased to a relatively constant value of 92.7 kJ/mol between 0.12 and 0.17 ML, when the second layer was growing (with an average heat in this range that varied by ±3.4 kJ/mol among runs). Above 0.2 ML, the heat of adsorption reached a nearly constant value, which averaged 80.6 ± 1.6 kJ/mol, within error bars of the bulk sublimation enthalpy at 150 K of 78.1 ± 2.2 kJ/mol. The higher heat at coverages in the second layer (~0.1 to 0.2 ML) indicates that the Pt(111) surface is still close enough to interact with azulene, in spite of the presence of an intervening layer of adsorbed azulene.

7.3.2 Adsorption Energies

DFT calculations of adsorbed large organic molecules are often performed for only one, rather high coverage to reduce the unit cell size and thus the computational effort. This restriction ignores the coverage dependence of many properties, including the adsorption energy. For comprehensive comparison with the coverage-dependent SCAC data, we calculated six different adsorbate structures in a wide range of coverages.

The DFT adsorption energies for the lowest calculated coverage [(7 × 7) structure, coverage of 0.020 ML] are −389 kJ/mol for azulene and −345 kJ/mol for naphthalene. These values decrease to −308 and −258 kJ/mol at the highest coverage [(3 × 3) structure, 0.111 ML], respectively. The adsorption energies for all calculated structures are compared to the experimental SCAC values in Figure 7.3. The SCAC data for naphthalene are taken from the literature.[66]

For a meaningful comparison of the integral electronic adsorption energies from theory with the differential experimental energies, the second-order polynomials obtained by fitting the experimental data were integrated. For a coverage of 0.083 ML, harmonic zero-point vibrational energy (ZPVE) and harmonic thermodynamic corrections for the DFT-derived values were performed, yielding the adsorption enthalpy in addition to the electronic adsorption energy directly produced by DFT.

For azulene, the calculated and measured adsorption energies agree remarkably well and deviate by an average of only 8 kJ/mol over the coverage range. In contrast, the adsorption energy of naphthalene is overestimated by an average of 53 kJ/mol. An overestimation by theory is expected, since the D3 dispersion correction is known for this shortcoming.[196,217,218] In previous work, DFT-D3 overestimated the adsorption energies of azulene and naphthalene on Cu(111) by 28 and 45 kJ/mol, respectively.[196] Considering the finite temperature of the measurements, neglecting anharmonicities in the calculations may additionally contribute to this overestimation: The vertical potential of the molecule on the surface is strongly anharmonic, resulting in an increased adsorption height and decreased adsorption energy at elevated temperatures.[219] The literature SCAC data for naphthalene were measured at 300 K,[66] whereas the SCAC data for azulene in this work were measured at 150 K. Therefore, the lowering effect of the elevated temperature on the adsorption energy should be stronger for naphthalene. It is, however, impossible to distinguish between these effects and the inherent limitations of DFT-D3.

The calculations correctly reproduce the higher adsorption energy of azulene and the general coverage dependences for both isomers. Considering their almost identical adsorption heights, it may be concluded that the latter (and the WF changes) are mainly determined by Pauli repulsion, whereas the extra adsorption energy of azulene is structurally mainly expressed in the

larger deformations of the molecule and the surface. However, the theoretical adsorption energies of the two isomers differ by 37−50 kJ/mol over the whole coverage range, which is distinctively smaller than the experimental difference of 85−116 kJ/mol. The harmonic zero-point vibrational and thermodynamic corrections change the adsorption energy only slightly to larger values (ZPVE: 1−2 kJ/mol, thermodynamic corrections: 5−7 kJ/mol). As shown in the bottom part of Figure 7.3, previous theoretical studies without dispersion corrections strongly underestimated the adsorption energy of naphthalene on Pt(111).[211,212] These deviations illustrate that dispersion corrections are also necessary in the case of chemisorption.[218] In our case, the dispersion attraction accounts for approximately one-third of the interaction energy.

7.4 Conclusions

The isomers azulene and naphthalene constitute a versatile molecular model system to study interfacial interactions of the topological pentagon−heptagon (5−7) defects in graphene. The experimental and theoretical analyses reveal that both molecules are chemisorbed on Pt(111) but azulene forms the stronger bond. Its differential adsorption energy, as measured by SCAC, is larger by 68 to 116 kJ/mol, depending on the coverage, and reaches 416 kJ/mol at zero coverage, compared to 300 kJ/mol for naphthalene. The stronger bond of azulene and the coverage dependencies of the adsorption energies are qualitatively correctly predicted by dispersion-corrected DFT calculations. DFT reveals rehybridization toward sp3 and a partially localized σ-character of the molecule−metal bond. The interfacial electron transfer occurs in both directions through donation and back-donation, resulting in the partial occupation (deoccupation) of orbitals that are unoccupied (occupied) in the free molecules, as shown by pEDA. Interpretation of the UP and NEXAFS spectra with an MO projection analysis supports the

occupation/deoccupation mechanism of the surface chemical bond. It also reveals that the molecular orbitals of azulene and naphthalene respond differently to adsorption. This observation connects the topology-related differences in the electronic structure (especially the HOMO−LUMO gap) with the different bonds to the surface. Our analysis shows that the π-topology of an aromatic ring system substantially influences its interaction at a metal/organic interface in the regime of strong chemisorption. Topology-related effects are therefore relevant for various applications, including metal/organic interfaces in organic (opto)electronic devices or catalytic reactions of aromatic hydrocarbons on transition-metal surfaces.

Acknowledgements

This research was funded by the Deutsche Forschungsgemeinschaft (DFG, German Research Foundation) through 223848855-SFB 1083. The authors acknowledge support for this work by the U.S. National Science Foundation under Grant No. CHE-1665077. We thank the synchrotron radiation facility BESSY-II of the Helmholtz-Zentrum für Materialien und Energie, Berlin, for allocation of beam time at the HE-SGM beamline and financial support. We thank Lukas Hellweg for assistance during the spectroscopy measurements. We further acknowledge computational resources from HRZ, Marburg; Goethe-CSC, Frankfurt; and HLRS Stuttgart. S.J.H. and R.J.M. acknowledge funding for a Ph.D. studentship through the EPSRC Centre for Doctoral Training in Molecular Analytical Science (EP/L015307/1) and computing resources via the EPSRC-funded HPC Midlands+ Computing Centre (EP/P020232/1) and the EPSRC-funded Materials Chemistry Consortium for the ARCHER U.K. National Supercomputing Service (EP/R029431/1). R.J.M. acknowledges support via a UKRI Future Leaders Fellowship (MR/S016023/1).

7.5 Figures

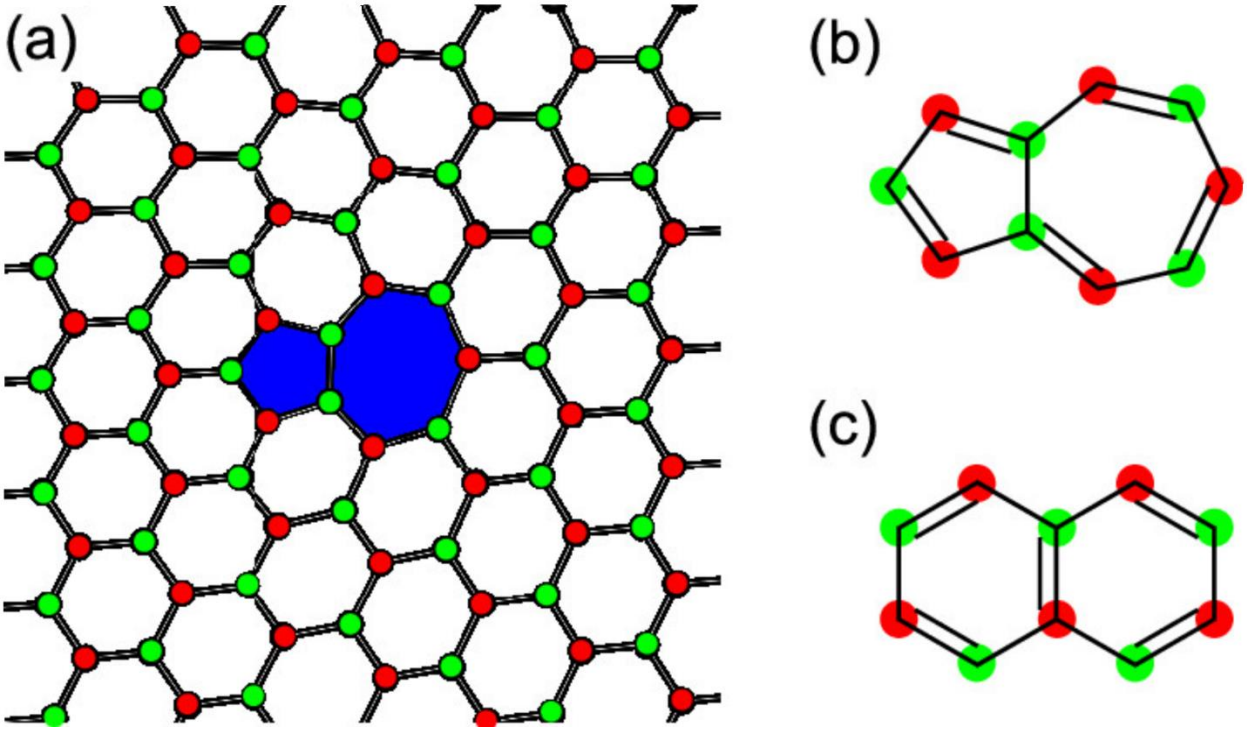

Figure 7.1 - (a) Graphene sheet with an embedded pentagon–heptagon (5–7) defect (blue). Molecular structures of (b) azulene and (c) naphthalene. The different topologies of the two isomers are illustrated by the color schemes: naphthalene has an alternant topology (only alternating or differently colored C centers are connected), whereas azulene has a nonalternant topology (two atoms with the same color are connected). As shown in (a), the 5–7 defect locally interrupts the alternant topology of regular graphene.

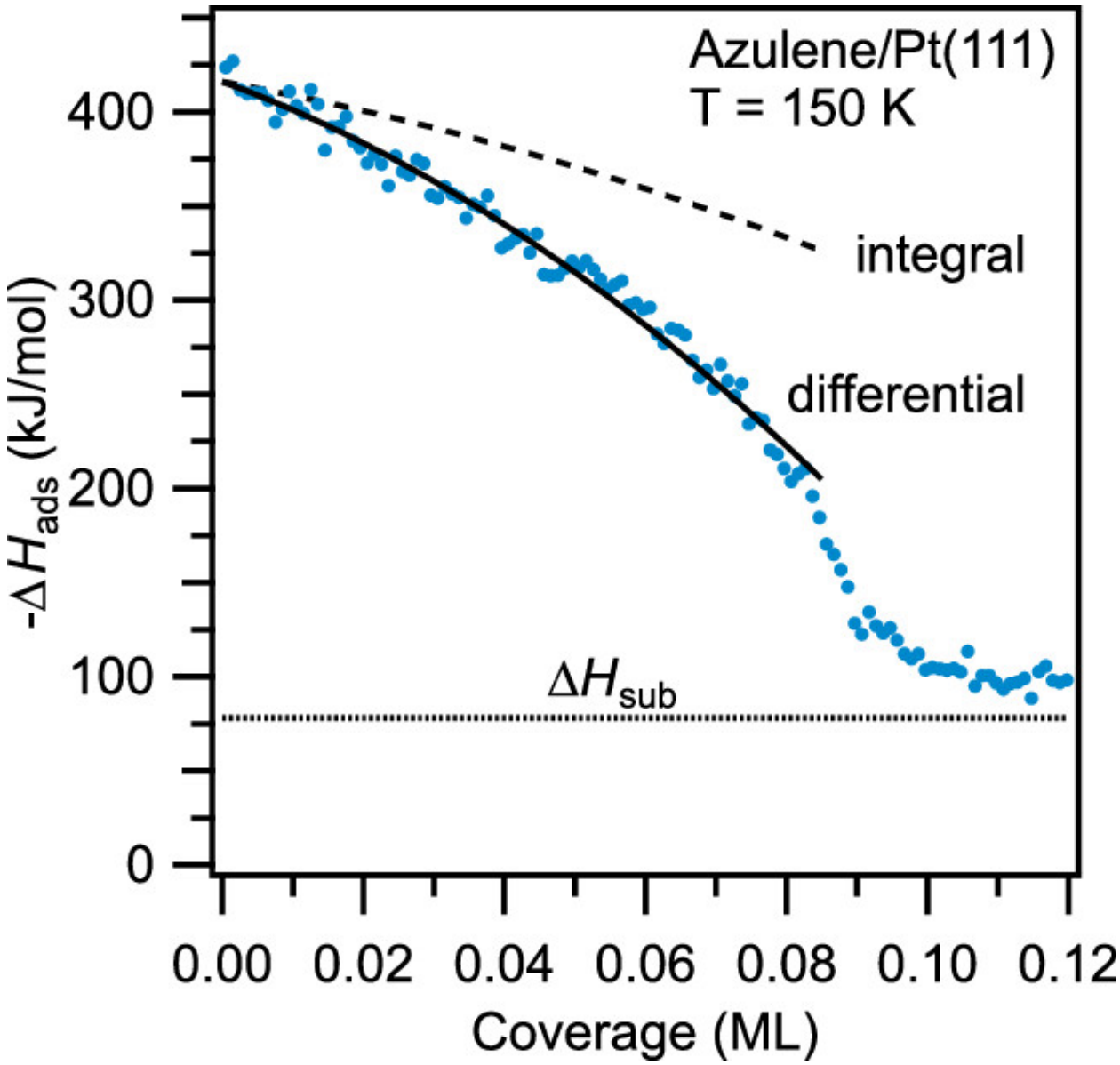

Figure 7.2 - Heat of adsorption of azulene on Pt(111) at 150 K as a function of coverage. Blue dots, experimental data; solid black line, fit function of the differential heat; dashed black line, integrated fit function. The dotted line shows the sublimation enthalpy (ΔH_{sub} = 78.1 ± 2.2 kJ/mol) reported in the literature[214] adjusted for the temperature of 150 K.

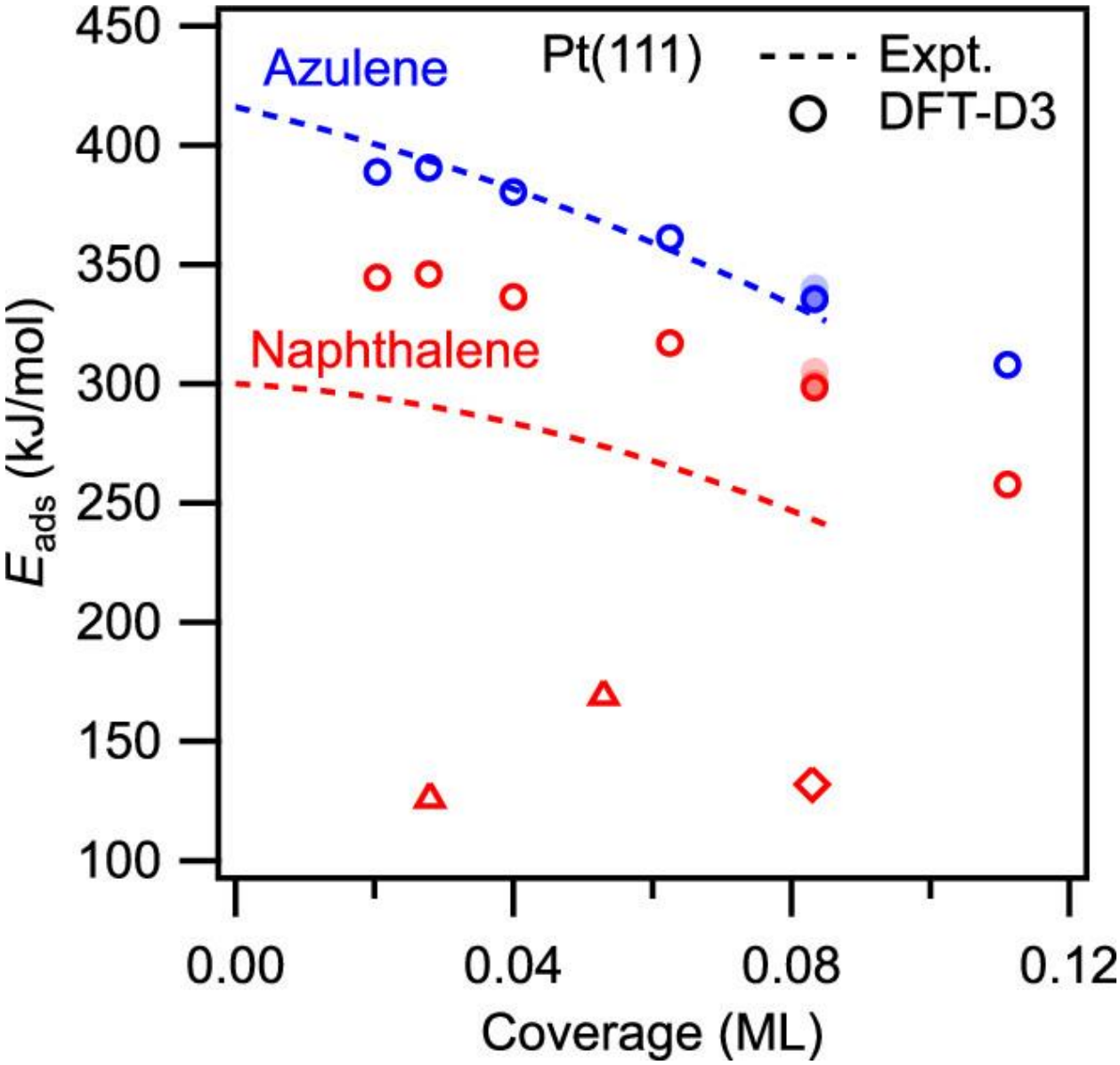

Figure 7.3 - Integral adsorption energies for azulene (blue) and naphthalene (red) on Pt(111). Experiment (Expt., dashed lines): second-order polynomials for the measured integral heats of adsorption taken from Figure 7.2 (azulene) and the literature (naphthalene).[66] Theory: adsorption energies for the six coverages calculated on the PBE-D3 level (open circles). Also included are previous DFT results for naphthalene (triangles[212] and diamonds[211]). The corrected DFT values for the coverage of 0.083 ML (harmonic zero-point vibrational energy, ZPVE and enthalpies) are plotted in progressively lighter colors (filled circles, overlapping).

Chapter 8 Conclusions

This dissertation reports experimental measurements of the energetics of the adsorption of small molecules and molecular fragments on model catalyst single-crystal surfaces. These energetics provide important benchmarks for validating the energy accuracy of developing DFT functionals and other modeling methods. This knowledge is crucial for both the improvement of our current catalyst-driven industrial processes and the development of new catalytic systems to meet growing energy needs.

Chapter 3 describes the study of the molecular adsorption of methanol on clean Ni(111) at 100 K as well as the dissociate adsorption of methanol on oxygen precovered Ni(111) to form adsorbed methoxy and hydroxyl between 100 and 190 K. At 100 K, the heat of molecular adsorption is well fit by the curve (63.2–23.9 θ) kJ/mol from 0–0.30 ML and (99.3–142.7 θ) kJ/mol from 0.30–0.40 ML. The dissociative adsorption of methanol on O-precovered Ni(111) produces adsorbed methoxy and hydroxyl and gives an integral heat of adsorption at 155 K of −70. kJ/mol at a coverage of 0.25 ML (of each product). This gives a heat of formation for adsorbed methoxy of −233 kJ/mol and its bond enthalpy to Ni(111) of 250. kJ/mol. We find a linear trend with a slope of 1 between the bond enthalpies of small oxygenates to Ni(111) and Pt(111) and their corresponding gas-phase hydrogen–ligand bond dissociation enthalpies. These values and trends improve our ability to understand the selectivity, reaction rate, and activity differences between metal surfaces in reactions involving adsorbed oxygenates.

Chapter 4 describes the study of the molecular adsorption of formic acid on Cu(111) at 120 K as well as the dissociative adsorption of formic acid on oxygen precovered Cu(111) to form adsorbed bidentate formate and gaseous water at 240 K. The enthalpy of formation and bond enthalpy of bidentate formate to Cu(111) are -465 kJ/mol and 335 kJ/mol, respectively, at

240 K and 0.20 ML. Corresponding enthalpies are estimated for monodentate formate on Cu(111), which give an enthalpy of formation of -437 kJ/mol and a bond enthalpy of 307 kJ/mol. A comparison to DFT calculations in the literature shows that DFT systematically underestimated the bond enthalpies of mono- and bidentate formate to Cu(111). In comparison to experimental measurements on Pt(111) and Ni(111), these enthalpy values indicate that formate binds ~15 kJ/mol more strongly to Cu(111) than to Ni(111), and ~85 kJ/mol more strongly than to Pt(111). At 240 K, the integral heat of the dissociative adsorption of formic acid on oxygen-predosed Cu(111) is well fit by (99.1 – 46.8θ) kJ/mol, which gives an integral (average) heat of 89.7 kJ/mol at 0.20 ML. The initial differential heat of adsorption is 99.1, which decreases linearly to 80.4 kJ/mol by 0.20 ML. At 120 K, the molecular adsorption of formic acid on clean Cu(111) has an initial differential heat of adsorption of 80.9 kJ/mol, which decreases to ~70 kJ/mol by 0.50 ML. Past that coverage, the heat remains at ~70 kJ/mol through 1.5 ML, after which it drops to a multilayer energy of 64.3 kJ/mol by 1.75 ML. Using the 120 K heat of adsorption curve measured out to multilayer coverages, we estimate the adhesion energy for liquid formic acid to Cu(111) to be 0.271 J/m^2. These results can serve as important experimental benchmarks for DFT calculations and efforts to improve the energy accuracy of computational models, as they are (to our knowledge) the first experimental measurements of the energy of *any* molecular fragment on *any* Cu surface. As formate is the simplest example of a carboxylate adsorbate, these results are applicable not only for systems with formate, but as well as other carboxylates and, more broadly, other oxygenates on Cu surfaces. These results further our understanding of fundamental energetic differences on catalyst surfaces, and can help explain differences in catalytic activity between late transition metal catalysts and guide the development of new catalysts and catalytic pathways.

Chapter 5 describes the study of the molecular adsorption of acetonitrile on Pt(111) at 100 and 180 K. At 180 K, the integral heat of adsorption is 74.3 kJ/mol at a saturation coverage of 0.25 ML and well fit at lower coverages by (82.9–34.4θ) kJ/mol. At 180 K, the initial differential heat of adsorption is 82.9 kJ/mol, which decreases to 63.2 kJ/mol by 0.25 ML. At 100 K, the initial heat of adsorption is 84.5 kJ/mol, which decreases to ~45 kJ/mol at the completion of the first layer (0.35 ML), and finally drops to a multilayer heat of 43.4 kJ/mol above coverages of 0.7 ML. This difference in saturation coverage of the first layer at 100 versus 180 K is a result of the formation of two different surface adsorbate configurations, μ and N-top, with the former being more energetically favorable but the latter arising in the presence of stearic constraints, which are present at 100 K due to lower adsorbate mobility across the surface. These present results agree well with recent TPD and RAIRS studies, and collectively these results provide a clear understanding of the nature of the interaction between acetonitrile, the simplest organic nitrile, and Pt(111). Using the 100 K heat of adsorption curve measured out to multilayer coverages, we estimate the adhesion energy for liquid acetonitrile to Pt(111) to be 0.198 J/m^2. This is slightly higher than that of formic acid and methanol to Pt(111) but considerably lower than that of water, benzene, and phenol. This adhesion energy is useful for estimating the effects of acetonitrile as a solvent on the adsorption energies of catalytic reaction intermediates of interest in liquid-phase catalytic and electrocatalytic reactions.

Chapter 6 describes the study of the molecular adsorption of *n*-decane on Pt(111) at 150 K. The initial heat of adsorption was nearly constant at 152 kJ/mol though 0.0455 ML (except for the first two points below 0.004 ML, which were ~17 kJ/mol higher and attributed to defect sites). The heat then dropped to ~90 kJ/mol by 0.091 ML, then decreased to the multilayer heat of adsorption of 84.9 kJ/mol above 0.27 ML. The integral heat of adsorption at the saturation

coverage of the first layer of adsorbed *n*-decane (0.091 ML) was 132.7 kJ/mol. This was close to that predicted based on desorption energies measured by TPD for shorter *n*-alkane on Pt(111) (C_1-C_6), which were found by Tait et al.[52] to increase nearly proportional to carbon number. Using the experimentally measured heat of adsorption versus coverage out to a bulk-like multilayer coverage, we estimate the adhesion energy of liquid *n*-decane on Pt(111) at room temperature to be 0.148 J/m^2. This is very close to the adhesion energy per unit area of *n*-hexane on Pt(111) estimated based on TPD desorption energies. Thus, linear alkanes have average heats of adsorption in close-packed islands on Pt(111) which approximately equal to a constant (13.3 kJ/mol per C atom) times their total number of CH_2 plus CH_3 groups, but because each CH_2 and CH_3 group occupies nearly the same area on the surface and has the same attraction energy to the surface per mole, the adhesion energy per unit area is also nearly a constant (0.15 J/m^2).

Chapter 7 describes the study of the molecular adsorption of azulene on Pt(111) at 150 K, with comparison to the previously measured molecular adsorption of naphthalene on Pt(111). The isomers azulene and naphthalene constitute a versatile molecular model system to study interfacial interactions of the topological pentagon−heptagon (5−7) defects in graphene. The experimental and theoretical analyses reveal that both molecules are chemisorbed on Pt(111) but azulene forms the stronger bond. Its differential adsorption energy, as measured by SCAC, is larger by 68 to 116 kJ/mol, depending on the coverage, and reaches 416 kJ/mol at zero coverage, compared to 300 kJ/mol for naphthalene. The stronger bond of azulene and the coverage dependencies of the adsorption energies are qualitatively correctly predicted by dispersion-corrected DFT calculations. DFT reveals rehybridization toward sp3 and a partially localized σ-character of the molecule−metal bond. The interfacial electron transfer occurs in both directions through donation and back-donation, resulting in the partial occupation (deoccupation) of

orbitals that are unoccupied (occupied) in the free molecules, as shown by pEDA. Interpretation of the UP and NEXAFS spectra with an MO projection analysis supports the occupation/deoccupation mechanism of the surface chemical bond. It also reveals that the molecular orbitals of azulene and naphthalene respond differently to adsorption. This observation connects the topology-related differences in the electronic structure (especially the HOMO−LUMO gap) with the different bonds to the surface. Our analysis shows that the π-topology of an aromatic ring system substantially influences its interaction at a metal/organic interface in the regime of strong chemisorption. Topology-related effects are therefore relevant for various applications, including metal/organic interfaces in organic (opto)electronic devices or catalytic reactions of aromatic hydrocarbons on transition-metal surfaces.

In sum, this work increases the available calorimetrically measured benchmarks of small molecules and molecular fragments on Pt, Ni and Cu(111), including the first experimentally determined heat of adsorption of any molecular fragment on any Cu surface. These benchmarks give DFT groups reference points to improve energy accuracy of their models. In addition, these benchmarks help explain why some catalysts historically used in industry are as selective and active as they are and provide pathways for the development of even better catalysts. The adsorption energies measured in this dissertation provide fundamental energies needed to develop the catalysts that will assist in meeting humanity's increasing energy requirements.

Chapter 9 References

1. Erisman, J. W., Sutton, M. A., Galloway, J., Klimont, Z. & Winiwarter, W. How a century of ammonia synthesis changed the world. *Nat. Geosci.* **1**, 636–639 (2008).
2. Bond, C. G. *Heterogeneous Catalysis: Principles and Applications*. (Oxford University Press, 1984).
3. Chorkendorff, I. & Niemantsverdriet, J. W. *Concepts of Modern Catalysis and Kinetics*. (2007).
4. Farrauto, R. J. & Bartholomew, C. H. *Fundamentals of Industrial Catalytic Processes*. (Blackie Academic & Professional, 1997).
5. Medford, A. J. *et al.* From the Sabatier principle to a predictive theory of transition-metal heterogeneous catalysis. *J. Catal.* **328**, 36–42 (2015).
6. Vedrine, J. C. *Metal Oxides in Heterogenous Catalysis*. (Elsevier, 2018).
7. Pascanu, V., González Miera, G., Inge, A. K. & Martín-Matute, B. Metal–Organic Frameworks as Catalysts for Organic Synthesis: A Critical Perspective. *J. Am. Chem. Soc.* **141**, 7223–7234 (2019).
8. Mondloch, J. E., Bayram, E. & Finke, R. G. A review of the kinetics and mechanisms of formation of supported-nanoparticle heterogeneous catalysts. *J. Mol. Catal. A Chem.* **355**, 1–38 (2012).
9. Lang, R. *et al.* Non defect-stabilized thermally stable single-atom catalyst. *Nat. Commun.* **10**, 234 (2019).
10. Mavrikakis, M. A search engine for catalysts. *Nat. Mater.* **5**, 847–848 (2006).
11. Nørskov, J. K., Abild-Pedersen, F., Studt, F. & Bligaard, T. Density functional theory in surface chemistry and catalysis. *Proc. Natl. Acad. Sci.* **108**, 937–943 (2011).

12. Greeley, J., Nørskov, J. K. & Mavrikakis, M. Electronic structure and catalysis on metal surfaces. *Annu. Rev. Phys. Chem.* **53**, 319–348 (2002).

13. Hammer, B. & Nørskov, J. K. Theoretical surface science and catalysis—calculations and concepts. in *Impact of Surface Science on Catalysis* vol. 45 71–129 (Academic Press, 2000).

14. Greeley, J. & Mavrikakis, M. Alloy catalysts designed from first principles. *Nat. Mater.* **3**, 810–815 (2004).

15. Studt, F. *et al.* Identification of Non-Precious Metal Alloy Catalysts for Selective Hydrogenation of Acetylene. *Science (80-.).* **320**, 1320–1322 (2008).

16. Greeley, J. & Nørskov, J. Large-scale, density functional theory-based screening of alloys for hydrogen evolution. *Surf. Sci.* **601**, 1590–1598 (2007).

17. Wellendorff, J. *et al.* A benchmark database for adsorption bond energies to transition metal surfaces and comparison to selected DFT functionals. *Surf. Sci.* **640**, 36–44 (2015).

18. Silbaugh, T. L. & Campbell, C. T. Energies of Formation Reactions Measured for Adsorbates on Late Transition Metal Surfaces. *J. Phys. Chem. C* **120**, 25161 (2016).

19. Redhead, P. A. Thermal desorption of gases. *Vacuum* **12**, 274 (1962).

20. Campbell, C. T. & Sellers, J. R. V. Enthalpies and Entropies of Adsorption on Well-Defined Oxide Surfaces: Experimental Measurements. *Chem. Rev.* **113**, 4106–4135 (2013).

21. Foo, K. Y. & Hameed, B. H. Insights into the modeling of adsorption isotherm systems. *Chem. Eng. J.* **156**, 2–10 (2010).

22. Brown, W. A., Kose, R. & King, D. A. Femtomole Adsorption Calorimetry on Single-Crystal Surfaces. *Chem. Rev.* **98**, 797 (1998).

23. Borroni-Bird, C. E. & King, D. A. An ultrahigh vacuum single crystal adsorption microcalorimeter. *Rev. Sci. Instrum.* **62**, 2177–2185 (1991).

24. Lew, W., Lytken, O., Farmer, J. A., Crowe, M. C. & Campbell, C. T. Improved pyroelectric detectors for single crystal adsorption calorimetry from 100 to 350 K. *Rev. Sci. Instrum.* **81**, 24102 (2010).

25. Ford, D. C., Xu, Y. & Mavrikakis, M. Atomic and molecular adsorption on Pt(1 1 1). *Surf. Sci.* **587**, 159–174 (2005).

26. Peng, G., Sibener, S. J., Schatz, G. C. & Mavrikakis, M. CO 2 hydrogenation to formic acid on Ni(110). *Surf. Sci.* **606**, 1050–1055 (2012).

27. Grabow, L. C. & Mavrikakis, M. Mechanism of methanol synthesis on cu through CO2 and CO hydrogenation. *ACS Catal.* **1**, 365–384 (2011).

28. Singh, N. & Campbell, C. T. A Simple Bond-Additivity Model Explains Large Decreases in Heats of Adsorption in Solvents Versus Gas Phase: A Case Study with Phenol on Pt(111) in Water. *ACS Catal.* **9**, 8116 (2019).

29. Akinola, J., Campbell, C. T. & Singh, N. Effects of Solvents on Adsorption Energies: a General Bond-Additivity Model. *J. Phys. Chem. C* **125**, 24371 (2021).

30. Rumptz, J. R. & Campbell, C. T. Adhesion Energies of Solvent Films to Pt(111) and Ni(111) Surfaces by Adsorption Calorimetry. *ACS Catal.* **9**, 11819 (2019).

31. Öström, H. *et al.* Methanol decomposition on Ni(111) and O/Ni(111). *J. Chem. Phys.* **156**, 24704 (2022).

32. Zhu, J. *et al.* Ni–In Synergy in CO2 Hydrogenation to Methanol. *ACS Catal.* **11**, 11371–11384 (2021).

33. Wasmus, S. & Küver, A. Methanol oxidation and direct methanol fuel cells: a selective

review1In honour of Professor W. Vielstich on the occasion of his 75th birthday and in appreciation of his contributions to electrochemistry as well as fuel cell development.1. *J. Electroanal. Chem.* **461**, 14–31 (1999).

34. Carey, S. J. *et al.* Energetics of Adsorbed Methanol and Methoxy on Ni(111): Comparisons to Pt(111). *ACS Catal.* **8**, 10089–10095 (2018).

35. Shiozawa, Y., Koitaya, T., Mukai, K., Yoshimoto, S. & Yoshinobu, J. The roles of step-site and zinc in surface chemistry of formic acid on clean and Zn-modified Cu(111) and Cu(997) surfaces studied by HR-XPS, TPD, and IRAS. *J. Chem. Phys.* **152**, 44703 (2020).

36. Gokhale, A. A., Dumesic, J. A. & Mavrikakis, M. On the mechanism of low-temperature water gas shift reaction on copper. *J. Am. Chem. Soc.* **130**, 1402–1414 (2008).

37. Zhang, R., Ludviksson, A. & Campbell, C. T. The chemisorption of methanol on Cu films on ZnO(000^{-}1)-O. *Catal. Letters* **25**, 277–292 (1994).

38. Lin, S., Johnson, R. S., Smith, G. K., Xie, D. & Guo, H. Pathways for methanol steam reforming involving adsorbed formaldehyde and hydroxyl intermediates on Cu(111): density functional theory studies. *Phys. Chem. Chem. Phys.* **13**, 9622–9631 (2011).

39. Ruehl, G., Harman, S. E., Gluth, O. M., LaVoy, D. H. & Campbell, C. T. Energetics of Adsorbed Formate and Formic Acid on Cu(111) by Calorimetry. *ACS Catal.* (2022) doi:https://doi.org/10.1021/acscatal.2c02608.

40. Villegas, I. & Weaver, M. J. Progressive cation solvation at Pt(111) model electrochemical interfaces in ultrahigh vacuum as probed by infrared spectroscopy and work-function measurements. *Electrochim. Acta* **41**, 661 (1996).

41. Baldelli, S., Mailhot, G., Ross, P., Shen, Y.-R. & Somorjai, G. A. Potential Dependent Orientation of Acetonitrile on Platinum (111) Electrode Surface Studied by Sum

Frequency Generation. *J. Phys. Chem. B* **105**, 654 (2001).

42. Feng, G., Huang, J., Sumpter, B. G., Meunier, V. & Qiao, R. Structure and dynamics of electrical double layers in organic electrolytes. *Phys. Chem. Chem. Phys.* **12**, 5468 (2010).

43. Pavlov, S. V & Kislenko, S. A. Effects of carbon surface topography on the electrode/electrolyte interface structure and relevance to Li–air batteries. *Phys. Chem. Chem. Phys.* **18**, 30830 (2016).

44. Foley, J. K., Korzeniewski, C. & Pons, S. Anodic and cathodic reactions in acetonitrile / tetra-n-butylammonium tetrafluoroborate: an electrochemical and infrared spectroelectrochemical study. *Can. J. Chem.* **66**, 201 (1988).

45. Kiss, L. Electrooxidation of low-permittivity solvents in acetonitrile and solubility of trihexylamine in acetonitrile. *J. Iran. Chem. Soc.* **17**, 67 (2020).

46. Yamada, Y. Unusual Stability of Acetonitrile-Based Superconcentrated Electrolytes for Fast-Charging Lithium-Ion Batteries. *J. Am. Chem. Soc.* **136**, 5039 (2014).

47. Lane, G. H. & Jezek, E. Electrochemical studies of acetonitrile based supercapacitor electrolytes containing alkali and alkaline earth metal cations. *Electrochim. Acta* **150**, 173 (2014).

48. Zhang, S. Insights into the effects of solvent properties in graphene based electric double-layer capacitors with organic electrolytes. *J. Power Sources* **334**, 162 (2016).

49. Trinh, N. D. An Artificial Lithium Protective Layer that Enables the Use of Acetonitrile-Based Electrolytes in Lithium Metal Batteries. *Angew. Chem., Int. Ed.* **57**, 5072 (2018).

50. Dou, Q. Safe and high-rate supercapacitors based on an ‘acetonitrile/water in salt’ hybrid electrolyte. *Energy Environ. Sci.* **11**, 3212 (2018).

51. Ruehl, G., Harman, S. E., Árnadóttir, L. & Campbell, C. T. Acetonitrile Adsorption and

Adhesion Energies onto the Pt(111) Surface by Calorimetry. *ACS Catal.* **12**, 156–163 (2022).

52. Tait, S. L., Dohnálek, Z., Campbell, C. T. & Kay, B. D. N-alkanes on Pt(111) and on C (0001) / Pt (111): Chain length dependence of kinetic desorption parameters. *J. Chem. Phys.* **125**, 1–15 (2006).

53. Harman, S. E., Ruehl, G. & Campbell, C. T. Adsorption and Adhesion Energies of n-Decane on the Pt(111) Surface by Calorimetry. *Surf. Sci.* 122166 (2022) doi:https://doi.org/10.1016/j.susc.2022.122166.

54. Campbell, C. T. & Rumptz, J. R. Adhesion Energies of Liquid Hydrocarbon Solvents onto Pt(111), MgO(100), Graphene, and TiO2(110) from Temperature-Programmed Desorption Energies. *J. Phys. Chem. C* **125**, 27931–27937 (2021).

55. Tsen, A. W. *et al.* Tailoring Electrical Transport across Grain Boundaries in Polycrystalline Graphene. *Science (80-.).* **336**, 1143 (2012).

56. Huang, P. Y. *et al.* Grains and grain boundaries in single-layer graphene atomic patchwork quilts. *Nature* **469**, 389–392 (2011).

57. Yazyev, O. V. & Louie, S. G. Electronic transport in polycrystalline graphene. *Nat. Mater.* **9**, 806–809 (2010).

58. Grantab, R., Shenoy, V. B. & Ruoff, R. S. Anomalous Strength Characteristics of Tilt Grain Boundaries in Graphene. *Science (80-.).* **330**, 946 (2010).

59. Rasool, H. I., Ophus, C., Klug, W. S., Zettl, A. & Gimzewski, J. K. Measurement of the Intrinsic Strength of Crystalline and Polycrystalline Graphene. *Nat. Commun.* **4**, 2811 (2013).

60. Ito, Y. *et al.* Correlation between Chemical Dopants and Topological Defects in

Catalytically Active Nanoporous Graphene. *Adv. Mater.* **28**, 10644 (2016).

61. Malola, S., Häkkinen, H. & Koskinen, P. Structural, Chemical, and Dynamical Trends in Graphene Grain Boundaries. *Phys. Rev. B* **81**, 165447 (2010).

62. Wei, Y. *et al.* The nature of strength enhancement and weakening by pentagong-heptagon defects in graphene. *Nat. Mater.* **11**, 759–763 (2012).

63. Shekhawat, A. & Ritchie, R. O. Toughness and Strength of Nanocrystalline Graphene. *Nat. Commun.* **7**, 10546 (2016).

64. Červenka, J., Katsnelson, M. I. & Flipse, C. F. J. Room-Temperature Ferromagnetism in Graphite Driven by Two-Dimensional Networks of Point defects. *Nat. Phys.* **5**, 840 (2009).

65. Klein, B. P. *et al.* Enhanced Bonding of Pentagon–Heptagon Defects in Graphene to Metal Surfaces: Insights from the Adsorption of Azulene and Naphthalene to Pt(111). *Chem. Mater.* **32**, 1041–1053 (2020).

66. Gottfried, J. M., Vestergaard, E. K., Bera, P. & Campbell, C. T. Heat of Adsorption of Naphthalene on Pt(111) Measured by Adsorption Calorimetry. *J. Phys. Chem. B* **110**, 17539 (2006).

67. Lytken, O., Lew, W. & Campbell, C. T. Catalytic reaction energetics by single crystal adsorption calorimetry: Hydrocarbons on Pt(111). *Chem. Soc. Rev.* **37**, 2172–2179 (2008).

68. Ajo, H. M., Ihm, H., Moilanen, D. E. & Campbell, C. T. Calorimeter for adsorption energies of larger molecules on single crystal surfaces. *Rev. Sci. Instrum.* **75**, 4471 (2004).

69. Stuckless, J. T., Frei, N. A. & Campbell, C. T. Pyroelectric detector for single-crystal adsorption microcalorimetry: Analysis of pulse shape and intensity. *Sensors Actuators, B Chem.* **62**, 13–22 (2000).

70. King, D. A. & Wells, M. G. Molecular Beam Investigation of Adsorption Kinetics on Bulk Metal Targets: Nitrogen on Tungsten. *Surf. Sci.* **29**, 454 (1972).

71. Erskine, J. L. & Bradshaw, A. M. The Electronic Structure and Orientation of the Surface Methoxy Species on Ni(111). *Chem. Phys. Lett.* **72**, 260 (1980).

72. Rubloff, G. W. & Demuth, J. E. Ultraviolet Photoemission and Flash-Desorption Studies of the Chemisorption and Decomposition of Methanol on Ni(111). *J. Vac. Sci. Technol.* **14**, 419 (1977).

73. Russell, J. N., Chorkendorff, I. & Yates, J. T. Methanol Decomposition on Ni(111): Investigation of the C-O Bond Scission Mechanism. *Surf. Sci.* **183**, 316 (1987).

74. Gates, S. M., Russell, J. N. & Yates, J. T. Observation of a Deuterium Kinetic Isotope Effect in the Chemisorption and Reaction of Methanol on Ni(111). *Surf. Sci.* **146**, 199 (1984).

75. Demuth, J. E. & Ibach, H. Observation of a Methoxy Species on Ni(111) by High-Resolution Electron Energy-Loss Spectroscopy. *Chem. Phys. Lett.* **60**, 395 (1979).

76. Zenobi, R., Xu, J., Yates, J. T., Persson, B. N. J. & Volokitin, A. I. FTIR Overtone Spectroscopy on Surfaces. The C—O Mode in Chemisorbed Methoxy on Ni(111). *Chem. Phys. Lett.* **208**, 414 (1993).

77. Schaff, O. *et al.* The Structure of the Surface Methoxy Species on Ni(111). *Surf. Sci.* **333**, 201 (1995).

78. Schaff, O. *et al.* Quantitative Determination of Molecular Adsorption Structures Using Photoelectron Diffraction: the Methoxy Species. *J. Electron Spectrosc. Relat. Phenom.* **75**, 117 (1995).

79. Gates, S. M., Russell, J. N. & Yates, J. T. Scanning Kinetic Spectroscopy (SKS): A New

Method for Investigation of Surface Reaction Processes. *Surf. Sci.* **159**, 233 (1985).

80. Amemiya, K. *et al.* Oxygen K-Edge x-Ray-Absorption Fine-Structure Study of Surface Methoxy Species on Cu(111) and Ni(111). *Phys. Rev. B Condens. Matter Mater. Phys.* **59**, 2307 (1999).

81. Karp, E. M., Silbaugh, T. L., Crowe, M. C. & Campbell, C. T. Energetics of Adsorbed Methanol and Methoxy on Pt(111) by Microcalorimetry. *J. Am. Chem. Soc.* **134**, 20388 (2012).

82. Zhao, W., Carey, S. J., Mao, Z. & Campbell, C. T. Adsorbed Hydroxyl and Water on Ni(111): Heats of Formation by Calorimetry. *ACS Catal.* **8**, 1485 (2018).

83. Zhao, W., Carey, S. J., Morgan, S. E. & Campbell, C. T. Energetics of Adsorbed Formate and Formic Acid on Ni(111) by Calorimetry. *J. Catal.* **352**, 300 (2017).

84. Karp, E. M., Silbaugh, T. L. & Campbell, C. T. Bond Energies of Molecular Fragments to Metal Surfaces Track Their Bond Energies to H Atoms. *J. Am. Chem. Soc.* **136**, 4137 (2014).

85. Lytken, O. *et al.* Energetics of Cyclohexene Adsorption and Reaction on Pt(111) by Low-Temperature Microcalorimetry. *J. Am. Chem. Soc.* **130**, 10247 (2008).

86. Zion, B. D., Hanbicki, A. T. & Sibener, S. J. Kinetic Energy Effects on the Oxidation of Ni(111) Using O2 Molecular Beams. *Surf. Sci.* **417**, L154 (1998).

87. Norton, P. R. & Tapping, R. L. Photoelectron Spectroscopic Study of the Interaction of Nickel and Oxygen. *Faraday Discuss. Chem. Soc.* **60**, 71 (1975).

88. Holloway, P. H. & Hudson, J. B. Kinetics of the Reaction of Oxygen with Clean Nickel Single Crystal Surfaces. *Surf. Sci.* **43**, 141 (1974).

89. Chao, J. & Rossini, F. D. Heats of Combustion, Formation, and Isomerization of Nineteen

Alkanols. *J. Chem. Eng. Data* **10**, 374 (1965).

90. Baber, A. E., Lawton, T. J. & Sykes, E. C. H. Hydrogen-Bonded Networks in Surface-Bound Methanol. *J. Phys. Chem. C* **115**, 9157 (2011).

91. Lawton, T. J., Carrasco, J., Baber, A. E., Michaelides, A. & Sykes, E. C. H. Hydrogen-Bonded Assembly of Methanol on Cu(111). *Phys. Chem. Chem. Phys.* **14**, 11846 (2012).

92. Murphy, C. J. *et al.* Structure and Energetics of Hydrogen-Bonded Networks of Methanol on Close Packed Transition Metal Surfaces. *J. Chem. Phys.* **141**, 14701 (2014).

93. Tauer, K. J. & Lipscomb, W. N. On the Crystal Structures, Residual Entropy and Dielectric Anomaly of Methanol. *Acta Crystallogr.* **5**, 606 (1952).

94. Carlson, H. G. & Westrum, E. F. Methanol: Heat Capacity, Enthalpies of Transition and Melting, and Thermodynamic Properties from 5 - 300 K. *J. Chem. Phys.* **54**, 1464 (1971).

95. Green, S. D. *et al.* Applying Laboratory Thermal Desorption Data in an Interstellar Context: Sublimation of Methanol Thin Films. *Mon. Not. R. Astron. Soc.* **398**, 357 (2009).

96. Lew, W., Crowe, M. C., Karp, E. & Campbell, C. T. Energy of Molecularly Adsorbed Water on Clean Pt(111) and Pt(111) with Coadsorbed Oxygen by Calorimetry. *J. Phys. Chem. C* **115**, 9164 (2011).

97. Sexton, B. A. Methanol Decomposition on Platinum (111). *Surf. Sci.* **102**, 271 (1981).

98. Tsang, W. *Energetics of Organic Free Radicals*. (1996).

99. Remediakis, I. N., Abild-Pedersen, F. & Nørskov, J. K. DFT Study of Formaldehyde and Methanol Synthesis from CO and H2 on Ni(111). *J. Phys. Chem. B* **108**, 14535 (2004).

100. Kelly, T. G., Stottlemyer, A. L., Ren, H. & Chen, J. G. Comparison of O-H, C-H, and C-O Bond Scission Sequence of Methanol on Tungsten Carbide Surfaces Modified by Ni, Rh, and Au. *J. Phys. Chem. C* **115**, 6644 (2011).

101. Kramer, Z. C., Gu, X. K., Zhou, D. D. Y., Li, W. X. & Skodje, R. T. Following Molecules through Reactive Networks: Surface Catalyzed Decomposition of Methanol on Pd(111), Pt(111), and Ni(111). *J. Phys. Chem. C* **118**, 12364 (2014).

102. Wang, G., Zhou, Y., Morikawa, Y. & Nakamura, J. Kinetic Mechanism of Methanol Decomposition on Ni (111) Surface: A Theoretical Study. *J. Phys. Chem. B* **109**, 12431 (2005).

103. Ren, R. *et al.* Why Is Metallic Pt the Best Catalyst for Methoxy Decomposition? *J. Nat. Gas Chem.* **20**, 90 (2011).

104. Carey, S. J., Zhao, W., Frehner, A., Campbell, C. T. & Jackson, B. Energetics of Adsorbed Methyl and Methyl Iodide on Ni(111) by Calorimetry: Comparison to Pt(111) and Implications for Catalysis. *ACS Catal.* **7**, 1286–1294 (2017).

105. Karp, E. M., Campbell, C. T., Studt, F., Abild-Pedersen, F. & Norskov, J. K. Energetics of Oxygen Adatoms, Hydroxyl Species and Water Dissociation on Pt(111). *J. Phys. Chem. C* **116**, 25772 (2012).

106. Karp, E. M., Silbaugh, T. L. & Campbell, C. T. Energetics of Adsorbed CH3 and CH on Pt(111) by Calorimetry: Dissociative Adsorption of CH3I. *J. Am. Chem. Soc.* **117**, 6325 (2013).

107. Lew, W. *et al.* The energy of adsorbed hydroxyl on Pt(111) by microcalorimetry. *J. Phys. Chem. C* **115**, 11586–11594 (2011).

108. Bryndza, H. E., Fong, L. K., Paciello, R. A., Tam, W. & Bercaw, J. E. Relative Metal-Hydrogen, -Oxygen, -Nitrogen, and -Carbon Bond Strengths for Organoruthenium and Organoplatinum Compounds; Equilibrium Studies of Cp*(PMe3)2RuX and (DPPE)MePtX Systems. *J. Am. Chem. Soc.* **109**, 1444 (1987).

109. Bryndza, H. E. *et al.* Comparison of Metal-Hydrogen, -Oxygen, -Nitrogen and -Carbon Bond Strengths and Evaluation of Functional Group Additivity Principles for Organoruthenium and Organoplatinum Compounds. *Polyhedron* **7**, 1441 (1988).

110. Bulls, A. R., Bercaw, J. E., Manriquez, J. M. & Thompson, M. E. Relative Bond Dissociation Energies for Early Transition Metal Alkyl, Aryl, Alkynyl and Hydride Compounds. Equilibration of Metallated Cyclopentadienyl Derivatives of Peralkylated Hafnocene and Scandocene with Hydrocarbons and Dihydrogen. *Polyhedron* **7**, 1409 (1988).

111. Silbaugh, T. L., Karp, E. M. & Campbell, C. T. Energetics of Formic Acid Conversion to Adsorbed Formates on Pt(111) by Transient Calorimetry. *J. Am. Chem. Soc.* **136**, 3964–3971 (2014).

112. Ihm, H., Ajo, H. M., Gottfried, J. M., Bera, P. & Campbell, C. T. Calorimetric Measurement of the Heat of Adsorption of Benzene on Pt(111). *J. Phys. Chem. B* **108**, 14627–14633 (2004).

113. Karp, E. M., Silbaugh, T. L. & Campbell, C. T. Energetics of Adsorbed CH3 on Pt(111) by Calorimetry. *J. Am. Chem. Soc.* **135**, 5208–5211 (2013).

114. Chen, B. W. J., Bhandari, S. & Mavrikakis, M. Role of Hydrogen-bonded Bimolecular Formic Acid–Formate Complexes for Formic Acid Decomposition on Copper: A Combined First-Principles and Microkinetic Modeling Study. *ACS Catal.* **11**, 4349–4361 (2021).

115. Li, S., Scaranto, J. & Mavrikakis, M. On the Structure Sensitivity of Formic Acid Decomposition on Cu Catalysts. *Top. Catal.* **59**, 1580–1588 (2016).

116. Baber, A. E. *et al.* Assisted deprotonation of formic acid on Cu(111) and self-assembly of

1D chains. *Phys. Chem. Chem. Phys.* **15**, 12291–12298 (2013).

117. Putra, S. E. M. *et al.* Van der Waals density functional study of formic acid adsorption and decomposition on Cu(111). *J. Chem. Phys.* **150**, 154707 (2019).

118. Putra, S. E. M. *et al.* Theoretical study on adsorption and reaction of polymeric formic acid on the Cu(111) surface. *Phys. Rev. Mater.* **5**, 75801 (2021).

119. Lynch, I. *et al.* The nanoparticle-protein complex as a biological entity; a complex fluids and surface science challenge for the 21st century. *Adv. Colloid Interface Sci.* **134**–**135**, 167–174 (2007).

120. Kasemo, B. Biological surface science. *Surf. Sci.* **500**, 656–677 (2002).

121. Barth, J. V, Costantini, G. & Kern, K. Engineering atomic and molecular nanostructures at surfaces. *Nature* **437**, 671–679 (2005).

122. Sarikaya, M., Tamerler, C., Jen, A. K.-Y., Schulten, K. & Baneyx, F. Molecular biomimetics: nanotechnology through biology. *Nat. Mater.* **2**, 577–585 (2003).

123. Durand, W. J., Peterson, A. A., Studt, F., Abild-Pedersen, F. & Nørskov, J. K. Structure effects on the energetics of the electrochemical reduction of CO2 by copper surfaces. *Surf. Sci.* **605**, 1354–1359 (2011).

124. Qiao, J., Liu, Y., Hong, F. & Zhang, J. A review of catalysts for the electroreduction of carbon dioxide to produce low-carbon fuels. *Chem. Soc. Rev.* **43**, 631–675 (2014).

125. Quan, J. *et al.* Vibration-driven reaction of CO2 on Cu surfaces via Eley–Rideal-type mechanism. *Nat. Chem.* **11**, 722–729 (2019).

126. Wang, Y.-F., Li, K. & Wang, G.-C. Formic acid decomposition on Pt1/Cu (111) single platinum atom catalyst: Insights from DFT calculations and energetic span model analysis. *Appl. Surf. Sci.* **436**, 631–638 (2018).

127. Yoo, J. S., Abild-Pedersen, F., Nørskov, J. K. & Studt, F. Theoretical Analysis of Transition-Metal Catalysts for Formic Acid Decomposition. *ACS Catal.* **4**, 1226–1233 (2014).

128. Herron, J. A., Scaranto, J., Ferrin, P., Li, S. & Mavrikakis, M. Trends in Formic Acid Decomposition on Model Transition Metal Surfaces: A Density Functional Theory study. *ACS Catal.* **4**, 4434–4445 (2014).

129. Pradhan, S., Reddy, A. S., Devi, R. N. & Chilukuri, S. Copper-based catalysts for water gas shift reaction: Influence of support on their catalytic activity. *Catal. Today* **141**, 72–76 (2009).

130. Appel, A. M. *et al.* Frontiers, Opportunities, and Challenges in Biochemical and Chemical Catalysis of CO2 Fixation. *Chem. Rev.* **113**, 6621–6658 (2013).

131. Hori, Y., Wakebe, H., Tsukamoto, T. & Koga, O. Electrocatalytic process of CO selectivity in electrochemical reduction of CO2 at metal electrodes in aqueous media. *Electrochim. Acta* **39**, 1833–1839 (1994).

132. Nie, X., Esopi, M. R., Janik, M. J. & Asthagiri, A. Selectivity of CO2 Reduction on Copper Electrodes: The Role of the Kinetics of Elementary Steps. *Angew. Chemie Int. Ed.* **52**, 2459–2462 (2013).

133. Babar, S. & Weaver, J. H. Optical constants of Cu, Ag, and Au revisited. *Appl. Opt.* **54**, 477–481 (2015).

134. Weaver, J. H., Krafka, C., Lynch, D. W. & Koch, E. E. Optical properties of metals. *Appl. Opt.* **20**, 1124_1----1125 (1981).

135. Marcinkowski, M. D. *et al.* Microscopic View of the Active Sites for Selective Dehydrogenation of Formic Acid on Cu(111). *ACS Catal.* **5**, 7371–7378 (2015).

136. Shiozawa, Y., Koitaya, T., Mukai, K., Yoshimoto, S. & Yoshinobu, J. Quantitative analysis of desorption and decomposition kinetics of formic acid on Cu(111): The importance of hydrogen bonding between adsorbed species. *J. Chem. Phys.* **143**, 234707 (2015).

137. Sotiropoulos, A., Milligan, P. K., Cowie, B. C. C. & Kadodwala, M. A structural study of formate on Cu(111). *Surf. Sci.* **444**, 52–60 (2000).

138. Wühn, M., Weckesser, J. & Wöll, C. Bonding and Orientational Ordering of Long-Chain Carboxylic Acids on Cu(111): Investigations Using X-ray Absorption Spectroscopy. *Langmuir* **17**, 7605–7612 (2001).

139. Nakano, H., Nakamura, I., Fujitani, T. & Nakamura, J. Structure-Dependent Kinetics for Synthesis and Decomposition of Formate Species over Cu(111) and Cu(110) Model Catalysts. *J. Phys. Chem. B* **105**, 1355–1365 (2001).

140. Stone, P., Poulston, S., Bennett, R. A., Price, N. J. & Bowker, M. An STM, TPD and XPS investigation of formic acid adsorption on the oxygen-precovered c(6×2) surface of Cu(110). *Surf. Sci.* **418**, 71–83 (1998).

141. Nishimura, H., Yatsu, T., Fujitani, T., Uchijima, T. & Nakamura, J. Synthesis and decomposition of formate on a Cu(111) surface — kinetic analysis. *J. Mol. Catal. A Chem.* **155**, 3–11 (2000).

142. Pöllmann, S., Bayer, A., Ammon, C. & Steinrück, H.-P. Adsorption and Reaction of Methanol on Clean and Oxygen Precovered Cu(111). *Zeitschrift für Phys. Chemie* **218**, 957–971 (2004).

143. Kolovos-Vellianitis, D., Kammler, T. & Küppers, J. Interaction of gaseous H atoms with Cu(100) surfaces: Adsorption, absorption, and abstraction. *Surf. Sci.* **454**, 316–319 (2000).

144. Bange, K., Grider, D. E., Madey, T. E. & Sass, J. K. The surface chemistry of H2O on clean and oxygen-covered Cu(110). *Surf. Sci.* **137**, 38–64 (1984).

145. Clendening, W. D., Rodriguez, J. A., Campbell, J. M. & Campbell, C. T. The chemisorption and coadsorption of water and oxygen on Cs-dosed Cu(110). *Surf. Sci.* **216**, 429–461 (1989).

146. Habraken, F. H. P. M., Kieffer, E. P. & Bootsma, G. A. A study of the kinetics of the interactions of O2 and N2O with a Cu(111) surface and of the reaction of CO with adsorbed oxygen using aes, LEED and ellipsometry. *Surf. Sci.* **83**, 45–59 (1979).

147. Acree, Jr., W. E. & Chickos, J. S. Phase Transition Enthalpy Measurements of Organic and Organometallic Compounds. in *NIST Standard Reference Database Number 69* (eds. Linstrom, P. J. & Mallard, W. G.) (National Institute of Standards and Technology, 2021).

148. Yaws, C. L. *Yaw's Handbook of Theromdynamic and Physical Properties of Chemical Compounds*. (Knovel, 2003).

149. Stephenson, R. M. & Malanowski, S. *Handbook of the thermodynamics of organic compounds*. (Elsevier, 1987).

150. Carey, S. J., Zhao, W., Mao, Z. & Campbell, C. T. Energetics of Adsorbed Phenol on Ni(111) and Pt(111) by Calorimetry. *J. Phys. Chem. C* **123**, 7627–7632 (2019).

151. Carey, S. J., Zhao, W. & Campbell, C. T. Energetics of adsorbed benzene on Ni(111) and Pt(111) by calorimetry. *Surf. Sci.* **676**, 9–16 (2018).

152. Dell, R. M., Stone, F. S. & Tiley, P. F. The adsorption of oxygen and other gases on copper. *Trans. Faraday Soc.* **49**, 195–201 (1953).

153. Giamello, E., Fubini, B., Lauro, P. & Bossi, A. A microcalorimetric method for the evaluation of copper surface area in Cu□ZnO catalyst. *J. Catal.* **87**, 443–451 (1984).

154. Wang, Y.-Q., Yan, L.-F. & Wang, G.-C. Oxygen-assisted water partial dissociation on copper: a model study. *Phys. Chem. Chem. Phys.* **17**, 8231–8238 (2015).

155. Carey, S. J., Zhao, W. & Campbell, C. T. Bond Energies of Adsorbed Intermediates to Metal Surfaces: Correlation with Hydrogen-Ligand and Hydrogen-Surface Bond Energies and Electronegativities. *Angew. Chem. Int. Ed. Engl.* **57**, 16877–16881 (2018).

156. Luo, Y.-R. *Comprehensive Handbook of Chemical Bond Energies*. (CRC Press, 2007).

157. Grabow, L. C., Gokhale, A. A., Evans, S. T., Dumesic, J. A. & Mavrikakis, M. Mechanism of the Water Gas Shift Reaction on Pt: First Principles, Experiments, and Microkinetic Modeling. *J. Phys. Chem. C* **112**, 4608–4617 (2008).

158. Haynes, W. M., Lide, D. R. & Bruno, T. J. *CRC Handbook of Chemistry and Physics*. (2016).

159. Ohtani, T. *et al.* IRAS and TPD study of adsorbed formic acid on Pt(110)-(1 × 2) surface. *Surf. Sci.* **368**, 270–274 (1996).

160. Chapman, D. 48. The infrared spectra of liquid and solid formic acid. *J. Chem. Soc.* 225–229 (1956) doi:10.1039/JR9560000225.

161. Zhang, Y. Direct conversion of cellulose and raw biomass to acetonitrile by catalytic fast pyrolysis in ammonia. *Green Chem.* **21**, 812 (2019).

162. Mellmer, M. A. *et al.* Solvent-enabled control of reactivity for liquid-phase reactions of biomass-derived compounds. *Nat. Catal.* **1**, 199–207 (2018).

163. Walker, T. W. *et al.* Universal kinetic solvent effects in acid-catalyzed reactions of biomass-derived oxygenates. *Energy Environ. Sci.* **11**, 617–628 (2018).

164. He, J. *et al.* Production of levoglucosenone and 5-hydroxymethylfurfural from cellulose in polar aprotic solvent–water mixtures. *Green Chem.* **19**, 3642–3653 (2017).

165. Kryachko, E. S. & Nguyen, M. T. Hydrogen Bonding between Phenol and Acetonitrile. *J. Phys. Chem. A* **106**, 4267 (2002).

166. Campbell, C. T. Energies of Adsorbed Catalytic Intermediates on Transition Metal Surfaces: Calorimetric Measurements and Benchmarks for Theory. *Acc. Chem. Res.* **52**, 984 (2019).

167. Silbaugh, T. L. & Campbell, C. T. Energies of formation reactions measured for adsorbates on late transition metal surfaces. *J. Phys. Chem. C* **120**, 25161–25172 (2016).

168. Tylinski, M., Smith, R. S. & Kay, B. D. Structure and Desorption Kinetics of Acetonitrile Thin Films on Pt (111) and on Graphene on Pt (111). *J. Phys. Chem. C* **124**, 2521 (2020).

169. Markovits, A. & Minot, C. Theoretical study of the acetonitrile flip-flop with the electric field orientation: adsorption on a Pt (111) electrode surface. *Catal. Lett.* **91**, 225 (2003).

170. Shayeghi, A. Adsorption of Acetonitrile, Benzene, and Benzonitrile on Pt(111): Single Crystal Adsorption Calorimetry and Density Functional Theory. *J. Phys. Chem. C* **121**, 21354 (2017).

171. Pašti, I. A., Markovic, A., Gavrilov, N. & Mentus, S. V. Adsorption of Acetonitrile on Platinum and its Effects on Oxygen Reduction Reaction in Acidic Aqueous Solutions ─ Combined Theoretical and Experimental Study. *Electrocatalysis* **7**, 235 (2016).

172. Domalski, E. S. & Hearing, E. D. Heat Capacities and Entropies of Organic Compounds in the Condensed Phase. Volume III. *J. Phys. Chem. Ref. Data* **25**, 1 (1996).

173. Yaws, C. L. *Yaw's Handbook of Theromdynamic and Physical Properties of Chemical Compounds*. (Knovel, 2003).

174. Garwood, G. A. & Hubbard, A. T. Superlattices formed by interaction of polar solvents with Pt(111) surfaces studied by LEED, Auger spectroscopy and thermal desorption mass

spectrometry. *Surf. Sci.* **118**, 223 (1982).

175. Gardin, D. E., Barbieri, A., Batteas, J. D., Van Hove, M. A. & Somorjai, G. A. Tensor LEED analysis of the Ni(111)-p(2×2)-CH3CN structure. *Surf. Sci.* **304**, 316 (1994).

176. Ou, E. C., Young, P. A. & Norton, P. R. Interaction of acetonitrile with platinum (111): more properties of the n2(C,N) state and new species in the submonolayer. *Surf. Sci.* **277**, 123 (1992).

177. Sexton, B. A. & Avery, N. R. Coordination of acetonitrile (CH3CN) to Platinum (111): evidence for an n2 (C,N) species. *Surf. Sci.* **129**, 21 (1983).

178. Waldrup, S. B. & Williams, C. T. Acetonitrile Adsorption on Polycrystalline Platinum: An In Situ Investigation Using Sum Frequency Spectroscopy. *J. Phys. Chem. C* **112**, 219 (2008).

179. Iyemperumal, S. K. & Deskins, N. A. Evaluating Solvent Effects at the Aqueous/Pt(111) Interface. *ChemPhysChem* **18**, 2171–2190 (2017).

180. Madon, R. J., O'Connell, J. P. & Boudart, M. Catalytic hydrogenation of cyclohexene: Part II. Liquid phase reaction on supported platinum in a gradientless slurry reactor. *AIChE J.* **24**, 904–911 (1978).

181. Gonzo, E. E. & Boudart, M. Catalytic hydrogenation of cyclohexene: 3. Gas-phase and liquid-phase reaction on supported palladium. *J. Catal.* **52**, 462–471 (1978).

182. Singh, N. *et al.* Aqueous phase catalytic and electrocatalytic hydrogenation of phenol and benzaldehyde over platinum group metals. *J. Catal.* **382**, 372–384 (2020).

183. Mellmer, M. A. *et al.* Solvent Effects in Acid-Catalyzed Biomass Conversion Reactions. *Angew. Chemie Int. Ed.* **53**, 11872–11875 (2014).

184. Campbell, J. M. & Campbell, C. T. The interactions of cyclopentane with clean and

bismuth-covered Pt(111). *Surf. Sci.* **210**, 46–68 (1989).

185. Bussell, M. E., Henn, F. C. & Campbell, C. T. A BPTDS and HREELS study of the interaction of cyclohexane with the platinum (111) surface. *J. Phys. Chem.* **96**, 5978–5982 (1992).

186. Freund, H. J., Nilius, N., Risse, T., Schauermann, S. & Schmidt, T. Innovative measurement techniques in surface science. *ChemPhysChem* **12**, 79–87 (2011).

187. Geim, A. K. & Novoselov, K. S. The Rise of Graphene. *Nat. Mater.* **6**, 183 (2007).

188. Kim, P. Graphene: Across the border. *Nat. Mater.* **9**, 792–793 (2010).

189. Yazyev, O. V & Louie, S. G. Electronic Transport in Polycrystalline Graphene. *Nat. Mater.* **9**, 806 (2010).

190. Kim, K. *et al.* Grain Boundary Mapping in Polycrystalline Graphene. *ACS Nano* **5**, 2142 (2011).

191. Wei, Y. *et al.* The Nature of Strength Enhancement and Weakening by Pentagon-Heptagon Defects in Graphene. *Nat. Mater.* **11**, 759 (2012).

192. Ni, B. *et al. Handbook of Graphene*. (2019).

193. Batzill, M. The Surface Science of Graphene: Metal Interfaces, CVD Synthesis, Nanoribbons, Chemical Modifications, and Defects. *Surf. Sci. Rep.* **67**, 83 (2012).

194. Wang, R. *et al.* Graphene Based Functional Devices: A Short Review. *Front. Phys.* **14**, 13603 (2019).

195. Cusati, T. *et al.* Electrical Properties of Graphene-Metal Contacts. *Sci. Rep.* **7**, 5109 (2017).

196. Klein, B. P. *et al.* Molecular Topology and the Surface Chemical Bond: Alternant Versus Nonalternant Aromatic Systems as Functional Structural Elements. *Phys. Rev. X* **9**, 11030

(2019).

197. Mallion, R. B. & Rouvray, D. H. The Golden Jubilee of the Coulson-Rushbrooke Pairing Theorem. *J. Math. Chem.* **5**, 1 (1990).

198. Coulson, C. A. & Rushbrooke, G. S. Note on the Method of Molecular Orbitals. *Math. Proc. Cambridge Philos. Soc.* **36**, 193 (1940).

199. Lide, D. R. *CRC Handbook of Chemistry and Physics*. (2010).

200. Xin, H. & Gao, X. Application of Azulene in Constructing Organic Optoelectronic Materials: New Tricks for an Old Dog. *Chempluschem* **82**, 945 (2017).

201. Koch, N. Organic Electronic Devices and Their Functional Interfaces. *ChemPhysChem* **8**, 1438 (2007).

202. Kahn, A., Koch, N. & Gao, W. Electronic Structure and Electrical Properties of Interfaces between Metals and π-Conjugated Molecular Films. *J. Polym. Sci., Part B Polym. Phys.* **41**, 2529 (2003).

203. Koch, N., Ueno, N. & Wee, A. T. S. *The Molecule-Metal Interface*. (2013).

204. Dahlgren, D. & Hemminger, J. C. Symmetry Extinction of Leed Beams for Naphthalene Adsorbed on Pt(111). *Surf. Sci.* **109**, L513 (1981).

205. Dahlgren, D. & Hemminger, J. C. Chemisorption and Thermal Chemistry of Azulene and Naphthalene Adsorbed on Pt(111). *Surf. Sci.* **114**, 459 (1982).

206. Dahlgren, D. & Hemminger, J. C. Chemisorption and Ordering of Naphthalene and Azulene on Pt[7(111) × (100)]: The Effect of Periodic Defects on Long Range Order. *Surf. Sci.* **134**, 836 (1983).

207. Gland, J. L. & Somorjai, G. A. Low Energy Eelektron Diffraction and Work Function Studies of Benzene, Naphthalene and Pyridine Adsorbed on Pt(111) and Pt(100) Single

Crystal Surfaces. *Surf. Sci.* **38**, 157 (1973).

208. Hallmark, V. M., Chiang, S., Brown, J. K. & Wöll, C. Real-Space Imaging of the Molecular Organization of Naphthalene on Pt(111). *Phys. Rev. Lett.* **66**, 48 (1991).

209. Hallmark, V. M., Chiang, S., Meinhardt, K.-P. & Hafner, K. Observation and Calculation of Internal Structure in Scanning Tunneling Microscopy Images of Related Molecules. *Phys. Rev. Lett.* **70**, 3740 (1993).

210. Hallmark, V. M. & Chiang, S. Imaging Structural Details in Closely Related Molecular Adsorbate Systems. *Surf. Sci.* **286**, 190 (1993).

211. Morin, C., Simon, D. & Sautet, P. Trends in the Chemisorption of Aromatic Molecules on a Pt(111) Surface: Benzene, Naphthalene, and Anthracene from First Principles Calculations. *J. Phys. Chem. B* **108**, 12084 (2004).

212. Santarossa, G., Iannuzzi, M., Vargas, A. & Baiker, A. Adsorption of Naphthalene and Quinoline on Pt, Pd and Rh: A DFT Study. *Chem. Phys. Chem.* **9**, 401 (2008).

213. Stuckless, J. T., Frei, N. A. & Campbell, C. T. A Novel Single-Crystal Adsorption Calorimeter and Additions for Determining Metal Adsorption and Adhesion Energies. *Rev. Sci. Instrum.* **69**, 2427 (1998).

214. Solomonov, B. N. *et al.* Solution Calorimetry as a Complementary Tool for the Determination of Enthalpies of Vaporization and Sublimation of Low Volatile Compounds at 298.15K. *Thermochim. Acta* **589**, 164 (2014).

215. Kováts, E., Günthard, H. H. & Plattner, P. A. Thermische Eigenschaften von Azulenen. *Helv. Chim. Acta* **38**, 1912 (1955).

216. Chickos, J., Hesse, D., Hosseini, S., Nichols, G. & Webb, P. Sublimation Enthalpies at 298.15k Using Correlation Gas Chromatography and Differential Scanning Calorimetry

Measurements. *Thermochim. Acta* **313**, 101 (1998).

217. Maurer, R. J., Ruiz, V. G. & Tkatchenko, A. Many-Body Dispersion Effects in the Binding of Adsorbates on Metal Surfaces. *J. Chem. Phys.* **143**, 102808 (2015).

218. Maurer, R. J. *et al.* Adsorption Structures and Energetics of Molecules on Metal Surfaces: Bridging Experiment and Theory. *Prog. Surf. Sci.* **91**, 72 (2016).

219. Maurer, R. J. *et al.* Thermal and Electronic Fluctuations of Flexible Adsorbed Molecules: Azobenzene on Ag(111). *Phys. Rev. Lett.* **116**, 146101 (2016).